CSR-TR-74-2

SURFACE ELECTRICAL PROPERTIES EXPERIMENT

FINAL REPORT, PART 2 OF 3

NASA CONTRACT NAS 9-11540

APRIL 1974

I

SURFACE ELECTRICAL PROPERTIES EXPERIMENT

Final Report, Part 2 of 3

NASA Contract NAS 9-11540

Theory of Radio-Frequency Interferometry in Geophysical Subsurface Probing

April 1974

Massachusetts Institute of Technology
Center for Space Research
Cambridge, Massachusetts 02139

II

Prepared by:

J. A. Kong and L. Tsang

Theory of Radio-Frequency Interferometry in Geophysical Subsurface Probing

Table of Contents

Preface

This report summarizes the work carried out in the past three years under the Lunar Surface Electric Properties (SEP) Project. It concerns primarily with the theory of radio-frequency interferometry used in geophysical subsurface probing. Parts of this report have been published in the following articles:

1. Kong, "Electromagnetic Fields Due to Dipole Antennas over Stratified Anisotropic Media," Geophysics, Vol. 37, pp. 985-996, 1972.

2. Shen, Tsang, and Kong, "Multifrequency Excitation of a Wire Antenna for an Invariant Radiation Pattern," IEEE Trans. on Ant. and Prop., 1972.

3. Kong, Tsang, and Simmons, "Lunar Subsurface Probing with Radio Frequency Interferometry," URSI Symposium, 1972.

4. Tsang, Kong, and Simmons, "Interference Patterns of a Horizontal Electric Dipole over Layered Dielectric Media," J. Geophysics Research, 1973.

5. Kong, Tsang, and Simmons, "Geophysical Subsurface Probing with Radio Frequency Interferometry," IEEE Trans. on Ant. and Prop., July, 1974.

6. Tsang, Brown, Kong, and Simmons, "Numerical Evaluation of Electromagnetic Fields due to Dipole Antennas in the Presence of Stratified Media," J. Geophysics Research, 1974.

Contributions are also made by L. Tsang, John Mallick, Winston Chan, Paul Palmer through their S.B. Theses, and by L. Tsang through his S.M. Thesis.

ACKNOWLEDGMENT

We wish to express our sincere appreciation to Professor J. V. Harrington for providing us with the opportunity, the support, and the encouragement to pursue research in this field. We are thankful to Professor Gene Simmons, Principal Investigator of the SEP Project, for his distinguished leadership and for his unswerving support. Acknowledgment is due to Dr. J. W. Meyer for many enlightening discussions and for his constant support, to Dr. J. DeBettencourt for his encouragement, and to Mr. L. E. Beckley for his support in administrative matters.

Financial support was provided by the DSR Account 73096 under the parent NASA Contract NAS 9-11540 through the Center for Space Research. Computations were done at the M.I.T. Computing Center. Support provided by the Research Laboratory of Electronics and the Department of Electrical Engineering is also acknowledged.

Chapter 1.

INTRODUCTION

The subsurface of planetary bodies, including the earth and its moon, can be examined with electromagnetic waves. In 1955, the radio-frequency interference fringes method was used on geophysical prospection of underground water in Egyptian desert (El Said, 1955a, 1956b). This report concerns with the experiment developed for Apollo 17 mission to measure the subsurface electromagnetic properties of the moon (Simmons et al, 1973). In the experiment, a transmitting antenna consisting of a pair of orthogonal dipoles is laid directly on the lunar surface. The antenna radiates sequentially at frequencies of 1, 2.1, 4, 8.1, 16 and 32.1 MHz in a time window of 100 millisecond for each frequency. The time window is sufficiently long that the experiment is effectively a continuous wave experiment. A receiving antenna consisting of three orthogonal loops is mounted on the lunar roving vehicle. As the LRV traverses the lunar surface, the strengths of magnetic field components are measured as a function of distance from the transmitting antenna. The data are recorded on magnetic tapes and returned to earth for analysis. The interference patterns of the field-distance plot contain information about the electromagnetic properties of the lunar subsurface. To test both equipment and theory, experiments have been performed on three glaciers (Strangway et al 1974) in Switzerland, Canada, and Alaska and on a scale model tank (Rossiter et al, 1974) in laboratory.

In this report, we present the theoretical basis of the experiment. The mathematical model is a stratified n-layer medium. Each layer is bounded by plane boundaries and possesses different electric permittivity, magnetic permeability, and thickness. Although dipole radiation in the presence of stratified media has been studied extensively (Sommerfeld 1949, Brekhovikih 1960, Banos 1962, Gudmaudsen 1972, Wait 1970, Felsen and Marcuvitz 1973, Kong 1972, Annan 1973), a proper account for the interference fringes method is still lacking. The geometrical optics approximation was the first approach used in calculating interference patterns (El Said 1956, Annan 1973, Tsang et al 1973). With the use of the reflection coefficient formulation (Kong 1972), all field components can be expressed in integral forms with a single variable of integration. In order to obtain explicit expressions for the six field components, the following three different approaches are used to evaluate the integrals: 1) geometrical optics approximation, 2) modal approach, and 3) direct numerical integration. Scattering effects are also discussed: the advantages and disadvantages of the various methods and their respective regions of validity are compared in the last Chapter. All numerical results for anisotropic as well as isotropic cases are presented in Appendices.

THEORETICAL FORMULATION

2.1 INTRODUCTION

The problem of radiation of a dipole source in the presence of stratified media has been extensively studied with application to geophysical explorations. An excellent review on the half-space case is contained in the book by Sommerfeld (1949) and in the monograph by Baños (1966). Propagation and Radiation in stratified media are treated by Wait (1970) amd Ward (1967). Wolf (1946), and Bhattacharya (1963) considered the case of dipoles on two layer earth. Wait (1951, 1953) solved the problem of electrical and magnetic dipoles over a stratified isotropic medium. The case of an anisotropic half-space was studied by Chetaev (1963) and Wait (1966a). Praus (1965), Sinha and Bhattacharya (1967) and Sinha (1968, 1969) treated electric and magnetic dipoles over a two layer anisotropic earth. Wait (1966b) formally solved the case of a horizontal dipole over a stratified anisotropic medium. All these works are carried out by means of Sommerfeld's Hertzian potential functions, and the primary interest is concentrated in the limits of high conductivity. Magnetic properties are almost entirely neglected; mainly because such model studies assume principal applications to the earth where the permeability is nearly equal to that of vacuum and the electric conductivity dominates at low frequencies. In events of other celestial bodies, such as the moon where the lack of moisture renders very low conductivity to the medium, a study of contributions due to all electric and magnetic properties then becomes important.

This Chapter is devoted to the case of radiation of various dipole sources in the presence of a stratified anisotropic media. The anisotropic medium is uniaxial and possesses both tensor permittivities and permeabilities. The principal axes are all perpendicular to the boundaries separating different media. Solutions to the problem are facilitated by decomposing a general wave field into TM and TE modes, employing the concept of propagation matrices and expressing the reflection coefficients in terms of continuous fractions. The primary excitation is separated entirely from contributions due to the medium. The reflection coefficients depend solely on the geometrical configurations as well as the physical properties of the stratified medium.

In studying the theory of electromagnetic wave propagation, it has been appreciated both classically and quantum mechanically (Kong, 1970) that introduction of a potential function is not necessary and sometimes complicates the algebra especially when anisotropic media are involved. With recognition of the fact that outside any source, two scalar functions are sufficient to determine all field quantities, two components of the field vectors can be chosen as the fundamental scalar functions. In our case, the preferred field components for TM and TE decomposition are clearly those along the principal axis and to boundaries of stratification. With the aid of propagation matrices (Kong, 1971), wave amplitudes in any region are easily calculated in terms of those in any other region. Writing in the form of continuous fractions, we obtain a closed form solution for the reflection

coefficients. All field components are expressed in terms of integrals which are ready for direct numerical evaluation. A discussion is given for the various special cases.

2.2 TRANSVERSE ELECTRIC AND MAGNETIC WAVES

Governing equations for electromagnetic fields in a region outside any source are the Maxwell's source free equations.

$$\nabla \times \bar{E} = i\omega\bar{\bar{\mu}} \cdot \bar{H} \tag{2.1a}$$

$$\nabla \times \bar{H} = -i\omega\bar{\bar{\epsilon}} \cdot \bar{E} \tag{2.1b}$$

where in (2.1a), $\bar{\bar{\mu}}$ is the permeability tensor of the media. The tensor $\bar{\bar{\epsilon}}$ in (2.1b) contains information about the dielectric constant and the conductivity of the medium. $\bar{\bar{\epsilon}} = \bar{\bar{\epsilon}}' + i\bar{\bar{\epsilon}}''$, where $\bar{\bar{\epsilon}}'$ is the permittivity tensor, and $\bar{\bar{\epsilon}}''$ is related to the conductivity tensor $\bar{\bar{\sigma}}$ by $\bar{\bar{\epsilon}}'' = \bar{\bar{\sigma}}/\omega$. Time harmonic excitations with time dependence $\exp(-i\omega t)$ have been assumed. The tensors $\bar{\bar{\epsilon}}$ and $\bar{\bar{\mu}}$ can be represented by hermitian matrices. In our case, we consider media which are uniaxially anisotropic, where

$$\bar{\bar{\epsilon}} = \begin{pmatrix} \epsilon & & \\ & \epsilon & \\ & & \epsilon_z \end{pmatrix} \tag{2.2a}$$

and

$$\bar{\bar{\mu}} = \begin{pmatrix} \mu & & \\ & \mu & \\ & & \mu_z \end{pmatrix} \tag{2.2b}$$

We employ cylindrical coordinates, and the plane transverse to the $\hat{z}$ axis is characterized by ρ and ϕ. Longitudinal electric and magnetic components E_z and H_z are used to derive TE and TM waves. The wave equations to be satisfied by E_z and H_z are immediately derived from equations (2.1) and (2.2). If we take the z component of (2.1b) in view of $\bar{\bar{\epsilon}}$ given by (2.2a), employ (2.1a) to eliminate transverse magnetic field components, and use the fact that $\nabla \cdot E = (1 - \alpha)\partial E_z/\partial z$, the equation for E_z is

$$(\nabla_t^2 + a \frac{\partial^2}{\partial z^2} + k^2 a)\ E_z = 0 \tag{2.3a}$$

By the same token, we obtain the wave equation for H_z:

$$(\nabla_t^2 + b \frac{\partial^2}{\partial z^2} + k^2 b)\ H_z = 0 \tag{2.3b}$$

In equations (2.3a) and (2.3b),

$$k = \omega\sqrt{\mu\epsilon} \tag{2.4}$$

$$a = \epsilon_z / \epsilon \tag{2.5a}$$

$$b = \mu_z / \mu \tag{2.5b}$$

and

$$\nabla_t^2 = \frac{1}{\rho}\frac{\partial}{\partial\rho}(\rho \frac{\partial}{\partial\rho}) + \frac{1}{\rho^2}\frac{\partial^2}{\partial\varphi^2} \tag{2.6}$$

is the transverse Laplacian operator expressed in cylindrical coordinates. It is seen from Eq.(3) that E_z and H_z are decoupled, which would not be true if the $\overline{\overline{\varepsilon}}$ abd $\overline{\overline{\mu}}$ tensors possess off-diagonal elements. A unique decomposition of the total wave into a transverse magnetic field (TM) mode derivable from E_z and a transverse electric field (TE) mode derivable from H_z is therefore plausible. We note that a pair of vector wave equations can be derived from (2.1) and (2.2):

$$\nabla^2\bar{E} + k^2\bar{E} + (a - 1)k^2E_z\hat{z} + (a - 1)\nabla(\partial E_z/\partial z) = 0 \qquad (2.7a)$$

$$\nabla^2\bar{H} + k^2\bar{H} + (b - 1)k^2H_z\hat{z} + (b - 1)\nabla(\partial H_z/\partial z) = 0 \qquad (2.7b)$$

Eq. (2.7a) is the vector wave equation for the electric fields of TM waves where $H_z = 0$, and (2.7b) is the wave equation for the magnetic fields of TE waves, where $E_z = 0$. The $\hat{z}$ component of the two vector equations (2.7) gives rise to equation (2.3).

Solutions of E_z and H_z to the wave equation (2.3) in cylindrical coordinates are well known. As a consequence of the Maxwell equations (2.1), all transverse-electric- and magnetic-field components can be expressed in terms of the longitudinal components E_z and H_z which, respectively, characterize the TM and the TE waves. In our problems we are interested in wave solutions which are outgoing in $\hat{\rho}$ direction and traveling or standing in $\hat{z}$ direction. Therefore, we obtain, for a fixed separation constant n,

$$\bar{E}^{TM} = \int_{-\infty}^{\infty} dk_\rho \begin{pmatrix} i \dfrac{a k_z^{(e)}}{k_\rho} \left(-Ae^{-ik_z^{(e)} z} + Be^{ik_z^{(e)} z} \right) H_n^{(1)'}(k_\rho \rho) S_n^{TM}(\varphi) \\ i \dfrac{a k_z^{(e)}}{k_\rho^2 \rho} \left(-Ae^{-ik_z^{(e)} z} + Be^{ik_z^{(e)} z} \right) H_n^{(1)}(k_\rho \rho) S_n^{TM'}(\varphi) \\ \left[A(k_\rho) e^{-ik_z^{(e)} z} + B(k_\rho) e^{ik_z^{(e)} z} \right] H_n^{(1)}(k_\rho \rho) S_n^{TM}(\varphi) \end{pmatrix} \tag{2.8a}$$

$$\bar{H}^{TM} = \int_{-\infty}^{\infty} dk_\rho \begin{pmatrix} -i \dfrac{a\omega\epsilon}{k_\rho^2 \rho} \left(Ae^{ik_z^{(e)} z} + Be^{ik_z^{(e)} z} \right) H_n^{(1)}(k_\rho \rho) S_n^{TM'}(\varphi) \\ i \dfrac{a\omega\epsilon}{k_\rho} \left(Ae^{-ik_z^{(e)} z} + Be^{ik_z^{(e)} z} \right) H_n^{(1)'}(k_\rho \rho) S_n^{TM}(\varphi) \\ 0 \end{pmatrix} \tag{2.8b}$$

$$\bar{E}^{TE} = \int_{-\infty}^{\infty} dk_\rho \begin{pmatrix} i \frac{b\omega\mu}{k_\rho^2} \left(Ce^{-ik_z^{(m)} z} + De^{ik_z^{(m)} z} \right) H_n^{(1)}(k_\rho \rho) S_n^{TE'}(\varphi) \\ -i \frac{b\omega\mu}{k_\rho} \left(Ce^{-ik_z^{(m)} z} + De^{ik_z^{(m)} z} \right) H_n^{(1)'}(k_\rho \rho) S_n^{TE}(\varphi) \\ 0 \end{pmatrix} \tag{2.8c}$$

$$\bar{H}^{TE} = \int_{-\infty}^{\infty} dk_\rho \begin{pmatrix} i \frac{bk_z^{(m)}}{k_\rho} \left(-Ce^{-ik_z^{(m)} z} + De^{ik_z^{(m)} z} \right) H_n^{(1)'}(k_\rho \rho) S_n^{TE}(\varphi) \\ i \frac{bk_z^{(m)}}{k_\rho^2 \rho} \left(-Ce^{-ik_z^{(m)} z} + De^{ik_z^{(m)} z} \right) H_n^{(1)}(k_\rho \rho) S_n^{TE'}(\varphi) \\ \left[C(k_\rho) e^{-ik_z^{(m)} z} + D(k_\rho) e^{ik_z^{(m)} z} \right] H_n^{(1)}(k_\rho \rho) S_n^{TE}(\varphi) \end{pmatrix} \tag{2.8c}$$

where superscripts TM and TE denote, respectively, TM and TE waves. We note that if the integrands for E_z and H_z are denoted, respectively, by $E_z(k_\rho)$ and $H_z(k_\rho)$ such that

$$E_z^{TM} = \int_{-\infty}^{\infty} dk_\rho E_z(k_\rho) \quad \text{and} \quad H_z^{TE} = \int_{-\infty}^{\infty} dk_\rho H_z(k_\rho),$$

then the integrands of the transverse components are related to $E_z(k\rho)$ and $H_z(k\rho)$ by the following relations:

$$E_t(k_\rho)^{TM} = \frac{a}{k_\rho^2} \nabla_t \left\{ \partial E_z(k_\rho)/\partial z \right\}, \quad H_t(k_\rho)^{TM} = -i \frac{a\omega\varepsilon}{k_\rho^2} \nabla_t \times E_z(k_\rho), \tag{2.9a}$$

and

$$H_t(k_\rho)^{TE} = \frac{b}{k_\rho^2} \nabla_t \left\{ \partial H_z(k_\rho)/\partial z \right\}, \quad E_t(k_\rho)^{TE} = -i \frac{b\omega\mu}{k_\rho^2} \nabla_t \times \bar{H}_z(k_\rho) \tag{2.9b}$$

where

$$\bar{E}_z = \hat{z} E_z, \quad \bar{H}_z = \hat{z} H_z, \quad \text{and} \quad \nabla_t = \hat{\rho} \frac{\partial}{\partial \rho} + \hat{\phi} \frac{1}{\rho} \frac{\partial}{\partial \rho}.$$

The fact that TM waves are extraordinary waves in the medium is signified in equation (2.8) by the superscript (e) on the $\hat{z}$-directed propagation constant $k_z^{(e)}$, which satisfies the dispersion relation

$$k_z^{(e)} = (k^2 - k_\rho^2/a)^{1/2}. \tag{2.10a}$$

TE waves are derived from H_z and satisfy the dispersion relation

$$k_z^{(m)} = (k^2 - k_\rho^2/b)^{1/2}, \tag{2.10b}$$

where the superscript (m) indicates the effect of magnetic anisotropy. In (2.8), the first element of the column matrices denotes $\hat{\rho}$ component, the second element of $\hat{\phi}$ component, and the third element the $\hat{z}$-conponent. The Hankel functions $H_n^{(1)}$ of the first kind and nth order represent outgoing waves in direction due to our choice of the time dependence $\exp(-i\omega t)$. $S_n(\phi)$ stands for sinusoidal functions of ϕ. Primes on $H_n^{(1)}(k_\rho\rho)$ and $S_n(\phi)$ denote differentiation with respect to the arguments. The k_ρ dependent functions A, B, C and D are to be determined by the appropriate boundary conditions.

2.3 PRIMARY EXCITATION

The explicit solution to the problem of dipole radiation over stratified medium depends on field excitations of the source, and the geometrical configuration and physical constituents of the medium. In the absence of the stratified medium, the solution of electromagnetic fields in an isotropic medium due to a dipole antenna, which we refer to as the primary excitation, is well-known (Adler, Chu and Fano, 1960). The solution is usually written in chperical coordinates. It can be transformed into cylindrical coordinates and represented by Hankel functions in the integral

form. Writing in the general form, we have

$$E_z = \int_{-\infty}^{\infty} dk_\rho \, E_o(k_\rho) \begin{cases} e^{ik_z z} \\ e^{-ik_z z} \end{cases} H_n^{(1)}(k_\rho \rho) \, S_n^{TM}(\varphi) \quad \begin{matrix} z > 0 \\ z < 0 \end{matrix} \qquad (2.11)$$

$$H_z = \int_{-\infty}^{\infty} dk_\rho \, H_o(k_\rho) \begin{cases} e^{ik_z z} \\ e^{-ik_z z} \end{cases} H_n^{(1)}(k_\rho \rho) \, S_n^{TE}(\varphi) \quad \begin{matrix} z > 0 \\ z < 0 \end{matrix} \qquad (2.12)$$

where E_o and H_o characterize the structure and excitation of the dipole. All field components follow from Eq. (2.8) with $B = D = 0$, $A = E_o$, $C = H_o$ for $z \leq 0$, and $A = C = 0$, $B = E_o$, $D = H_o$ for $z \geq 0$.

For the elementary dipoles under consideration, we obtain for:

1) Vertical electric dipole: $n = 0$, $S_n^{TM}(\varphi) = 1$

$$E_o = -\frac{Ilk_\rho^3}{8\pi\omega\epsilon k_z} \qquad (2.13a)$$

$$H_o = 0 \qquad (2.13b)$$

2) Horizontal electric dipole along $\hat{x}$-direction

$$E_o = \pm i \frac{Ilk_\rho^2}{8\pi\omega\epsilon} \quad z \gtrless 0 \quad S_1^{TM} = \cos\varphi \tag{2.14a}$$

$$H_o = i \frac{Ilk_\rho^2}{8\pi k_z} \quad S_1^{TE} = -\sin\varphi \tag{2.14b}$$

3) Vertical magnetic dipole: $n = 0$, $S_n^{TE}(\varphi) = 1$

$$H_o = -i \frac{IAk_\rho^3}{8\pi k_z} \tag{2.15a}$$

$$E_o = 0 \tag{2.15b}$$

4) Horizontal magnetic dipole along $\hat{x}$-direction

$$H_o = \mp \frac{IAk_\rho^2}{8\pi} \quad z \gtrless 0 \quad S_1^{TM} = \cos\varphi \tag{2.16a}$$

$$E_o = -\frac{IA\omega\mu k_\rho^2}{8\pi k_z} \quad S_1^{TE} = -\sin\varphi \tag{2.16b}$$

In the following, we derive Eq. (2.14) from well-known potential solutions for the dipole. Similar derivation, comparetively simpler, applies to Eqs. (2.13), (2.15) and (2.16). The vector potential solution for the horizontal electric dipole is

$$\bar{A} = A(\hat{\rho}\cos\phi - \hat{\phi}\sin\phi)$$

where $A = \frac{I\ell}{4\pi} e^{ikr}/r$

The electromagnetic fields are obtained from

$$\bar{H} = \nabla \times \bar{A}$$

and

$$\bar{E} = i \frac{1}{\omega E} \{\nabla(\nabla \cdot \bar{A}) + k^2 \bar{A}\}$$

Using the identity (Sommerfeld, 1949)

$$\frac{e^{ikr}}{r} = \frac{i}{2} \int_{-\infty}^{\infty} dk_\rho \frac{k_\rho}{k_z} H_o^{(1)}(k_\rho \rho) e^{\pm ik_z z}$$

the field components can all be written in the integral form. For the z-component,

$$H_z = - \sin\phi \, \partial A/\partial\rho$$

$$E_z = i \frac{1}{\omega\varepsilon} \cos\phi \, \partial^2 A/\partial\rho\partial z$$

The results are Eq. (2.14).

In Eqs. (2.13) - (2.16) I is the current that drives the dipole, l the equivalent lingth of the electric dipole, A the area of the current loop that constitutes the magnetric dipole. Horizontal dipoles can be simply obtained by a rotation of coordinates, which ammounts to change $\cos\phi$ to $\sin\phi$ and $\sin\phi$ to $-\cos\phi$. We note that a vertical electric dipole excites TM wave only and a vertical magnetic dipole excites TE wave only, both involve

Hankel functions of zeroth order; whereas horizontal dipoles excite both TM and TE waves and require Hankel functions of first order. An arbitrary oriented dipole can be treated as a linear combination of three dipoles along $\hat{x}$, $\hat{y}$, and $\hat{z}$ axes which are just described.

2.4 DIPOLE ANTENNAS OVER STRATIFIED ANISOTROPIC MEDIA

Giometrical configuration of the problem is shown in Fig. 2.1. There are n slab regions, and the last region is numbered t instead of $n+1$, for the sake of simplifying writings. In each region labelled i, solutions of electromagnetic field components take the form Eq. (2.8) with all quantities subscripted by i. In the 0th region where we have the antennas, $A_0 = E_0$ and $C_0 = H_0$ which are known from (2.13) - (2.16) for the three types of antennas under consideration. In the last region namely region t, it is semi-infinite and we do not expect reflected waves, therefore, $B_t = D_t = 0$.

Boundary conditions at all interfaces are that all tagential electromagnetic field components must be continuous for all ρ and ϕ. Consider the boundary at $z = -d_i$, the continuity of tangential electric fields and the continuity of tangential magnetic fields yields, for the TM waves,

$$k_{iz}^{(e)} \{ - A_i e^{ik_{iz}^{(e)} d_i} + B_i e^{-ik_{iz}^{(e)} d_i} \}$$

$$= k_{(i+1)z}^{(e)} \{ - A_{i+1} e^{ik_{(i+1)z}^{(e)} d_i} + B_{i+1} e^{-ik_{(i+1)z}^{(e)} d_i} \} \qquad (2.17a)$$

$$\varepsilon_i \{A_i e^{ik_{iz}^{(e)} d_i} + B_i e^{-ik_{iz}^{(e)} d_i}\}$$

$$= \varepsilon_{i+1}\{ A_{i+1} e^{ik_{(i+1)z}^{(e)} d_i} + B_{i+1} e^{-ik_{(i+1)z}^{(e)} d_i}\} \quad (2.17b)$$

and for the TE waves

$$\mu_i\{ C_i e^{ik_{iz}^{(m)} d_i} + D_i e^{-ik_{iz}^{(m)} d_i}\}$$

$$= \mu_{i+1}\{ C_{i+1} e^{ik_{(i+1)z}^{(m)} d_i} + D_{i+1} e^{-ik_{(i+1)z}^{(m)} d_i}\} \quad (2.18a)$$

$$\hat{k}_{iz}^{(m)}\{ -C_i e^{ik_{iz}^{(m)} d_i} + D_i e^{-ik_{iz}^{(m)} d_i}\}$$

$$= k_{(i+1)z}^{(m)}\{ -C_{i+1} e^{ik_{(i+1)z}^{(m)} d_i} + D_{i+1} e^{-ik_{(i+1)z}^{(m)} d_i}\} \quad (2.18b)$$

The reason that we can treat the TM and TE cases separately is because that 1) for vertical dipole case, only TM or TE is excited; 2) for horizontal dipole case, although the total tangential field components consist of both TM and TE waves, the coefficients of $H_1^{(1)}$ and $H_1^{(1)'}$ separates TM and TE cases.

We now illustrate the derivation for the upward propagation matrix M_i^{i+1} for TM cases. From (2.17a) and (2.17b) it is straight-forward to solve for $A_i \exp ik_{kz}^{(e)} d_i$ and $B_i \exp - ik_{iz}^{(e)} d_i$ in terms of A_{i+1} and B_{i+1}. Define

$$a_i = A_i \exp (ik_{iz}^{(e)} d_i) \quad (2.19a)$$

$$b_i = B_i \exp\left(- ik_{iz}^{(e)} d_i \right) \tag{2.19b}$$

We have

$$a_i = \frac{1}{2} \{\varepsilon(+)_i^{i+1} e(+)_i^{(e)} a_{i+1} + \varepsilon(-)_i^{i+1} e(-)_i^{(e)} b_{i+1}\} \tag{2.20a}$$

$$b_i = \frac{1}{2} \{\varepsilon(-)_i^{i+1} e(+)_i^{(e)} a_{i+1} + \varepsilon(+)_i^{i+1} e(-)_i^{(e)} b_{i+1}\} \tag{2.20b}$$

The upward propagation matrix for TM waves from (i + 1)th region to ith region is defined to be

$$M_i^{i+1} = \frac{1}{2} \begin{pmatrix} \varepsilon(+)_i^{i+1} e(+)_i^{(e)} & \varepsilon(-)_i^{i+1} e(-)_i^{(e)} \\ \varepsilon(-)_i^{i+1} e(+)_i^{(e)} & \varepsilon(+)_i^{i+1} e(-)_i^{(e)} \end{pmatrix} \tag{2.21}$$

where

$$\varepsilon(\pm)_q^p = \left(\frac{\varepsilon_p}{\varepsilon_q} \pm \frac{k_{pz}^{(e)}}{k_{qz}^{(e)}} \right)$$

$$e(\pm)_i^{(e)} = \exp[\pm ik_{(i+1)z}^{(e)} (d_i - d_{i+1})]$$

$$k_{iz}^{(e)} = \sqrt{k_i^2 - k_\rho^2}/a$$

Equation (2.20) can be written as

$$\begin{pmatrix} a_i \\ \\ b_i \end{pmatrix} = M_i^{i+1} \begin{pmatrix} a_{i+1} \\ \\ b_{i+1} \end{pmatrix} \tag{2.22}$$

Note that, with R^{TM} denoting reflection coefficients and T^{TM} denoting transmission coefficients, we can write

$$a_0 = E_0 \exp\ (ik_z^{(e)}\ d_0\ ) \tag{2.23a}$$

$$b_0 = R^{TM}\ E_0\ \exp\ (\ -\ ik_z^{(e)}\ d_0\ ) \tag{2.23b}$$

$$a_t = T^{TM}\ E_0\ \exp\ (ik_z^{(e)}\ d_t\ ) \tag{2.23c}$$

and that $b_t = 0$ because there is no reflected wave in the last region. The parameter d_t in (2.23c) is introduced for convenience, it does not correspond to any distance and is always multiplied by $e(-)_n^{(e)}$ to yield $\exp(ik_{nz}^{(e)}\ d_n)$. The definition of the propagation matrix is a useful one. Once wave amplitudes in any region are known, those in the regions above this one are all determined by

(2.22). Thus the propagation matrix (2.21) propagates wave amplitudes upward. We can also define a propagation matrix M_{i+1}^{i} which propagates wave amplitudes downward.

$$M_{i+1}^{i} = \frac{1}{2} \begin{pmatrix} \epsilon(+)_{i+1}^{i}\, e(-)_{i}^{(e)} & \epsilon(-)_{i+1}^{i}\, e(-)_{i}^{(e)} \\ \epsilon(-)_{i+1}^{i}\, e(+)_{i}^{(e)} & \epsilon(+)_{i+1}^{i}\, e(+)_{i}^{(e)} \end{pmatrix} \tag{2.24a}$$

and $$\begin{pmatrix} a_{i+1} \\ b_{i+1} \end{pmatrix} = M_{i+1}^{i} \begin{pmatrix} a_i \\ b_i \end{pmatrix} \tag{2.24b}$$

It is easily shown that

$$M_{i}^{i+1}\, M_{i+1}^{i} = 1 \tag{2.25}$$

Following a parallel analysis of the above, we define a downward propagation matrix N_{i+1}^{i} for TE waves.

$$N_{i+1}^{i} = \frac{1}{2} \begin{pmatrix} \mu(+)_{i+1}^{i}\, e(-)_{i}^{(m)} & \mu(-)_{i+1}^{i}\, e(-)_{i}^{(m)} \\ \mu(-)_{i+1}^{i}\, e(+)_{i}^{(m)} & \mu(+)_{i+1}^{i}\, e(+)_{i}^{(m)} \end{pmatrix} \tag{2.26a}$$

$$\begin{pmatrix} c_{i+1} \\ d_{i+1} \end{pmatrix} = N_{i+1}^{i} \begin{pmatrix} c_i \\ d_i \end{pmatrix} \tag{2.26b}$$

An upward propagation matrix N_i^{i+1} is defined as the inverse of N_{i+1}^{i}

$$N_i^{i+1} = \frac{1}{2} \begin{pmatrix} \mu(+)_i^{i+1} \, e(+)_i^{(m)} & \mu(-)_i^{i+1} \, e(-)_i^{(m)} \\ \mu(-)_i^{i+1} \, e(+)_i^{(m)} & \mu(+)_i^{i+1} \, e(-)_i^{(m)} \end{pmatrix} \tag{2.27a}$$

$$\begin{pmatrix} c_i \\ d_i \end{pmatrix} = N_i^{i+1} \begin{pmatrix} c_{i+1} \\ d_{i+1} \end{pmatrix} \tag{2.27b}$$

In (2.26) and (2.27)

$$\mu(\pm)_q^p = \frac{\mu_p}{\mu_q} \pm \frac{k_{pz}^{(m)}}{k_{qz}^{(m)}} \tag{2.28}$$

$$c_i = C_i \exp(ik_{iz}^{(m)} d_i) \tag{2.29a}$$

$$d_i = D_i \exp(-ik_{iz}^{(m)} d_i) \tag{2.29b}$$

$$k_{iz}^{(m)} = \sqrt{k_i^2 - k^2/b} \tag{2.29c}$$

Also $c_0 = H_0$, $d_0 = R^{TE}H_0$, $c_t = T^{TE}H_0$ and $d_t = 0$. We note that for vertical magnetic or electric dipoles, only the TM waves or the TE waves, respectively, are excited. In the case of either a horizontal electric dipole or a horizontal magnetic dipole, both TM and TE waves are excited.d

2.5 REFLECTION COEFFICIENTS

In the interferometry method, our primary interest is the reflected wave fields. From the preceding section, we have established that when the wave amplitudes in region 0 are known, solutions in any other region can be determined by using the downward propagation matrices (2.24) and (2.26). In this section, we derive for the reflection coefficients, a formula which is expressed in continuous fractions. We observe from Eq. (2.23) that $b_t/a_t = 0$ and b_0/a_0 gives rise to the reflection coefficients R^{TM}. And from (2.22), an expression for b_i/a_i in terms of b_{i+1}/a_{i+1} can be easily extablished. In view of (2.21), (2.22) gives

$$\frac{b_i}{a_i} = \frac{\epsilon(+)_i^{i+1}}{\epsilon(-)_i^{i+1}} \left(1 - \frac{\epsilon(+)_i^{i+1} / \epsilon(-)_i^{i+1} - \epsilon(-)_i^{i+1} / \epsilon(+)_i^{i+1}}{\epsilon(+)_i^{i+1} / \epsilon(-)_i^{i+1} + (e(-)_i^{(e)})^2 (b_{i+1}/a_{i+1})} \right) \tag{2.30}$$

Making use of (2.30), we obtain a formula in continuous fraction for the reflection coefficient R^{TM}

$$R_n^{TM} = \exp(i2k_z^{(e)} d_0) \frac{\epsilon(+)_0^1}{\epsilon(-)_0^1} \{1 - \frac{\epsilon(+)_0^1 / \epsilon(-)_0^1 - \epsilon(-)_0^1 / \epsilon(+)_0^1}{\epsilon(+)_0^1 / \epsilon(-)_0^1}$$

$$+ \exp(i2k_{1z}^{(e)} (d_1 - d_0)) \frac{\epsilon(+)_1^2}{\epsilon(-)_1^2} [1 - \frac{\epsilon(+)_1^2 / \epsilon(-)_1^2 - \epsilon(-)_1^2 / \epsilon(+)_1^2}{\epsilon(+)_1^2 / \epsilon(-)_1^2}$$

$$+ \ldots\ldots .. + \exp(i2k_{nz}^{(e)} (d_n - d_{n-1})) \frac{\epsilon(-)_n^t}{\epsilon(+)_n^t} \ldots\ldots]\}. \quad (2.31)$$

Likewise, we obtain the reflection coefficient for TE waves

$$R_n^{TE} = \exp(i2k_z^{(m)} d_o) \frac{\mu(+)_0^1}{\mu(-)_0^1} \{ 1 - \frac{\mu(+)_0^1 / \mu(-)_0^1 - \mu(-)_0^1 / \mu(+)_0^1}{\mu(+)_0^1 / \mu(-)_0^1}$$

$$+ \exp(i2k_{1z}^{(m)} (d_1 - d_0)) \frac{\mu(+)_1^2}{\mu(-)_1^2} [1 - \frac{\mu(+)_1^2 / \mu(-)_1^2 - \mu(-)_1^2 / \mu(+)_1^2}{\mu(+)_1^2 / \mu(-)_1^2}$$

$$+ .... + \exp(i2k_{nz}^{(m)} (d_n - d_{n-1})) \frac{\mu(-)_n^t}{\mu(+)_n^t} \ldots\ldots]\}. \quad (2.32)$$

The subscript n on R^{TM} and R^{TE} denotes the number of layers involved.

2.6 SUMMARY

With the reflection coefficients determined in the last section, we can now summarize the formulas for all field quantities in region 0, where interference patterns are calculated. We have decomposed total wave fields into a summation of the TM and TE wave modes.

$$\bar{E} = \bar{E}^{TM} + \bar{E}^{TE} \tag{2.33}$$

$$\bar{H} = \bar{H}^{TM} + \bar{H}^{TE} \tag{2.34}$$

The TM and TE solutions are

1) For a vertical electric dipole

$$\bar{E}^{TM} = \int_{-\infty}^{\infty} dk_\rho \left(-\frac{I\ell}{8\pi\omega\epsilon}\right) \begin{pmatrix} ik_\rho^2 (\pm e^{\mp ik_z^{(e)} z} + R^{TM} E^{ik_z^{(e)} z}) H_0^{(1)'}(k_\rho \rho) \\ 0 \\ \frac{k_\rho^3}{k_z^{(e)}} (e^{\mp ik_z^{(e)} z} + R^{TM} e^{ik_z^{(e)} z}) H_0^{(1)}(k_\rho \rho) \end{pmatrix} \tag{2.35a}$$

$$\bar{H}^{TM} = \int_{-\infty}^{\infty} dk_\rho \left(-\frac{I\ell}{8\pi}\right) \begin{pmatrix} 0 \\ i\frac{k_\rho^2}{k_z^{(e)}} (e^{\mp ik_z^{(e)} z} + R^{TM} e^{ik_z^{(e)} z}) H_0^{(1)'}(k_\rho \rho) \\ 0 \end{pmatrix} \tag{2.35b}$$

$$\bar{E}^{TE} = \bar{H}^{TE} = 0$$

2) For a vertical magnetic dipole

$$\bar{E}^{TE} = \int_{-\infty}^{\infty} dk_\rho \left(-i \frac{IA\omega\mu}{8\pi}\right) \begin{pmatrix} 0 \\ -i \frac{k_\rho^2}{k_z^{(m)}} \left(e^{\mp ik_z^{(m)} z} + R^{TE} e^{ik_z^{(m)} z}\right) H_0^{(1)'}(k_\rho \rho) \\ 0 \end{pmatrix} \tag{2.36a}$$

$$\bar{H}^{TE} = \int_{-\infty}^{\infty} dk_\rho \left(-i \frac{IA}{8\pi}\right) \begin{pmatrix} ik_\rho^2 \left(\mp e^{\mp ik_z^{(m)} z} + R^{TE} e^{ik_z^{(m)} z}\right) H_0^{(1)'}(k_\rho \rho) \\ 0 \\ \frac{k_\rho^3}{k_z} \left(e^{\mp ik_z^{(m)} z} + R^{TE} e^{ik_z^{(m)} z}\right) H_0^{(1)}(k_\rho \rho) \end{pmatrix} \tag{2.36b}$$

$$\bar{E}^{TM} = \bar{H}^{TM} = 0$$

3) For a horizontal electric dipole along $\hat{x}$-direction

$$\bar{E}^{TM} = \int_{-\infty}^{\infty} dk_\rho \left(i \frac{I\ell}{8\pi\omega\epsilon}\right) \begin{pmatrix} iak_z^{(e)} k_\rho \left(e^{\mp ik_z^{(e)} z} - R^{TM} e^{ik_z^{(e)} z}\right) H_1^{(1)'}(k_\rho\rho)\cos\varphi \\ -a \frac{k_z^{(e)}}{\rho}\left(e^{\mp ik_z^{(e)} z} - R^{TM} e^{ik_z^{(e)} z}\right) H_1^{(1)}(k_\rho\rho)\sin\varphi \\ k_\rho^2 \left(\mp e^{\mp ik_z^{(e)} z} - R^{TM} e^{ik_z^{(e)} z}\right) H_1^{(1)}(k_\rho\rho)\cos\varphi \end{pmatrix}$$

(2.37a)

$$\bar{H}^{TM} = \int_{-\infty}^{\infty} dk_\rho \left(\frac{I\ell}{8\pi}\right) \begin{pmatrix} -\frac{a}{\rho}\left(\mp e^{\mp ik_z^{(e)} z} - R^{TM} e^{ik_z^{(e)} z}\right) H_1^{(1)}(k_\rho\rho)\sin\varphi \\ -ak_\rho \left(\mp e^{\mp ik_z^{(e)} z} - R^{TM} e^{ik_z^{(e)} z}\right) H_1^{(1)'}(k_\rho\rho)\cos\varphi \\ 0 \end{pmatrix}$$

(2.37b)

$$\bar{E}^{TE} = \int_{-\infty}^{\infty} dk_\rho \left(\frac{I\ell\omega\mu}{8\pi}\right) \begin{pmatrix} -\frac{b}{k_z^{(m)}\rho}\left(e^{\mp ik_z^{(m)} z} + R^{TE} e^{ik_z^{(m)} z}\right) H_1^{(1)}(k_\rho\rho)\cos\varphi \\ b\frac{k_\rho}{k_z^{(m)}}\left(e^{\mp ik_z^{(m)} z} + R^{TE} e^{ik_z^{(m)} z}\right) H_1^{(1)'}(k_\rho\rho)\sin\varphi \\ 0 \end{pmatrix}$$

(2.37c)

$$\bar{H}^{TE} = \int_{-\infty}^{\infty} dk_\rho \, (i \frac{I\ell}{8\pi}) \begin{pmatrix} ibk_\rho (\mp e^{\mp ik_z^{(m)} z} + R^{TE} e^{ik_z^{(m)} z}) H_1^{(1)'}(k_\rho \rho) \sin\varphi \\ \frac{ib}{\rho} (\mp e^{\mp ik_z^{(m)} z} + R^{TE} e^{ik_z^{(m)} z}) H_1^{(1)}(k_\rho \rho) \cos\varphi \\ \frac{k_\rho^2}{k_z^{(m)}} (e^{\mp ik_z^{(m)} z} + R^{TE} e^{ik_z^{(m)} z}) H_1^{(1)}(k_\rho \rho) \sin\varphi \end{pmatrix}$$

(2.37d)

4) For a horizontal magnetic dipole along $\hat{x}$-direction

$$\bar{E}^{TM} = \int_{-\infty}^{\infty} dk_\rho \, (-\frac{IA\omega\mu}{8\pi}) \begin{pmatrix} iak_\rho (\mp e^{\mp ik_z^{(e)} z} + R^{TE} e^{ik_z^{(e)} z}) H_1^{(1)'}(k_\rho \rho) \sin\varphi \\ \frac{ia}{} (\mp e^{\mp ik_z^{(e)} z} + R^{TE} e^{ik_z^{(e)} z}) H_1^{(1)}(k_\rho \rho) \cos\phi \\ -\frac{k_\rho^2}{k_z^{(e)}} (e^{\mp ik_z^{(e)} z} + R^{TE} e^{ik_z^{(e)} z}) H_1^{(1)}(k_\rho \rho) \sin\varphi \end{pmatrix}$$

(2.38a)

$$\bar{H}^{TM} = \int_{-\infty}^{\infty} dk_\rho \, (-\frac{IAk^2}{8\pi}) \begin{pmatrix} -i\frac{a}{k_z^{(e)}\rho} (e^{\mp ik_z^{(e)} z} + R^{TE} e^{ik_z^{(e)} z}) H_1^{(1)}(k_\rho \rho) \cos\varphi \\ i\frac{ak_\rho}{k_z^{(e)}} (e^{\mp ik_z^{(e)} z} + R^{TE} e^{ik_z^{(e)} z}) H_1^{(1)'}(k_\rho \rho) \sin\varphi \\ 0 \end{pmatrix}$$

(2.38b)

$$\bar{E}^{TE} = \int_{-\infty}^{\infty} dk_\rho \left(i \frac{IA\omega\mu}{8\pi}\right) \begin{pmatrix} -\frac{b}{\rho}\left(\mp e^{\mp ik_z^{(m)} z} + R^{TE} e^{ik_z^{(m)} z}\right) H_1^{(1)}(k_\rho \rho)\cos\varphi \\ -bk_\rho \left(\mp e^{\mp ik_z^{(m)} z} + R^{TE} e^{ik_z^{(m)} z}\right) H_1^{(1)\prime}(k_\rho \rho)\cos\varphi \\ 0 \end{pmatrix} \tag{2.38c}$$

$$\bar{H}^{TE} = \int_{-\infty}^{\infty} dk_\rho \left(\frac{IA}{8\pi}\right) \begin{pmatrix} ibk_z^{(m)} k_\rho \left(-e^{\mp ik_z^{(m)} z} + R^{TE} e^{ik_z^{(m)} z}\right) H_1^{(1)\prime}(k_\rho \rho)\cos\varphi \\ -i\frac{bk_z^{(m)}}{\rho}\left(-e^{\mp ik_z^{(m)} z} + R^{TE} e^{ik_z^{(m)} z}\right) H_1^{(1)}(k_\rho \rho)\sin\varphi \\ k_\rho^2 \left(\mp e^{\mp ik_z^{(m)} z} + R^{TE} e^{ik_z^{(m)} z}\right) H_1^{(1)}(k_\rho \rho)\cos\varphi \end{pmatrix} \tag{2.38d}$$

2.7 DISCUSSIONS

The problem of radiation of various dipole antennas over a stratified anisotropic medium has been solved. In view of the general formalism as presented in sections V and VI, we can make the following observations:

1) All medium properties such as the constitutive parameters and the geometrical configuration are all absorbed into the reflection coefficients R^{TM} and R^{TE}, which is readily computed by Eqs. (2.31) and (2.32). Clearly, when all regions possess the same constitutive parameters, namely when there is no stratification, $R^{TM} = R^{TE} = 0$.

2) Since the anisotropy in permittivity appears only in $\epsilon(\pm)$ and the anisotropy in permeability appears only in $\mu(\pm)$, it is seen from (2.31)-(2.34) that R^{TM} does not depend on the magnetic anisotropy and R^{TE} does not depend on the electric anisotropy. Both R^{TM} and R^{TE} are seen to be even functions of k_ρ.

3) It is obvious from (2.35)-(2.38) that a vertical electric dipole excites TM waves only and a vertical magnetic dipole excites TE waves only. Whereas both horizontal electric and magnetic dipoles excite both TM and TE waves. In the case when permeability is isotropic, the TM waves are extraordinary waves and the TE waves are ordinary waves. A turnstile antenna which consists of two dipoles perpendicular to each other and driven 90 degrees out of phase also excites both TM and TE waves.

4) The above formulation can be compared with the potential approach for the various cases that are existing. In the case of no stratified medium, the results are checked by using the identities

$$H_1^{(1)\prime} + \frac{1}{k_\rho \rho} H_1^{(1)} = H_o^{(1)} \tag{2.39}$$

and

$$\frac{i}{2} \int_{-\infty}^{\infty} dk_\rho e^{ik_z z} \frac{k_\rho}{k_z} H_o^{(1)}(k_\rho \rho) = \exp\left(ik\sqrt{\rho^2 + z^2}\right)/\sqrt{\rho^2 + z^2} \tag{2.40}$$

where $r^2 = \rho^2 + z^2$ in spherical coordinates. We define the number of layers of a stratified medium equal to the number of boundaries. The medium below the nth boundary is called the tth layer.

5) The one layer case (or half space) has been extensively studied. We obtain from (2.31) and (2.32)

$$R^{TM} = \frac{\epsilon(-)_0^1}{\epsilon(+)_0^1} \exp\left(i2k_z^{(e)} d_0\right) \tag{2.41a}$$

$$R^{TE} = \frac{\mu(-)_0^1}{\mu(+)_0^1} \exp\left(i2k_z^{(m)} d_0\right) \tag{2.41b}$$

In the case of a perfectly conducting half space,

$\epsilon = \epsilon_3 \to \infty$. Eq. (2.41) gives $R^{TM} = 1$ and $R^{TE} = -1$.

6) Observe that all contributions due to all layers below the first are lumped into the reflection coefficient R_{n-1}, such that

$$R_n^{TM} = \exp(i2k_z^{(e)}d_o)\,\frac{\varepsilon(+)_o^1}{\varepsilon(-)_o^1}\left(1 - \frac{\varepsilon(+)_o^1/\varepsilon(-)_o^1 - \varepsilon(-)_o^1/\varepsilon(+)_o^1}{\varepsilon(+)_o^1/\varepsilon(-)_o^1 + \exp(-i2k_{1z}^{(e)}d_o)R_{n-1}^{TM}}\right) \tag{2.42}$$

$$R_n^{TE} = \exp(i2k_z^{(m)}d_o)\,\frac{\mu(+)_o^1}{\mu(-)_o^1}\left(1 - \frac{\mu(+)_o^1/\mu(-)_o^1 - \mu(-)_o^1/\mu(+)_o^1}{\mu(+)_o^1/\mu(-)_o^1 + \exp(-i2k_{iz}^{(m)}d_o)R_{n-1}^{TE}}\right) \tag{2.43}$$

The definitions for R_{n-1}^{TM} and R_{n-1}^{TE} follow directly from (2.31) and (2.32).

In order to make effective use of the results obtained for the one layer case, we follow Wait (1953) to define a stratification factor for conductivity dominated media such as the earth. For a vertical electric dipole on the ground, the electromagnetic field quantities can be written in terms of one single integral

$$J_e = \int_{-\infty}^{\infty} \frac{k_\rho H_o^{(1)}(k_\rho\rho)e^{ik_z z}}{k_z + Q_e\frac{\varepsilon}{\varepsilon_1}k_{1z}}\,dk_\rho \tag{2.44}$$

The field components are

$$H_\phi = \left(-\frac{I\ell}{4\pi}\right)\frac{\partial J_e}{\partial\rho} \tag{2.45}$$

$$E_\rho = \left(-\frac{I\ell}{4\pi\omega\varepsilon}\right)\frac{\partial^2 J_e}{\partial\rho\,\partial z} \tag{2.46}$$

$$E_z = \left(-\frac{I\ell}{4\pi\omega\varepsilon}\right)\left(\frac{\partial^2}{\partial z^2} + k^2\right)J_e \tag{2.47}$$

The integral J_e follows from Eq. (2.35). The stratification factor Q_e is determined to be

$$Q_e = \frac{1 - R_{n-1}^{TM}}{1 + R_{n-1}^{TM}} \tag{2.48}$$

Under the assumption that the stratified medium is conductivity dominated such that $k_{iz}^{(e)} = k_i$, Q_e is then seen to be a constant. $k_{pz}/k_{qz} \approx \sqrt{\varepsilon_p/\varepsilon_q}$, and J_e becomes

$$J_e = 2 \frac{e^{ikr}}{r} [1 + (\pi p_1)^{1/2} e^{-p_2} \operatorname{erfc}(i\sqrt{p_2})] \tag{2.49}$$

Eq. (2.49) is obtained from (2.44) for far field and observation point near the surface such that $k\rho >> 1$ and $z/\rho << 1$. In (2.49),

$$p_1 = i \frac{k^3 \rho}{2k_1^2} \quad , \quad p_2 = p_1 \left(1 + \frac{k_1 z}{k_o} \right)^2 \tag{2.50}$$

and erfc is the complementary error function. Replacing k_1 by $Q_e k_1$, we obtain an analytic solution for a vertical electric dipole on top of an N layer stratified media.

For the case of a vertical magnetic dipole on a stratified medium, all electromagnetic field components can also be written in terms of one single integral J_m. The stratification factor Q_m can similarly be determined from the reflection

coefficient R^{TE} . Under the assumption of high conductivity,

$$Q_m \simeq \frac{1 - R^{TE}_{n-1}}{1 + R^{TE}_{n-1}} \tag{2.51}$$

$$J_m \simeq - \frac{k_\rho H_o^{(1)}(k_\rho \rho) e^{ik_z z}}{k_z + Q_m \frac{\mu}{\mu_1} k_1} \tag{2.52}$$

Eqs. (2.51) and (2.52) are dual to (2.48) and (2.49). The stratification factors Q_e for a two layer ground has been calculated by Wait (1953). In Figs. 2.1 and 2.2 the amplitude and the phase Q_m are plotted versas $\sqrt{\omega\mu\sigma_1}\, d_1$ for the two layer case. Q_m is seen to drop to near unity as $\sqrt{\omega\mu\sigma_1}\, d_1$ becomes larger than 1. Thus the effect of the second layer diminishes as $d_1 > (\omega\mu\sigma_1)^{-1/2}$. In Figs. 3-6, the amplitudes and phases of both Q_e and Q_m are depicted. The depth of the first layer is assumed to be $d_1 \simeq 2(\omega\mu\sigma_1)^{-1/2}$. The ratio $(\sigma_2/\sigma_1)^{1/2}$ is set to 0.5, and $(\sigma_3/\sigma_2)^{1/2}$ is used as a parameter. As $d_2 - d_1$ becomes larger than $1.2(\omega\mu\sigma_2)^{-1/2}$, both $|Q_e|$ and $|Q_m|$ drop to within about 6 percent of its final value. Beyond that we can safely omit contributions from the last layer.

7) The integrals as presented in (2.35)-(2.38) can be directly programmed with a computer or analyzed analytically. Asymptotic evaluations of the integrals and numerical results for the electromagnetic field quantities under various circumstances constitute topics of the subsequent papers.

Chapter 3.

DIPOLE ANTENNAS ON A HALF SPACE MEDIUM

3-1 FIELDS IN THE LOWER MEDIUM

For a horizontal electric dipole above a lossy dielectric half space, the electromagnetic field components in the lower medium (i.e. the field components of the transmitted wave) are listed as follows:

$$\bar{E}^{TE} = \int_{-\infty}^{\infty} dk_\rho \left(\frac{I\ell\omega\mu_t}{8\pi}\right) \frac{2}{\mu_t/\mu + k_{tz}^{(m)}/k_z} e^{-ik_{tz}^{(m)}z} \begin{bmatrix} -\frac{1}{k_z\rho} H_1^{(1)}(k_\rho\rho)\cos\phi \\ \frac{k_\rho}{k_z} H_1^{(1)'}(k_\rho\rho)\sin\phi \\ 0 \end{bmatrix} \tag{3.1}$$

$$\bar{E} = \int_{-\infty}^{\infty} dk_\rho \frac{I\ell}{8\pi} \frac{2}{\mu_t/\mu + k_{tz}^{(m)}/k_z} e^{-ik_{tz}^{(m)}z} \sin\phi \begin{bmatrix} \frac{k_{tz}^{(m)}}{k_z} H_1^{(1)'}(k_\rho\rho) \sin \\ \frac{k_{tz}^{(m)}}{k_z\rho} H_1^{(1)}(k_\rho\rho)\cos\phi \\ i\frac{k_\rho^2}{b\,k_z} H_1^{(1)}(k_\rho\rho)\sin\phi \end{bmatrix} \tag{3.2}$$

$$\bar{E}^{TM} = \int_{-\infty}^{\infty} dk_\rho \; \frac{I\ell}{8\pi\omega\epsilon} \; - \frac{2}{\frac{\epsilon_t}{\epsilon} + \frac{k_{tz}^{(e)}}{k_z}} \; e^{-ik_{tz}^{(e)} z} \begin{bmatrix} - k_\rho \, k_{tz}^{(e)} \, H_1^{(1)'}(k_\rho \rho) \cos\phi \\ \frac{k_{tz}^{(e)}}{\rho} \, H_1^{(1)}(k_\rho \rho) \sin\phi \\ - \frac{i}{a} \, k_\rho^2 \, H_1^{(1)}(k_\rho \rho) \cos\phi \end{bmatrix} \tag{3.3}$$

$$\bar{H}^{TM} = \int_{-\infty}^{\infty} dk \; \frac{I\ell\epsilon_t}{8\pi\epsilon} \; - \frac{2}{\frac{\epsilon_t}{\epsilon} + \frac{k_{tz}^{(e)}}{k_z}} \; e^{-ik_{tz}^{(e)} z} \begin{bmatrix} H_1^{(1)}(k_\rho \rho) \sin\phi \\ k_\rho \, H_1^{(1)'}(k_\rho \rho) \cos\phi \\ 0 \end{bmatrix} \tag{3.4}$$

A typical integral to be solved takes the following form

$$I = \int_{-\infty}^{\infty} \frac{k_\rho}{k_{iz}} A(k_\rho) e^{-ik_{iz} z} H_0^{(1)}(k_\rho \rho) \, dk_\rho \quad ; \quad z < 0 \tag{3.5}$$

The first order Hankel function is the negative of the derivative of the zeroth order Hankel function. In the above integral

$$A(k_\rho) = \frac{k_{iz}}{k_z + k_{iz}}$$

Two points are to be noted:

1. The path of integration along the real axis of k_ρ is actually undefined for strictly real k because the branch point $k_\rho = k$ then lies on the path. There are two remedies. One is to assume a vanishingly small imaginary part for k. The other is to choose the Sommerfeld path of integration.
2. Taking remedy into account, we notice that there are two double-valued functions in the integrand viz. k_z and k_{1z}. They must be well-defined along the path of integration. They are defined as follows: Along the path, $Re\ k_{1z} > 0$, $Im\ k_{1z} > 0$;

$$Re\ k_z > 0 \ , \quad Im\ k_z > 0 \ .$$

To facilitate solution of the integral, the conformal transformation $k_\rho = k_1 \sin\beta$ is made , so that the integral becomes

$$I = k_1 \int_C \sin\beta\ A(\beta)\, e^{-ik_{1z}\cos\beta}\, H_0^{(1)}(k_1 \rho \sin\beta)\, d\beta$$

where

$$A(\beta) = \frac{k_1 \cos\beta}{k_1 \cos\beta + k_z}$$

C is the original path in the β plane. If k_1 is strictly real , C first runs from $-\frac{\pi}{2} + i\infty$ to $-\frac{\pi}{2}$ and then along the real β axis

to $\frac{\pi}{2}$ and then from $\frac{\pi}{2}$ to $\frac{\pi}{2} - i\infty$. When k_1 is slightly conductive, C is slightly shifted with its position as shown in figure 3.1.

Now, in this β plane, only $k_z = \sqrt{k^2 - k_1^2 \sin^2\beta}$ is a double-valued function. The branch cut $\text{Im } k_z = 0$ is drawn. On the top sheet, $\text{Im } k_z > 0$, and on the lower sheet $\text{Im } k_z < 0$. The path of integration C lies on the top sheet. The path C is then detoured to a path such that along the new path, the argument of the Hankel function is always big so that the Hankel function can be expanded asymtotically.

$$H_0^{(1)}(k_1 \rho \sin\beta) = e^{i(k_1 \rho \sin\beta - \frac{\pi}{4})} \sqrt{\frac{2}{\pi k_1 \rho \sin\beta}} \left(1 + \frac{1}{8ik_1 \rho \sin\beta}\right)$$

$$I = \sqrt{\frac{2k_1}{\pi\rho}}\, e^{-i\frac{\pi}{4}} \int_C \sin^{\frac{1}{2}}\beta\, A(\beta)\, e^{-ik_1 z\cos\beta + ik_1\rho\sin\beta} \left(1 + \frac{1}{8ik_1\rho\sin\beta}\right) d\beta$$

The exponential arising from the asymtotic expansion of the Hankel function, combines with the exponential in front to give $ik_1 R\cos(\beta - \alpha)$ where $\alpha = \tan^{-1}\frac{\rho}{|z|}$. Therefore, there is a saddle point at $\beta = \alpha$. The branch point due to k_z is at $\theta_0 = \theta_0' + i\theta_0''$. Because k_1 has a small imaginary part, therefore θ_0 is complex. For slightly conductive material, θ_0' is approximately the critical angle. θ_0'' , on the other hand, is very small but negative.

The location of the branch point and branch cut are all marked in figure 3.1.

The problem, that is next faced, is to detour the original path C to the saddle point steepest descent path. There are two different detours for two different regions of interest. For α smaller than θ_0', the detoured path starts at $-\frac{\pi}{2} + i\infty$, goes to $-\frac{\pi}{2} + \alpha + i\infty$, and then goes down the path of steepest descent passing through the saddle point crossing the branch cut twice and crossing the real axis at the saddle point in between, and then goes down to $\frac{\pi}{2} + \alpha - i\infty$ and from then back to the end of the original contour at $\frac{\pi}{2} - i\infty$. On crossing the branch cut once, the contour gets onto the lower sheet. On crossing the branch cut again it crosses back onto the upper sheet. The dotted portion of the path lies on the lower sheet.

The integrand is analytic within the domain of the enclosed contour and along the path, and by Cauchy's integral theorem, the line integral of the original contour is equal to the line integral of the new contour. Notice that although the domain enclosed by the two contours lies on different sheets, the function is still analytic along the contour and in the domain. On jumping to the lower sheet, the function retains its continuity. On the other hand, if it jumps acoss the branch cut and stays on the same sheet, the function is discontinuous at the jump. Also, in this case, since

the new contour crosses the branch cut twice, going down and coming up again to the upper sheet, it can meet the other end of the original contour and forms a closed loop.

Therefore, for α less than θ_0' ,

$$I = \frac{2}{i} \frac{e^{ik_1 R}}{R} \left[A(\alpha) + \frac{1}{2ik_1 R} \left(A''(\alpha) + \cot \alpha \, A'(\alpha) \right) \right]$$

where

$$A(\alpha) = \frac{k_1 \cos \alpha}{k_1 \cos \alpha + \sqrt{k^2 - k_1^2 \sin^2 \alpha}}$$

In the above expression, the double-valued function $k_z = \sqrt{k^2 - k_1^2 \sin^2 \alpha}$ assumes a positive real part and a negative imaginary part. This is because the saddle point, as can be clearly seen from figure 2a, lies on the dotted portion of the curve and thus lies on the lower sheet. And , on the lower sheet, $\operatorname{Im} k_z < 0$.

Physically, the saddle point corresponds to the angle of observation in the lower medium.

For α bigger than θ_0' , i.e. the observation angle greater than the critical angle, the branch point contribution has to be included and the original path C is detoured in the following way. (Figure 3.1b). It starts at $-\frac{\pi}{2} + i\infty$ and goes to $0 + i\infty$, goes down the left side of the branch cut

on the upper Rieman sheet, goes around the branch point, back to $0 + i\infty$ on the right side of the branch cut on the upper sheet. It then crosses the branch cut onto the lower Rieman surface, goes to $-\frac{\pi}{2} + \alpha + i\infty$ and from there, follows the steepest descent path, crosses the branch cut again back to the upper Rieman surface, crosses the real axis at saddle point α, goes to $\frac{\pi}{2} + \alpha - i\infty$ and finally connects back to the end of the original contour at $\frac{\pi}{2} - i\infty$. Therefore, summing up, there are two contributions to I : the saddle point path contribution I_1, and the branch cut contribution I_2. The saddle point lies on the upper sheet. Therefore

$$I_1 = \frac{2}{i} \frac{e^{ik_1 R}}{R} \left[A(\alpha) + \frac{1}{2ik_1 R} \left(A''(\alpha) + \cot\alpha \, A'(\alpha) \right) \right]$$

where,

$$A(\alpha) = \frac{k_1 \cos\alpha}{k_1 \cos\alpha + \sqrt{k^2 - k_1^2 \sin^2\alpha}}$$

and k_z assumes a positive imaginary part and a corresponding negative imaginary part in the above expression since on the upper sheet, $\mathrm{Im}\, k_z > 0$.

At this point, it is convenient to adopt the following convention. We denote $\sqrt{k^2 - k_1^2 \sin^2\alpha}$ (the square root sign) as always having a positive real part. Therefore, going back to our analysis, k_z can be either $+\sqrt{k^2 - k_1^2 \sin^2\alpha}$, or $-\sqrt{k^2 - k_1^2 \sin^2\alpha}$ depending on the sheet the path is lying on. With this convention, the solution

is rewritten as follows:

for α less than θ_0' ,

$$I = \frac{2}{i}\frac{e^{ik_1R}}{R}\left[A(\alpha) + \frac{1}{2ik_1R}\left(A''(\alpha) + \cot\alpha\, A'(\alpha)\right)\right]$$

where,

$$A(\alpha) = \frac{k_1\cos\alpha}{k_1\cos\alpha + \sqrt{k^2 - k_1^2\sin^2\alpha}}$$

for α greater than θ_0' ,

$$I_1 = \frac{2}{i}\frac{e^{ik_1R}}{R}\left[A(\alpha) + \frac{1}{2ik_1R}\left(A''(\alpha) + \cot\alpha\, A'(\alpha)\right)\right]$$

where,

$$A(\alpha) = \frac{k_1\cos\alpha}{k_1\cos\alpha - \sqrt{k^2 - k_1^2\sin^2\alpha}}$$

To evaluate the branch cut contribution I_2, much care has to be exercised. The branch cut is defined by $\mathrm{Im}\, k_z = 0$. On the left side of the branch cut $\mathrm{Re}\, k_z > 0$, while on the right side of the branch cut $\mathrm{Re}\, k_z < 0$. Denoting the positive side by B_+ and the negative side by B_-,

$$I_2 = \sqrt{\frac{2k_1}{\pi\rho}}\, e^{-i\frac{\pi}{4}} \int_{\substack{\text{down } B_+ \\ \text{up } B_-}} \sin^{\frac{1}{2}}\beta\, A(\beta)\, e^{ik_1R\cos(\beta-\alpha)}\, d\beta$$

$$= \sqrt{\frac{2k_1}{\pi\rho}}\, e^{-i\frac{\pi}{4}}\left[\int_{\text{up } B_+} -\sin^{\frac{1}{2}}\beta\, A(\beta)\, e^{ik_1R\cos(\beta-\alpha)}\, d\beta\right.$$

$$\left. + \int_{\text{up } B_-} \sin^{\frac{1}{2}}\beta\, A(\beta)\, e^{ik_1R\cos(\beta-\alpha)}\, d\beta\right]$$

(Up means from branch point to ∞ .)

The above integral can be combined in two forms, either by changging B_- into B_+ so that both integrals are written as B_+ , or alternatively, by converting B_+ into B_- to have both integrals in terms of B_- . Thus, there are two forms of I_2 :

$$I_2 = \sqrt{\frac{2k_1}{\pi\rho}}\, e^{-i\frac{\pi}{4}} \int_{up\ B_+} \sin^{\frac{1}{2}}\beta\ \frac{2k_{1z}k_z}{k_{1z}^2 - k_z^2}\, e^{ik_1 R\cos(\beta-\alpha)}\, d\beta$$

or

$$I_2 = \sqrt{\frac{2k_1}{\pi\rho}}\, e^{-i\frac{\pi}{4}} \int_{up\ B_-} \sin^{\frac{1}{2}}\beta\ \frac{-2k_{1z}k_z}{k_{1z}^2 - k_z^2}\, e^{ik_1 R\cos(\beta-\alpha)}\, d\beta$$

Both give the same answer.

The next step is to detour the path, either B_+ or B_- , to the steepest descent path passing through the branch point. (Note: one must distinguish between the steepest descent path passing through the branch point and the steepest descent path passing through the saddle point.) The position of the steepest descent path BS through the branch point is clearly depicted in figure 2b. It lies to the left of the branch cut. Therefore B_- can be detoured to BS by simple application of Cauchy's theorem. Therefore

$$I_2 = \sqrt{\frac{2k_1}{\pi\rho}}\, e^{-i\frac{\pi}{4}} \int_{BS} \sin^{\frac{1}{2}}\beta\ k_1\cos\beta\, e^{ik_1 R\cos(\beta-\alpha)}\, \frac{-2k_z}{k_1^2\cos^2\beta - k^2 + k_1^2\sin^2\beta}\, d\beta$$

On the other hand, if B_+ is to be detoured to BS , one needs to cross onto the lower sheet and subsequent calculation

needs to be performed on the lower sheet. This is unadvisable. If , it is quite plausible, one is not careful enough to follow the above step by step, one can easily just detour B_+ to BS and arrive at

$$I_2 = \sqrt{\frac{2k_1}{\pi\rho}}\, e^{-i\frac{\pi}{4}} \int_{BS} \sin^{\frac{1}{2}}\beta\, k_1 \cos\beta\, e^{ik_1 R\cos(\beta-\alpha)} \frac{2k_z}{k_1^2\cos^2\beta - k^2 + k_1^2\sin^2\beta}\, d\beta$$

This is the negative of the correct answer and is wrong.

The contribution of BS mainly comes from around the branch point. By applying the method of steepest descent to the above integral, one obtains (Appendix I)

$$I_2 = \frac{2}{\rho^2}\frac{k}{a^2}\frac{e^{-ia z + ik\rho}}{(1-\cot\alpha\tan\theta_0)^{3/2}} \quad ; \quad a = \sqrt{k_1^2 - k^2}$$

Finally, in summary,

for α less than θ_0' ,

$$I = \frac{2}{i}\frac{e^{ik_1 R}}{R}\left[A(\alpha) + \frac{1}{2ik_1 R}\left(A''(\alpha) + \cot\alpha\, A'(\alpha)\right)\right]$$

where

$$A(\alpha) = \frac{k_1\cos\alpha}{k_1\cos\alpha + \sqrt{k^2 - k_1^2\sin^2\alpha}} \quad ; \quad \mathrm{Im}\ k_z < 0$$

for α greater θ_0' ,

$$I = \frac{2}{i}\,\frac{e^{ik_1R}}{R}\left[A(\alpha) + \frac{1}{2ik_1R}\left(A''(\alpha) + \cot\alpha\, A'(\alpha)\right)\right]$$

$$+ \frac{2}{\rho^2}\,\frac{k}{a^2}\,\frac{e^{-ia z + ik\rho}}{(1-\cot\alpha\tan\theta_0)^{3/2}} \qquad ; \qquad \mathrm{Im}\ k_z > 0$$

where,

$$A(\alpha) = \frac{k_1\cos\alpha}{k_1\cos\alpha - \sqrt{k^2 - k_1^2\sin^2\alpha}}$$

Several physical observations can be made. For α greater than θ_0' , there are two waves, represented respectively by the first and term in I. The first term corresponds to the spherical direct wave, and the second term corresponds to the flank wave. From the equation, one also notices that if k_1 is strictly real, both terms blow up at $\alpha = \theta_0$. Mathematically, this is to be expected because the saddle point collides with the branch point. Actually when the saddle point approaches the branch point and gets near to it (this also applies to the case of complex k_1 where α is never exactly equal to θ_0 .) , the saddle point method breaks down. The area $\alpha \doteq \theta_0$, is the area in which the two waves interact and they have to be considered together and not separately. A detailed discussion is given in the book by Brekhovskih[3] .

by most authors. The advantage of using this branch cut is that it can be detoured to the steepest descent path passing through the branch point. In the following, it is shown that the same answer will be arrived at even if a different branch cut is chosen. The different branch cut is $\mathrm{Re}\ k_z = 0$. Solution with a different branch cut yields the same answer means that the choice of different signs for k_z in the two regions $\alpha < \theta_o'$ and $\alpha > \theta_o'$ is absolute and is not arbitrary.

With the branch cut $\mathrm{Re}\ k_z = 0$, and after the $k_\rho = k_1 \sin\beta$ transformation is made, the same integral is obtained but with the picture in the complex plane changed as in figure 3.2. BS is the steepest descent path passing through the branch point. On the top sheet $\mathrm{Re}\ k_z > 0$, and on the lower sheet $\mathrm{Re}\ k_z < 0$. On the top sheet, where the original path lies, there is the positive side of the branch cut B_+ where $\mathrm{Im}\ k_z > 0$, and the negative side of the branch cut B_- where $\mathrm{Im}\ k_z < 0$. The most important observation is that, in this case, the branch cut , no matter whether the B_+ side or the B_- side, cannot be detoured to the steepest descent path BS through the branch point.

Analysing the integral as the case with the branch cut $\mathrm{Im}\ k_z = 0$, for $\alpha < \theta_o'$, the saddle point lies on the upper sheet and $\mathrm{Re}\ k_z > 0$.

$$I = \frac{2}{i} \frac{e^{ik_1 R}}{R} \left[A(\alpha) + \frac{1}{2ik_1 R} \left(A''(\alpha) + \cot\alpha\, A'(\alpha) \right) \right]$$

Notice that the saddle point contribution in this case is different from the corresponding I_1 in the case $\text{Im } k_z = 0$ because in that case $\text{Im } k_z > 0$ and in this case $\text{Re } k_z > 0$.

Analysing I_2 the branch cut contribution,

$$I_2 = \sqrt{\frac{2k_1}{\pi\rho}}\, e^{-i\frac{\pi}{4}} \int_{\substack{\text{down } B_- \\ \text{up } B_+}} \sin^{\frac{1}{2}}\beta\, A(\beta)\, e^{ik_1 R\cos(\beta-\alpha)} \left(1 + \frac{1}{8ik_1\rho\sin\beta}\right) d\beta$$

$$= \sqrt{\frac{2k_1}{\pi\rho}}\, e^{-i\frac{\pi}{4}} \int_{\text{up } B_-} \sin^{\frac{1}{2}}\beta\, k_1\cos\beta\, e^{ik_1 R\cos(\beta-\alpha)} \left(1 + \frac{1}{8ik_1\rho\sin\beta}\right) \frac{2k_z}{k_1^2\cos^2\beta - k^2 + k_1^2\sin^2\beta}\, d\beta$$

$$= \sqrt{\frac{2k_1}{\pi\rho}}\, e^{-i\frac{\pi}{4}} \int_{\text{up } B_-} \sin^{\frac{1}{2}}\beta\, e^{ik_1 R\cos(\beta-\alpha)} \left(1 + \frac{1}{8ik_1\rho\sin\beta}\right) D(\beta)\, d\beta$$

(Again, up means from branch point to ∞ .)

where,

$$D(\beta) = \frac{2\, k_z\, k_1\cos\beta}{k_1^2\cos^2\beta - k^2 + k_1^2\sin^2\beta} \quad ; \quad \text{Re } k_z > 0$$

where,

$$A(\alpha) = \frac{k_1 \cos\alpha}{k_1 \cos\alpha + \sqrt{k^2 - k_1^2 \sin^2\alpha}} \quad ; \quad Re\ k_z > 0$$

Therefore, the answer checks with the case with branch cut $\text{Im}\ k_z = 0$.

In the case $\alpha > \theta_0'$, there are , as in the case with branch cut $\text{Im}\ k_z = 0$, two contributions ; one due to the steepest descent path passing through the saddle point and the other due to the branch cut. The branch cut contribution, however, as opposed to the case of branch cut $\text{Im}\ k_z = o$, is of first order effect.

Set

$$I = I_1 + I_2$$

where I_1 = contribution due to steepest descent path through saddle point.

I_2 = branch cut contribution

then,

$$I_I = \frac{2}{i} \frac{e^{ik_1 R}}{R} \left[A(\alpha) + \frac{1}{2ik_1 R} \left(A''(\alpha) + \cot\alpha\, A'(\alpha) \right) \right]$$

where,

$$A(\alpha) = \frac{k_1 \cos\alpha}{k_1 \cos\alpha + \sqrt{k^2 - k_1^2 \sin^2\alpha}} \quad ; \quad Re\ k_z > 0.$$

The path B_- cannot be detoured to BS. To evaluate the contour integral along B_-, the path B_- is detoured to a path consisting of two parts: the first part L_1 extending from the branch point to the saddle point, and the second part L_2 extending from the saddle point to down the steepest descent path. By Cauchy's theorem

$$\int_{L_1} = \int_{BS} + \int_{\Gamma'}$$

Therefore,

$$I_2 = \int_{L_1} + \int_{L_2} = \int_{BS} + \int_{\Gamma'} + \int_{L_2}$$

$$= \int_{BS} + \int_{\Gamma}$$

$$= \frac{2}{\pi} \frac{e^{ik_1 R}}{R} \left[D(\alpha) + \frac{1}{2ik_1 R} \left(D''(\alpha) + \cot\alpha \, D'(\alpha) \right) \right]$$

$$+ \frac{2}{\rho^2} \frac{k}{a^2} \frac{e^{-ia z + ik\rho}}{(1 - \cot\alpha \tan\theta_0)^{3/2}}$$

where

$$D(\alpha) = \frac{2\sqrt{k^2 - k_1^2 \sin^2\alpha} \; k_1 \cos\alpha}{k_1^2 \cos^2\alpha - k^2 + k_1^2 \sin^2\alpha}$$

Combining these expressions, one has

$$I = I_1 + I_2$$

$$= \frac{2}{i}\frac{e^{ik_1R}}{R}\left[G(\alpha) + \frac{1}{2ik_1R}\left(G''(\alpha) + G'(\alpha)\cot\alpha\right)\right]$$

$$+ \frac{2}{\rho^2}\frac{k}{a^2}\frac{e^{-iaz+ik\rho}}{(1-\cot\alpha\tan\theta_0)^{3/2}}$$

where $G(\alpha) = A(\alpha) + D(\alpha)$

$= A(\alpha)$ of the case of branch cut $\operatorname{Im} k_z = 0$.

Therefore, in summary, the answers are identical whether the branch cut $\operatorname{Re} k_z = 0$ or $\operatorname{Im} k_z = 0$ is chosen.

For TM waves of nonmagnetic material, on the top sheet, there is a Sommerfeld pole at $\sin\theta_{p1} = \frac{k}{\sqrt{k^2+k_1^2}}$ in the denominator. Its effect can be neglected by the following reasoning. When $\alpha < \theta_0'$, α lies on the lower sheet (branch cut $\operatorname{Im} k_z = 0$ is chosen.), while θ_{p1} lies on the upper sheet. Thus the pole is not enclosed between the original contour and the detoured contour. The pole does not contribute anything. When $\alpha > \theta_0'$, the analysis is slightly more complicated. When the original path C is detoured to the saddle point path Γ , two contributions need to be considered : one due to the branch

cut B, the other due to the residue of the pole P_1 because in this case, the pole does lie between the original contour and the detoured contour. But, in evaluating B, it is detoured to the steepest descent path BS, and on this detour, P_1 is again enclosed, and this time, its contribution is exactly the negative of the residue and thus cancels out exactly the previous contribution. Summing up, P_1 does not contribute both for $\alpha < \theta_o'$ and $\alpha > \theta_o'$. The only contributions come from the saddle point and the branch, both of which have been discussed already.

3.2 RADIATION PATTERNS

In this section, we analyse the radiation pattern of the horizontal dipole for the half space case. The radiation pattern gives information of the angular distribution of the radiated energy. This information is of crucial importance if the interference patterns for the two layer case are to be explained in terms of ray optics.

The radiation fields are of $1/r$ dependence. The $1/r$ term, in this case, corresponds to the first order term in the saddle point contribution.

For the half space case, with the dipole on the surface, the reflection coefficients are

$$R^{TE} = \frac{\mu_1 k_z - \mu k_{1z}}{\mu_1 k_z + \mu k_{1z}} \quad ; \quad R^{TM} = \frac{\epsilon_1 k_z - \epsilon k_{1z}}{\epsilon_1 k_z + \epsilon k_{1z}}$$

The electromagnetic fields , to first order are the following.

For the upper medium:

$$H_z^{TE} = -\frac{Il}{4\pi}\frac{e^{ikr}}{r} ik \sin\theta X_{01}(\theta) \sin\phi$$

$$E_\phi^{TE} = \frac{Il\omega\mu_0}{4\pi i}\frac{e^{ikr}}{r} X_{01}(\theta) \sin\phi$$

$$H_\rho^{TE} = -\frac{Il}{4\pi i}\frac{e^{ikr}}{r} k\cos\theta X_{01}(\theta) \sin\phi$$

$$E_\rho^{TM} = -\frac{Il}{4\pi i\omega\varepsilon}\frac{e^{ikr}}{r} k^2\cos^2\theta Y_{10}(\theta) \cos\phi$$

$$E_z^{TM} = -\frac{Il}{4\pi\omega\varepsilon}\frac{e^{ikr}}{r} ik^2 \sin\theta\cos\theta Y_{10}(\theta) \cos\phi$$

$$H_\phi^{TM} = -\frac{Il}{4\pi i}\frac{e^{ikr}}{r} k\cos\theta Y_{10}(\theta) \cos\phi$$

For the lower medium :

$$H_z^{TE} = -\frac{Il}{4\pi}\frac{e^{ik_1r}}{r} ik_1 \sin\alpha X_{10}(\alpha) \sin\phi$$

$$E_\phi^{TE} = \frac{Il\omega\mu_1}{4\pi i}\frac{e^{ik_1r}}{r} X_{10}(\alpha) \sin\phi$$

$$H_\rho^{TE} = \frac{Il}{4\pi i}\frac{e^{ik_1r}}{r} k_1\cos\alpha X_{10}(\alpha) \sin\phi$$

$$E_\rho^{TM} = -\frac{Il}{4\pi i\omega\varepsilon_1}\frac{e^{ik_1r}}{r} k_1^2\cos^2\alpha Y_{01}(\alpha) \cos\phi$$

$$E_z^{TM} = \frac{Il}{4\pi\omega\varepsilon_1}\frac{e^{ik_1r}}{r} ik_1^2 \sin\alpha\cos\alpha Y_{01}(\alpha) \cos\phi$$

$$H_\phi^{TM} = \frac{I\ell}{4\pi i}\frac{e^{ik_1 r}}{r} k_1 \cos\alpha \; Y_{01}(\alpha)\cos\phi$$

where,

$$R_{ij} = \frac{\mu_j k_{iz} - \mu_i k_{jz}}{\mu_j k_{iz} + \mu_i k_{jz}}$$

$$S_{ij} = \frac{\varepsilon_j k_{iz} - \varepsilon_i k_{jz}}{\varepsilon_j k_{iz} + \varepsilon_i k_{jz}}$$

$$X_{ij} = 1 + R_{ij} = \frac{2\mu_j k_{iz}}{\mu_j k_{iz} + \mu_i k_{jz}}$$

$$Y_{ij} = 1 + S_{ij} = \frac{2\varepsilon_j k_{iz}}{\varepsilon_j k_{iz} + \varepsilon_i k_{jz}}$$

θ is the observation angle in the upper medium and α is the observation angle in the lower medium.

The Poynting vector is $\bar{S} = Re\left(\frac{1}{2}(\bar{E}\times\bar{H}^*)\right)$

Denoting the radial component of the Poynting vector by S_r, we obtain, for the upper medium

$$S_r = \frac{1}{2}\left(\frac{I\ell}{4\pi}\right)^2\left[\frac{\omega\mu}{r^2} k X_{01}^2(\theta)\sin^2\phi + \frac{\omega\mu}{r^2} k \cos^2\theta \; Y_{10}^2(\theta)\cos^2\phi\right]$$

for the lower medium,

$$S_r = \frac{1}{2}\left(\frac{I\ell}{4\pi}\right)^2\left[\frac{\omega\mu_1}{r^2} k_1 \left|X_{10}(\alpha)\right|^2 \sin^2\phi + \frac{\omega\mu_1}{r^2} k_1 \cos^2\alpha \left|Y_{01}(\alpha)\right|^2 \cos^2\phi\right]$$

The maximum power radiated into the lower medium is at the critical angle for broadside ($\phi = 90°$) and at the angle $\sin^{-1}\sqrt{\frac{2n^2}{(1+n^2)}}$ for endfire ($\phi = 0°$). These values can be obtained by setting the derivative of S_r with respect to the observation angle equal to zero. Another interesting observation is that for the endfire radiation pattern, S_r is precisely null at the critical angle. A quick way to explain this is that the free space radiation power is zero along the endfire surface, so that there is no " incident field " into the dielectric at $\theta = 90°$ when the dipole antenna is put on top of the dielectric medium. Another observation is that along the surface, fields are of second order effect, and thus the radiation power is zero along the surface. If k_1 contains an imaginary part (for conductive medium), however small, the radiation is null in the lower half plane, because, by definition, the radiation pattern is measured at infinity. The $\mathrm{Im}\, k_1$ gives rise to an exponential attenuation with distance and the power vanishes at infinity.

3.3 FIELDS IN THE UPPER SPACE

In actual experiment, the receiver is placed above ground, so that, we are actually interested in the region $z > 0$ for the half space problem. The transmitted wave for $z < 0$ is interested not in the

half space problem, but, as has been mentioned, its solution sheds light on the two layer problem which will be discussed in the next section.

For $z > 0$, a typical integral to be solved is

$$I = \int_{-\infty}^{\infty} \frac{k_\rho}{k_z} \frac{k_z}{k_z + k_{1z}} H_0^{(1)}(k_\rho \rho) e^{ik_z z} \, dk_\rho$$

Notice that this integral is different from the transmitted wave integral in that k_{1z} is replaced by k_z. Let

$$B(k_\rho) = \frac{k_z}{k_z + k_{1z}}$$

In this case, the conformal transformation is

$$k_\rho = k \sin\beta$$

The saddle point is at θ, where θ is the observation angle in the upper medium, $\theta = \tan^{-1}\frac{\rho}{z}$.
The branch point is at $\theta_1 = \sin^{-1}\frac{k_1}{k} = \theta_1' - i\theta_1''$
The branch cut chosen is $\operatorname{Im} k_{1z} = 0$. The equation of the steepest descent path Γ passing through the saddle point is $\operatorname{Re} kR\cos(\beta - \theta) = kR$. Let's take k_1 to be strictly real for the time being, so that $\theta_1' = \frac{\pi}{2}$, $\cosh\theta_1'' = \frac{k_1}{k}$. The steepest descent path passes through the branch point when

$$\operatorname{Re} kR\cos(\theta_1 - \theta) = kR$$

$$\cos(\theta_1' - \theta)\cosh\theta_1'' = 1$$

$$\therefore \sin\theta = \frac{k}{k_1}$$

and this turns out to be θ_o , quite a coincidence. Therefore, for $\theta < \theta_o$, only saddle point contribution is needed, while for $\theta > \theta_o$, branch cut contribution needs to be included too. The branch cut contribution is to be carefully manipulated by the B_+ and B_- approach, and also by using the method of steepest descent. For the Tm wave, the Sommerfeld pole does not contribute by similar reasoning.

In summary, extending also to slightly conductive k_1 too,

for $\theta < \theta_o$,

$$I = \frac{2}{i} \frac{e^{ikR}}{R} \left[B(\theta) + \frac{1}{2ikR} \left(B'(\theta) \cot \theta + B''(\theta) \right) \right]$$

for $\theta > \theta_o$

$$I = \frac{2}{i} \frac{e^{ikR}}{R} \left[B(\theta) + \frac{1}{2ikR} \left(B'(\theta) \cot \theta + B''(\theta) \right) \right]$$

$$- \frac{2k_1}{\rho^2 a^2} \frac{e^{-az + ik_1 \rho}}{(1 + i \sec \theta_o \cot \theta)^{3/2}}$$

The double-valued function k_{1z} has its imaginary part bigger than 0 on the upper sheet. Since for both regions of interest $\theta < \theta_o$ and $\theta > \theta_o$ the saddle point occurs on the upper sheet, therefore Im $k_{1z} > 0$

in the above expressions.

As can be seen from the expressions, for $\theta > \theta_0$, there are two waves , the first term representing the direct wave , and the second term the inhomegeneous wave. The inhomegeneous wave decays exponentially away from the surface. Its magnitude is greatest on the surface where it interferes most significantly with the direct wave. To do detection of electromagnetic properties, we know that for two waves with different wave vectors k and k_1 , the peaks and troughs are separated by a distance of

$$\Delta = \frac{2\pi}{k_1 - k}$$

On the other hand, if we know Δ , then k_1 can be determined.

On the surface,

$$I = \frac{2}{\rho^2}\frac{k}{a^2} e^{ik\rho} - \frac{2k_1}{\rho^2 a^2} e^{ik_1\rho}$$

Actually, the exact answer can be obtained by the following steps of algebra due to Van Der Pol. Use is made of the following identity :

$$\frac{e^{ikR}}{R} = \frac{i}{2}\int_{-\infty}^{\infty} \frac{k_\rho}{k_z} e^{ik_z z} H_0^{(1)}(k_\rho \rho)\, dk_\rho$$

The integral is

$$I = \int_{-\infty}^{\infty} \frac{k_\rho}{k_z + k_{1z}} H_0^{(1)}(k_\rho \rho)\, dk_\rho$$

$$= \frac{1}{k^2 - k_1^2} \int_{-\infty}^{\infty} (k_\rho k_z - k_\rho k_{1z}) H_0^{(1)}(k_\rho \rho)\, dk_\rho$$

$$\int_{-\infty}^{\infty} k_\rho k_z H_0^{(1)}(k_\rho \rho)\, dk_\rho = \left[-\frac{\partial^2}{\partial z^2} \frac{2}{i} \frac{e^{ikR}}{R} \right]_{z=0}$$

$$\int_{-\infty}^{\infty} k_\rho k_{1z} H_0^{(1)}(k_\rho \rho)\, dk_\rho = \left[-\frac{\partial^2}{\partial z^2} \frac{2}{i} \frac{e^{ik_1 R}}{R} \right]_{z=0}$$

$$\therefore \quad I = \frac{1}{a^2} \left[\frac{2}{i} \frac{e^{ik\rho}}{\rho^2} (ik - \frac{1}{\rho}) - \frac{2}{i} \frac{e^{ik_1 \rho}}{\rho^2} (ik_1 - \frac{1}{\rho}) \right]$$

The various interference and radiation patterns due to different half-space medium compositions are presented in Appendix A.

FIGURE CAPTIONS

3.1 a. The complex β plane for the transmitted wave with the observation angle smaller than the critical angle.

b. The complex β plane for the transmitted wave with the observation angle greater than the critical angle.

3.2 The complex β plane for the transmitted wave with a different branch cut, Re $k_z = 0$, L_1 is the contour joining the branch point to the saddle point. L_2 is that part of the saddle point steepest descent path extending from the saddle point to $-i\infty$. Γ' is that part of the saddle point steepest descent path extending from $+i\infty$ to the saddle point.

3.3 The complex β plane: waves in the upper medium in the half space case. The transformation is $k_\rho = k \sin \beta$. The branch cut is Im $k_{1z} = 0$.

Figure 3.1a

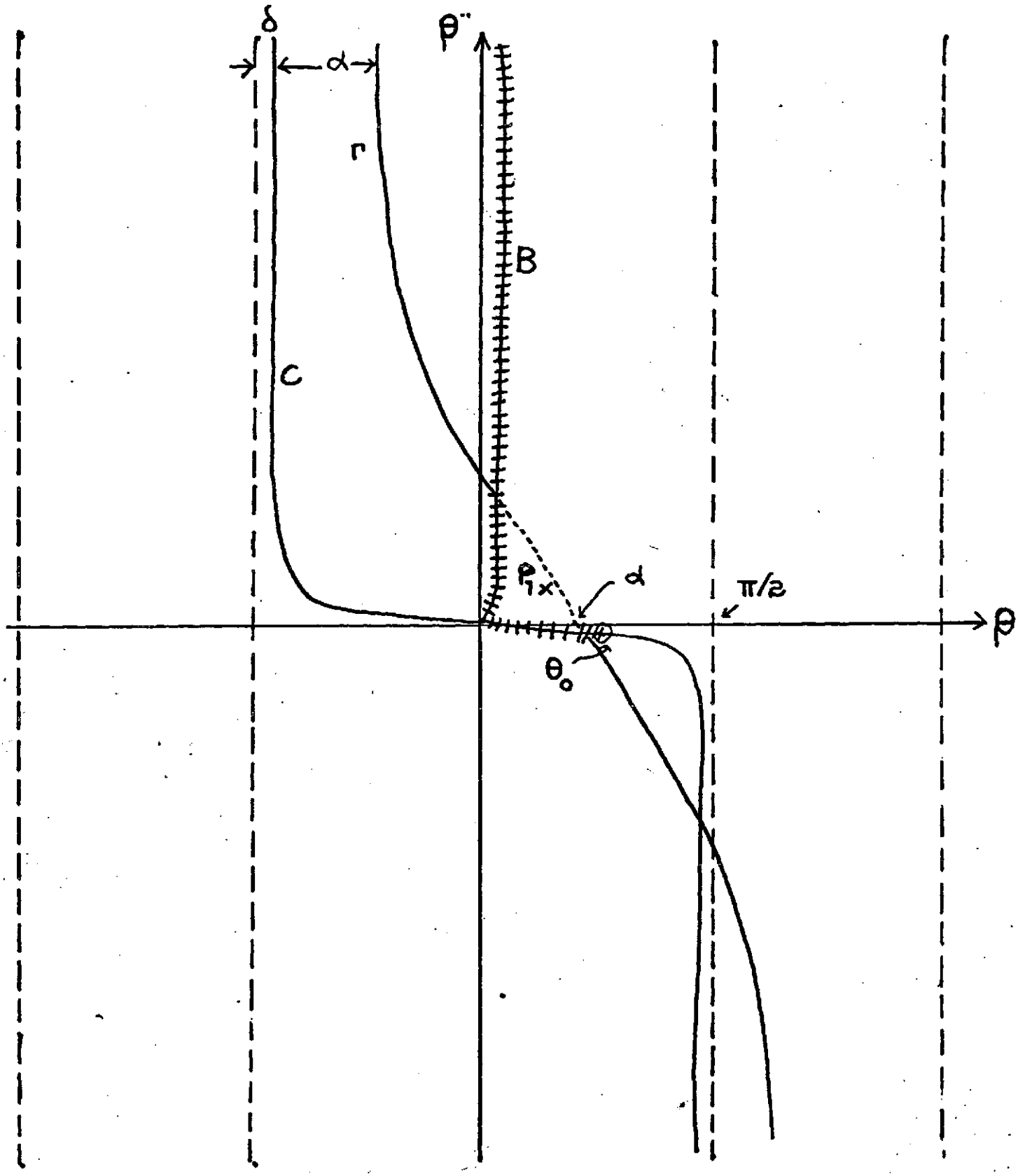

Figure 3.1b

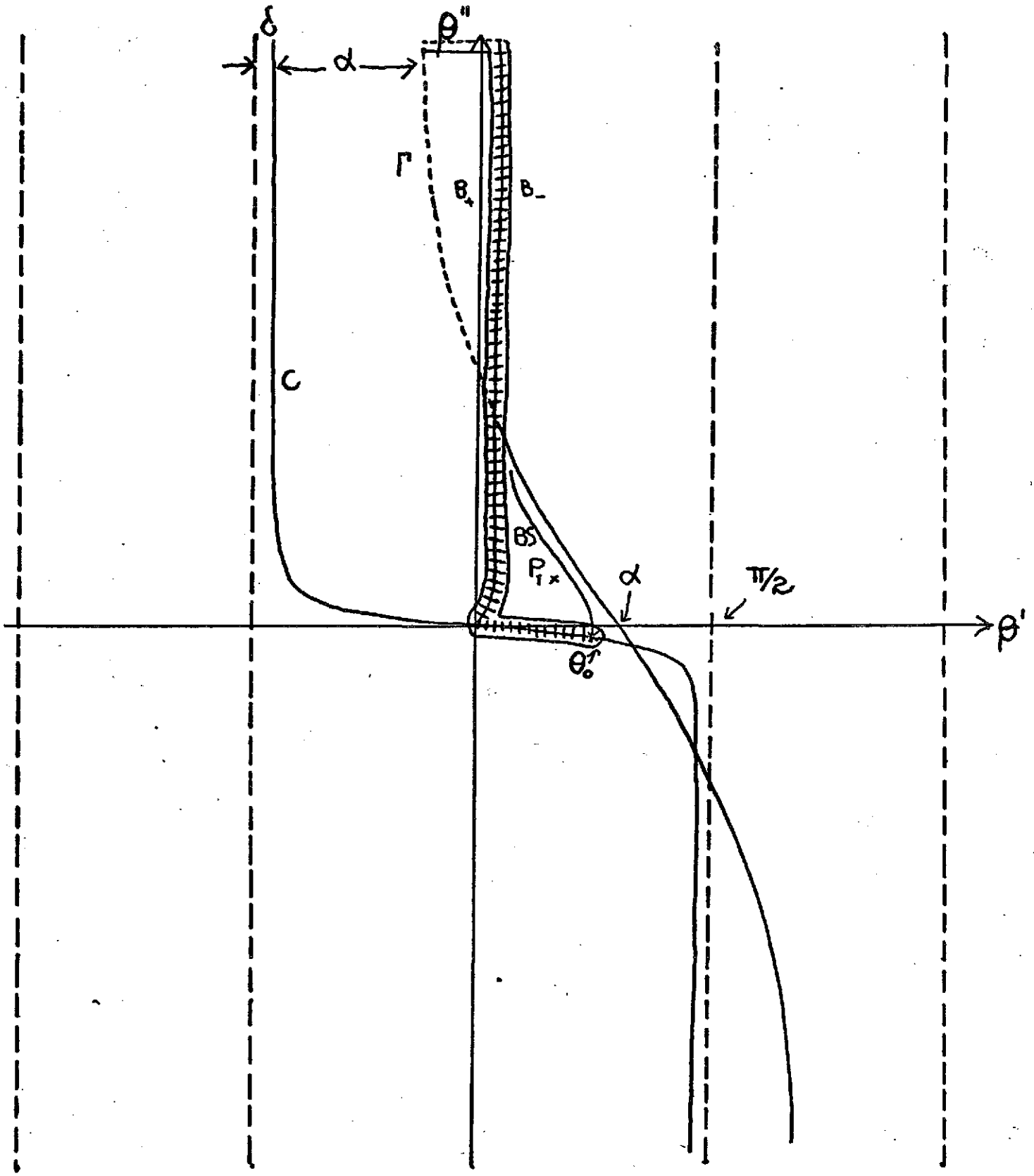

Figure 3.2

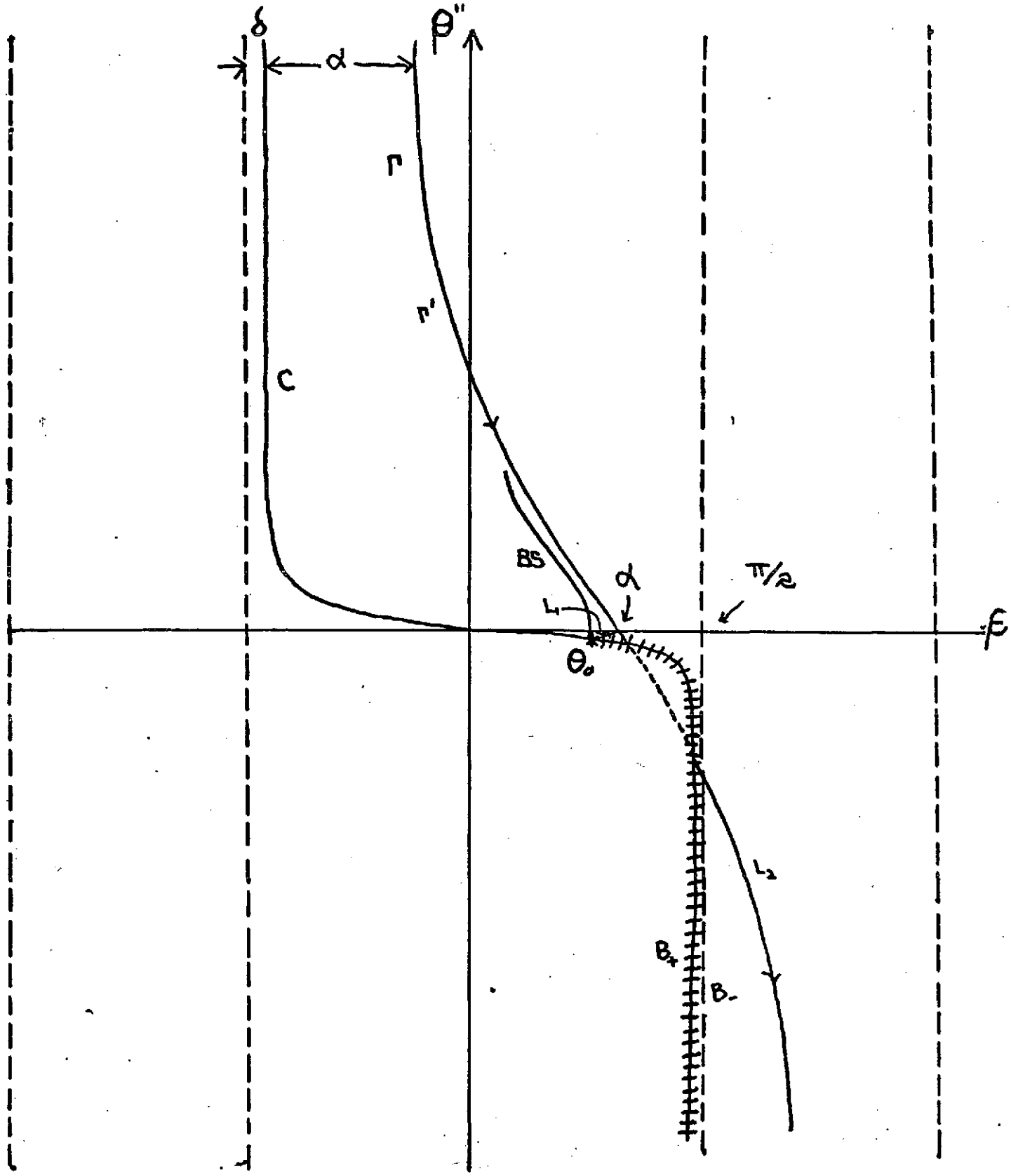

Figure 3.3

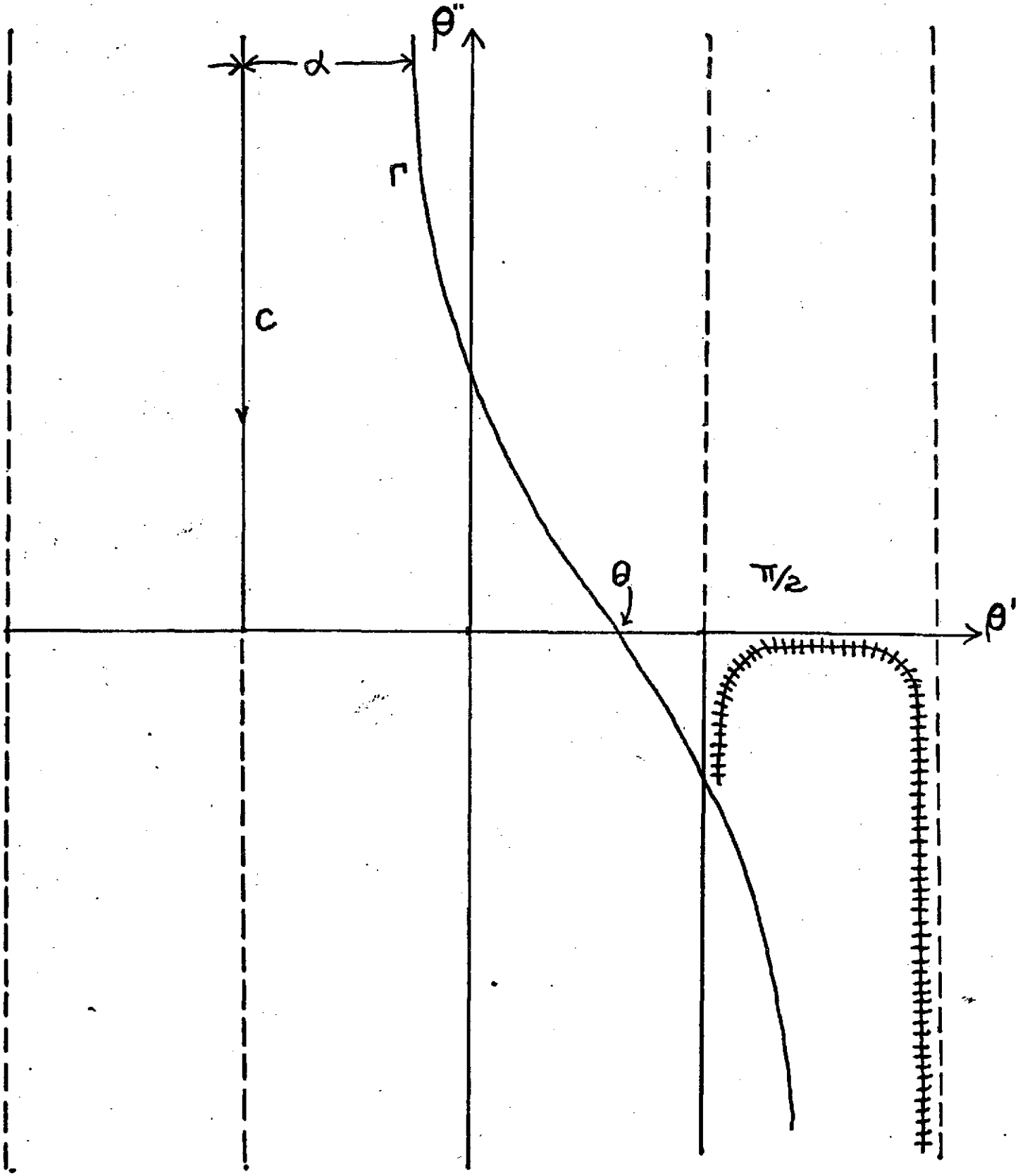

Chapter 4.

GEOMETRICAL OPTICS APPROACH

4.1 TWO LAYER MEDIA

We first consider solutions to the reflection coefficients for a two layer medium:

$$R^{TE} = \frac{1}{R_{01}}\left[1 - \frac{1/R_{01} - R_{01}}{1/R_{01} + R_{12}\exp(i2k_{1z}d)}\right]$$

and

$$R^{TM} = \frac{1}{S_{01}}\left[1 - \frac{1/S_{01} - S_{01}}{1/S_{01} + S_{12}\exp(i2k_{1z}d)}\right]$$

$$1 + R^{TE} = \frac{1 + R_{12}\exp(i2k_{1z}d)}{1 + R_{01}R_{12}\exp(i2k_{1z}d)}\,X_{01}$$

$$1 - R^{TM} = \frac{1 - S_{12}\exp(i2k_{1z}d)}{1 + S_{01}S_{12}\exp(i2k_{1z}d)}\,Y_{10}$$

In the geometrical optics approximation, the interference pattern is determined by three waves:

1. the direct wave from the antenna
2. the inhomogeneous wave excited by the antenna on the surface, and
3. the wave reflected in the subsurface following ray optics paths (Figure 4.1).

The denominators in $1 + R^{TE}$ and $1 + R^{TM}$ are expanded in power series :

$$1 + R^{TE} = X_{01}\left[1 + \sum_{m=1}^{\infty} X_{10} R_{10}^{m-1} R_{12}^{m} \exp(i2k_{1z} md)\right]$$

$$1 - R^{TM} = Y_{10}\left[1 - \sum_{m=1}^{\infty} Y_{01} S_{10}^{m-1} S_{12}^{m} \exp(i2k_{1z} md)\right]$$

The first term in the power series gives rise to the half space solution which consists of the first two kind of waves, both of which have been dealt with in the section on half space. Mathematically, the direct wave corresponds to the saddle point contribution, and the inhomogeneous wave correponds to the branch point contribution due to k_{1z}. The summation term gives rise to all reflections from the subsurface. At each observation point, the number of reflections from the bottom layer can be determined by exercising ray optics. Each optical path can be traced back to an image source.

The integral for the "reflected terms of images" is of the following form

$$I_g = \sum_{m=1}^{\infty} \int_{-\infty}^{\infty} dk_\rho\, D(k_\rho)\, e^{ik_z z} H_0^{(1)}(k_\rho \rho)\, X_{01} X_{10} e^{2ik_{1z} md} R_{10}^{m-1} R_{12}^{m}$$

By rearranging terms in the integral

$$I_g = \sum_{m=1}^{\infty} \int_{-\infty}^{\infty} dk_\rho \frac{k_\rho}{k_{1z}} \left\{\frac{k_{1z}}{k_\rho} D(k_\rho) X_{01} X_{10} R_{10}^{m-1} R_{12}^{m} e^{ik_z z}\right\} e^{2ik_{1z} md} H_0^{(1)}(k_\rho \rho)$$

If z is small, the important observation is that each of the integrals in the summation is of the form of the half space transmitted wave, (that is why the half space transmitted wave is solved first.) , where 2md now plays the role that was played by z in the half space transmitted wave case. The $k_\rho = k_1 \sin\beta$ transformation is made, the saddle point contribution is,

$$I_g = \sum_{m=1}^{\infty} \left\{ \frac{2}{i} \frac{e^{ik_1 R_m}}{R_m} D(k_\rho) \frac{k_{12}}{k_\rho} X_{01} X_{10} R_{10}^{m-1} R_{12}^{m} e^{ik_2 z} \right\}_{k_\rho = k_1 \sin\alpha_m} ;$$

$$R_m = \sqrt{\rho^2 + (2md)^2}$$

$$\alpha_m = \tan^{-1} \frac{\rho}{2md}$$

The saddle point is at $\alpha_m = \tan^{-1} \frac{\rho}{2md}$

The above results hold for $k_1 d \gg 1$ and $d \gg z$. When α_m exceeds the critical angle, then branch cut contribution needs to be included. The branch cut is evaluated by deforming to a steepest descent path through the branch point. In geometrical optics approximation, integrals along the BS's , the steepest descent paths passing through the branch points , are usually neglected. In deforming the branch cuts to the steepest descent path through the branch point and before deciding that the final contribution due to the latter is negligible, it must be shown that the deformation is valid. If the deformation is invalid, two alternative approaches can be taken. One alternative is to choose another path and the other alternative is to choose a different branch cut.

In the complex β plane, there are two double-valued functions, k_z and k_{2z}, and their values are to be defined. In analogy to the transmitted wave case, therefore, for $\alpha_m < \theta_o'$

$$Im\ k_z < 0\ ;$$

for $\alpha_m > \theta_o'$

$$Im\ k_z > 0$$

By the same argument as presented in the transmitted wave case, the contribution of the Sommerfeld pole P_1, ($\sin\theta_{p1} = \frac{k}{\sqrt{k^2+k_1^2}}$), is well taken care of by the steepest descent path BS . The net contribution is the saddle point path Γ and the branch cut steepest descent path BS. BS is to be neglected in geometrical optics approximation.

For the double-valued function k_{2z}, it is to be discussed under two different cases: one case with a good subsurface conductor, the other case when the subsurface is a good dielectric.

When the subsurface is a good conductor, the branch point $\theta_2 = \sin^{-1}\frac{k_2}{k_1}$ and various singularities are shown in figure 4.2. For this case, the branch cut $Im\ k_{2z} = 0$ is chosen because this branch cut can be detoured to BS_2, the steepest descent path passing through the branch θ_2. BS_2

is of second order effect so that it is neglected in geometrical optics approximation. With respect to k_{2z}, there are two sheets. On the first sheet, on which the original contour C lies, $\text{Im } k_{2z} > 0$, on the bottom sheet $\text{Im } k_{2z} < 0$. Since the saddle point occurs on the first sheet, therefore the value to be taken for k_{2z}, in the above expression for saddle point contribution, is such that its imaginary part is bigger than 0. The Sommerfeld pole P_2, ($\sin\theta_{p2} = \frac{k_2}{\sqrt{k_1^2+k_2^2}}$), as can be seen from its position in figure 6, is never included between the original contour and the detoured contour. It, however, may affect the saddle point α_m if α_m is getting close to $\frac{\pi}{2}$. In our regions of interest of big d and moderately large ρ, this is never the case. Thus, the effect of P_2 can be safely disregarded. Therefore, in summary, the values of double-valued functions k_z and k_{2z} are to be chosen in the following manner.

$$\text{for } \alpha_m < \theta_0' \quad , \quad \text{Im } k_z < 0 \quad , \quad \text{Im } k_{2z} > 0 \ ;$$

$$\text{for } \alpha_m > \theta_0' \quad , \quad \text{Im } k_z > 0 \quad , \quad \text{Im } k_{2z} > 0$$

When the subsurface is a good dielectric medium, the various singularites and contours are shown in figure 4.3. The following observations are made:

1. This case contrasts with the previous case in that $\theta_2 = \sin^{-1}\frac{k_2}{k_1}$ is at a drastically different location.
2. The branch cut $\text{Im } k_{2z} = 0$ cannot be detoured to the

steepest descent path BS_2 because the detour involves passing through regions where the exponential blows up. It is to be emphasized that, in geometrical optics approximation, it is the BS_2 , steepest descent path passing through branch point, that is negligible, and not any arbitrary branch cut one defines. The prescription, in this case, is to define a different branch cut such that it can be detoured to BS_2 . The branch cut chosen is $\mathrm{Re}\ k_{2z} = 0$ which can fulfill the function.

3. With respect to k_{2z} , again, there are two sheets. On the first sheet $\mathrm{Re}\ k_{2z} > 0$, while on the second sheet, $\mathrm{Re}\ k_{2z} < 0$. The branch cut $\mathrm{Re}\ k_{2z} = 0$ can be detoured to the steepest descent path BS_2 which is neglected in geometrical optics approximation. Since the saddle point always occur on the upper sheet with respect to this branch cut, therefore $\mathrm{Re}\ k_{2z} > 0$ is the value to be taken in our expression. In summary, the values of the double-valued functions k_z and k_{2z} are to be chosen in the following manner:

$$\text{for } \alpha_m < \theta_0' \,,\ \mathrm{Im}\ k_z < 0 \,,\ \mathrm{Re}\ k_{2z} > 0 \,;$$

$$\text{for } \alpha_m > \theta_0' \,,\ \mathrm{Im}\ k_z > 0 \,,\ \mathrm{Re}\ k_{2z} > 0$$

The two layer case is different from the half space case in one other important aspect. In the half space case, the receiver is close to the surface, so that the saddle point is always close to $\frac{\pi}{2}$. On the other hand, for the two layer case , the saddle point for the "reflected terms of images" have their saddle points α_m moving along the real β axis as ρ and 2md are changed. When the saddle point α_m approaches the branch point θ_0 , the saddle point method crumbles. Using Watson's Lemma, the criterion for the validity of the saddle point method is found to be

$$\left| \frac{k_1 R_m (\sin\theta_0 - \sin\alpha_m)^2}{n-1} \right| \gg 1$$

The above condition can be achieved by either making k_1 more conductive so that k_1 has a bigger imaginary part or by making R_m bigger. But both of these procedures will lead to a decay of the reflections and thus decrease the interference effects; they are largely undesirable.

4.2 SOLUTIONS FOR THE FIELD COMPONENTS

By making full use of the mathematics

developed in Appendix I and previous sections, the field components have been derived. In the vicnity of the surface, i. e. $z \ll d, \rho$, the six electromagnetic field components are listed in the following:

$$H_z^{TE} = -\frac{Il}{4\pi}\frac{e^{ikr}}{r}\left[\sin\theta\left(ik-\frac{1}{r}\right)X_{01}(\theta)+\frac{3}{2r}\cos\theta\,X_{01}'(\theta)\right.$$

$$\left.+\frac{\sin\theta}{2r}X_{01}''(\theta)\right]\sin\phi$$

$$-\frac{Il}{4\pi}\frac{\mu}{\mu_1}\frac{2k_1^2}{\rho^2a^2}\frac{e^{-az+ik_1\rho}}{(1+i\sin\theta_0\cot\theta)^{3/2}}\sin\phi$$

$$-\frac{Il}{4\pi}\frac{\mu_1}{\mu}\sum_{m=1}^{\infty}\left[X_{10}^2\,R_{10}^{m-1}\,R_{12}^m\,ik_1\sin\alpha_m\,e^{ik_z z}\right]_{k_\rho=k_1\sin\alpha_m}\frac{e^{ik_1R_m}}{R_m}\sin\phi$$

$$E_\phi^{TE} = \frac{Il\omega\mu}{4\pi i}\frac{e^{ikr}}{r}\left[X_{01}(\theta)+\frac{1}{2ikr}\left(\cot\theta\,X_{01}'(\theta)+X_{01}''(\theta)\right)\right]\sin\phi$$

$$-\frac{Il\omega\mu}{4\pi}\frac{2k_1}{\rho^2a^2}\frac{e^{-az+ik_1\rho}}{(1+i\sec\theta_0\cot\theta)^{3/2}}\frac{\mu}{\mu_1}\sin\phi$$

$$+\frac{Il\omega\mu}{4\pi i}\frac{\mu_1}{\mu}\sum_{m=1}^{\infty}\left[X_{10}^2\,R_{10}^{m-1}\,R_{12}^m\,e^{ik_z z}\right]_{k_\rho=k_1\sin\alpha_m}\frac{e^{ik_1R_m}}{R_m}\sin\phi$$

$$H_\rho^{TE} = -\frac{I\ell}{4\pi i}\frac{e^{ikr}}{r}\left[P(\theta) + \frac{1}{2ikr}\left(\cot\theta P'(\theta) + P''(\theta)\right)\right]\sin\phi$$

$$-\frac{I\ell}{4\pi}\frac{\mu}{\mu_1}\frac{2ik_1}{\rho^2 a}\frac{e^{-az+ik_1\rho}}{(1+i\sec\theta_0\cot\theta)^{3/2}}\sin\phi$$

$$-\frac{I\ell}{4\pi i}\sum_{m=1}^{\infty}\left[k_{1z}X_{01}X_{10}R_{10}^{m-1}R_{12}^{m}e^{ik_z z}\right]_{k_\rho = k_1\sin\alpha_m}\frac{e^{ik_1 R_m}}{R_m}\sin\phi$$

$$E_z^{TM} = -\frac{I\ell}{4\pi\omega\varepsilon}\frac{e^{ikr}}{r}\left[\left(ik - \frac{1}{r}\right)\sin\theta\, Q(\theta) + \frac{3\cos\theta}{2r}Q'(\theta)\right.$$

$$\left. + \frac{1}{2r}\sin\theta\, Q''(\theta)\right]\cos\phi$$

$$+\frac{I\ell}{4\pi\omega\varepsilon}\frac{\varepsilon}{\varepsilon_1}\frac{2ik_z^2}{\rho^2 a}\frac{e^{-az+ik_1\rho}}{(1+i\sec\theta_0\cot\theta)^{3/2}}\cos\phi$$

$$+\frac{I\ell}{4\pi\omega\varepsilon}\sum_{m=1}^{\infty}\left[k_{1z}\Gamma_{10}\Gamma_{01}S_{12}^{m}S_{10}^{m-1}e^{ik_z z}\right]_{k_\rho = k_1\sin\alpha_m} ik_1\sin\alpha_m$$

$$\frac{e^{ik_1 R_m}}{R_m}\cos\phi$$

$$E_\rho^{TM} = -\frac{I\ell}{4\pi i\omega\varepsilon}\frac{e^{ikr}}{r}\left[Q_1(\theta) + \frac{1}{2ikr}\left(\cot\theta\, Q_1'(\theta) + Q_2''(\theta)\right)\right]\cos\phi$$

$$+\frac{I\ell}{4\pi\omega\varepsilon}\frac{\varepsilon}{\varepsilon_1}\frac{2k_1}{\rho^2}\frac{e^{-az+ik_1\rho}}{(1+i\sec\theta_0\cot\theta)^{3/2}}\cos\phi$$

$$+\frac{I\ell}{4\pi\omega\varepsilon i}\sum_{m=1}^{\infty}\left[k_{1z}Y_{10}Y_{01}S_{12}^{m}S_{10}^{m-1}e^{ik_1z}\right]_{k_\rho=k_1\sin\alpha_m}\frac{e^{ik_1R_m}}{R_m}\cos\phi$$

$$H_\phi^{TM} = -\frac{I\ell}{4\pi i}\frac{e^{ikr}}{r}\left[Q(\theta) + \frac{1}{2ikr}\left(\cot\theta\, Q'(\theta) + Q''(\theta)\right)\right]\cos\phi$$

$$-\frac{I\ell}{4\pi}\frac{2ik_1}{\rho^2 a}\frac{e^{-az+ik_1\rho}}{(1+i\sec\theta_0\cot\theta)^{3/2}}\frac{\varepsilon}{\varepsilon_1}\cos\phi$$

$$+\frac{I\ell}{4\pi i}\sum_{m=1}^{\infty}\left[k_{1z}Y_{10}Y_{01}S_{10}^{m-1}S_{12}^{m}e^{ik_1z}\right]_{k_\rho=k_1\sin\alpha_m}\frac{e^{ik_1R_m}}{R_m}\cos\phi$$

where $P(\theta) = k\cos\theta\, X_{01}(\theta)$

$Q(\theta) = k\cos\theta\, Y_{10}(\theta)$

$Q_1(\theta) = k^2\cos^2\theta\, Y_{10}(\theta)$

Several points are to be noted in the above fomula:

1. The first term is the direct wave. The second term correponds to the inhomogeneous wave. The third term correponds to the reflected terms of the images.
2. In the first term, which is the saddle point contribution, the first order term correponds to the radiation field.
3. At $z \ll \rho$, i.e. the receiver being close to the surface, the terms $X_{01}(\theta)$ and $Q(\theta)$ are much smaller than their derivatives, $X'_{01}(\theta)$, $X''_{01}(\theta)$, $Q'(\theta)$, and $Q''(\theta)$. This is because of the $\cos\theta$ dependence.

4.3 NUMERICAL RESULTS

The interference patterns for the six electromagnetic field components for different configuration and media are illustrated in Appendix B. In the diagrams, the magnetic field components have been normalized by

$$H = \frac{I\ell}{4\pi\lambda^2} H_{norm.}$$

while the electric field components have been normalized by

$$E = i\frac{I\ell\omega\mu}{4\pi\lambda} E_{norm.}$$

The interference patterns may be best understood by separating the contributions of the various waves. Thus we depict in Figures 4.4 - 4.5, two typical field

components H_z and E_z separated into the half space solutions and the waves reflected from the first boundary. We note that H_z together with H_ρ and E_ϕ are the field components measured broadside, i.e. $\phi = \frac{\pi}{2}$; while E_z , E_ρ and H_ϕ are those measured endfire, i.e. $\phi = 0$. The maximum of the first reflected waves for H_z and E_z occur at different locations.

To explain this difference, we consider the radiation pattern due to the dipole lying on the lunar surface. Under the geometrical optics approximation, the maximum of the wave reflected from the subsurface correponds to the angle of the Poynting power that is radiated into the first layer. For a HED at $\phi = \pi/2$, the maximum power occurs at the critical angle $\sin^{-1}(k/k_1)$ and k_1 is assumed to be real. But for $\phi = 0$, we find that the maximum occurs at an angle $\sin^{-1}\sqrt{2n^2/(1+n^2)}$, where $n = k/k_1$.

The following observations are made:

1. In the direction of maximum power, not all field components have to be maximum. e.g H_z and H_ρ have maximum at different locations.
2. A change of permeability from μ_o to $\mu > \mu_o$ merely changes the magnitude of k_2 . If μ becomes complex, then the positions of the various singularities change, and the integrals must be re-evaluated on the new complex plane.

3. A small loss tangent change has small effect on the positions of peaks and troughs but changes the amplitudes of the field components drastically.

The results of this thesis are now compared with previous findings. Brekhovskih[3], in his solution made the kind of mistake due to the wrong approach to B_+ and B_- as discussed in the section on half space solution. He got the negative of the correct answer. Thus, if one plugs in $z = 0$ in equations 19.36 and 21.14, one obtains

$$\frac{2}{\rho^2}\frac{k_2}{a^2}e^{ik\rho} + \frac{2k_1}{\rho^2 a^2}e^{ik_1\rho}$$

and thus, fails to reproduce Van Der Pol's exact answer.

The validity of the calculations of this thesis can be verified by carrying out exact solutions of the integrals. Tsang (1972) obtained such solutions by numerical integration with a computer. The computation is extremely time consuming and a single comparison is shown. In Figure 4.6 , the exact solution may be compared with the asymtotic solution under the geometrical optics approximation. It can be seen that the geometrical optics approximation is not good near peaks in the interference curves. Mathematically, the peaks are those regions where the saddle point α_m approaches the branch point θ_0 . The saddle point method crumbles

One more point requires discussion. In the geometrical optics approximation, BS and BS_2,

the branch point steepest descent paths contributions, have been neglected. These contributions correspond physically to the reflections of the lateral waves from the bottom layer. Thus, it is implicitly assumed that the energy arriving at the upper surface of layer 1 due to the reflected lateral waves is small. For a better approximation, these effects should be included.

The calculated results using the geometrical optics approach are presented in Appendix B. Both a vertical magnetic dipole and a horizontal electric dipole are considered.

Rossiter et al (1972), has performed the model tank experiment with a dipole over a tank of dielectric over a perfect conductor. The theoretical results are compared with experimental findings in Figure 4.7.

Experiments have been done on glaciers to check both theory and experiment. The Athabasca glacier, located about 75 miles south of Jasper, Alberta, has been thoroughly studied by others with such methods as seismology, gravity, resistivity measurements and drill holes. In Figure 4.8 is a single comparison. The thickness of the ice determined by our theoretical curves is 180 meters which agrees very well with the thickness determined independently from the drill hole.

4.4 STRATIFIED MEDIUM WITH MORE THAN TWO LAYERS

Cases of more than two layers can be dealt with in similar ways, using geometrical optics approximation. The steps are the same: the denominators of $1 + R^{TE}$ and $1 - R^{TM}$ are expanded and combined with other terms in the integrand. A suitable transformation is made e.g. $k_\rho = k_1 \sin\beta$, $k_\rho = k_2 \sin\beta$, $k_\rho = k_3 \sin\beta$ etc., depending on the predominant term in the exponential.

By expanding the denominators in the n-layer reflection coefficient, one can get, in general, two terms: the first being exactly the same as the $n - 1$ layer solution, the second term corresponding to the reflections generated by an additional boundary. This, indeed, has been the case for the two layer problem where we get back the half space solution plus the "reflected terms of images". The three layer problem is illustrated in the following:

$$1 + R^{TE} = X_{01} \left[1 + \sum_{m=1}^{\infty} X_{10} R_{10}^{m-1} R_{12}'^{m} e^{2i k_{1z} m d_1} \right]$$

where,

$$R_{12}' = \frac{1}{R_{12}} \left[1 - \frac{\frac{1}{R_{12}} - R_{12}}{\frac{1}{R_{12}} + e^{2i k_{2z}(d_2 - d_1)} R_{23}} \right]$$

$$R'_{12} = R_{12} + X_{12} X_{21} \sum_{m=1}^{\infty} R_{21}^{m-1} R_{23}^{m} e^{2ik_{2z} m (d_2 - d_1)}$$

$$= g + f$$

$$g = R_{12}$$

$$f = \frac{X_{12} X_{21}}{R_{21}} \sum_{n=1}^{\infty} R_{21}^{n} R_{23}^{n} e^{2ik_{2z} n (d_2 - d_1)}$$

$$\therefore \quad R'^{m}_{12} = g^{m} + \sum_{l=1}^{m} C_l^m g^{m-l} f^{l}$$

where C_1^m is the binomial coefficient.

$$f^{l} = \frac{X_{12}^{l} X_{21}^{l}}{R_{21}^{l}} \left[\frac{1}{1 - R_{21} R_{23} e^{2ik_{2z}(d_2 - d_1)}} - 1 \right]^{l}$$

If

$$X = R_{21} R_{23} e^{2ik_{2z}(d_2 - d_1)}$$

then

$$f^{l} = \frac{X_{12}^{l} X_{21}^{l}}{R_{21}^{l}} X^{l} \sum_{p=0}^{\infty} C_p^{-l} (-X)^{p}$$

$$\therefore \quad 1 + R^{TE} = X_{01} \left[1 + \sum_{m=1}^{\infty} X_{10} R_{10}^{m-1} g^{m} e^{2ik_{1z} m d_1} \right.$$

$$\left. + \sum_{m=1}^{\infty} X_{10} R_{10}^{m-1} e^{2ik_{1z} m d_1} \sum_{l=1}^{m} C_l^m g^{m-l} f^{l} \right]$$

Thus, there are three factors, viz.,

$$X_{01} \quad ; \quad \sum_{m=1}^{\infty} X_{01} X_{10} R_{10}^{m-1} g^{m} e^{2ik_{12}md_1} \quad ;$$

$$\sum_{m=1}^{\infty} \sum_{\ell=1}^{m} \sum_{p=0}^{\infty} X_{01} X_{10} R_{10}^{m-1} e^{2ik_{12}md_1} C_{\ell}^{m} R_{12}^{m-\ell} \frac{X_{12}^{\ell} X_{21}^{\ell}}{R_{21}^{2\ell}} C_{p}^{-\ell}$$

$$(-1)^{p} \left\{ R_{21} R_{23} e^{2ik_{22}(d_2-d_1)} \right\}^{p+\ell}$$

The first two terms combined is just the two layer solution. To find the location of the saddle point in the last term, we observe that the exponential is

$$ik_{\rho}\rho + 2ik_{12}md_1 + 2ik_{22}(p+\ell)(d_2-d_1)$$

so that the two equations to be solved are

$$k_{\rho} = k_1 \sin\theta_1 = k_2 \sin\theta_2$$

$$2md_1 \tan\theta_1 + 2(p+\ell)(d_2-d_1)\tan\theta_2 = \rho$$

where θ_1 is the saddle point in the $k_{\rho} = k_1 \sin\beta$ transformation, θ_2 is the saddle point in the $k_{\rho} = k_2 \sin\beta$ transformation.

Note that physically, the above equations correspond to the ray paths given rise by the multiple reflections in geometrical optics when there are several boundaries of reflection.

For complex k_1 and k_2, there are actually four equations and four unknowns as both the real and imaginary parts of the equations are to be taken. For slightly conductive k_1 and k_2, the real parts are solved first to get an approximate answer first. The imaginary parts are then taken into account and the final answers are obtained by perturbing around the approximate answers using Newton's method of solving roots of equation.

Either the transformation $k_\rho = k_1 \sin\beta$ or the transformation $k_\rho = k_2 \sin\beta$ is made, depending on which layer is thicker. Care has also to be exercised in choosing the values of double-valued functions, the k_z's, in the complex β plane as in the two layer case.

FIGURE CAPTIONS

4.1 The image diagram for the two layer case.

4.2 The complex β plane for the two layer case with a good subsurface conductor.

4.3 The complex β plane for the two layer case with a subsurface dielectric.

4.4 The half space solution for H_z and also the first few reflected terms.

4.5 The half space solution for E_z and also the first few reflected terms. Comparing figure 12 and 13 show that the maximum for the reflected terms occurs at different location for the two components.

4.6 Comparison of geometrical optics approximation with exact numerical integration.

4.7 Comparison of model tank results with geometrical optics approximation. Dotted curve is G. O. A. (Geometrical Optics Approximation). Solid curve is experimental measurement. Vertical scale is 15 db. per inch.

4.8 Comparison of G. O. A. and Athabasca Glacier data measurement. The stratified diagram gives the parameters of the G. O. A. curve. Vertical scale is 8 db. per inch.

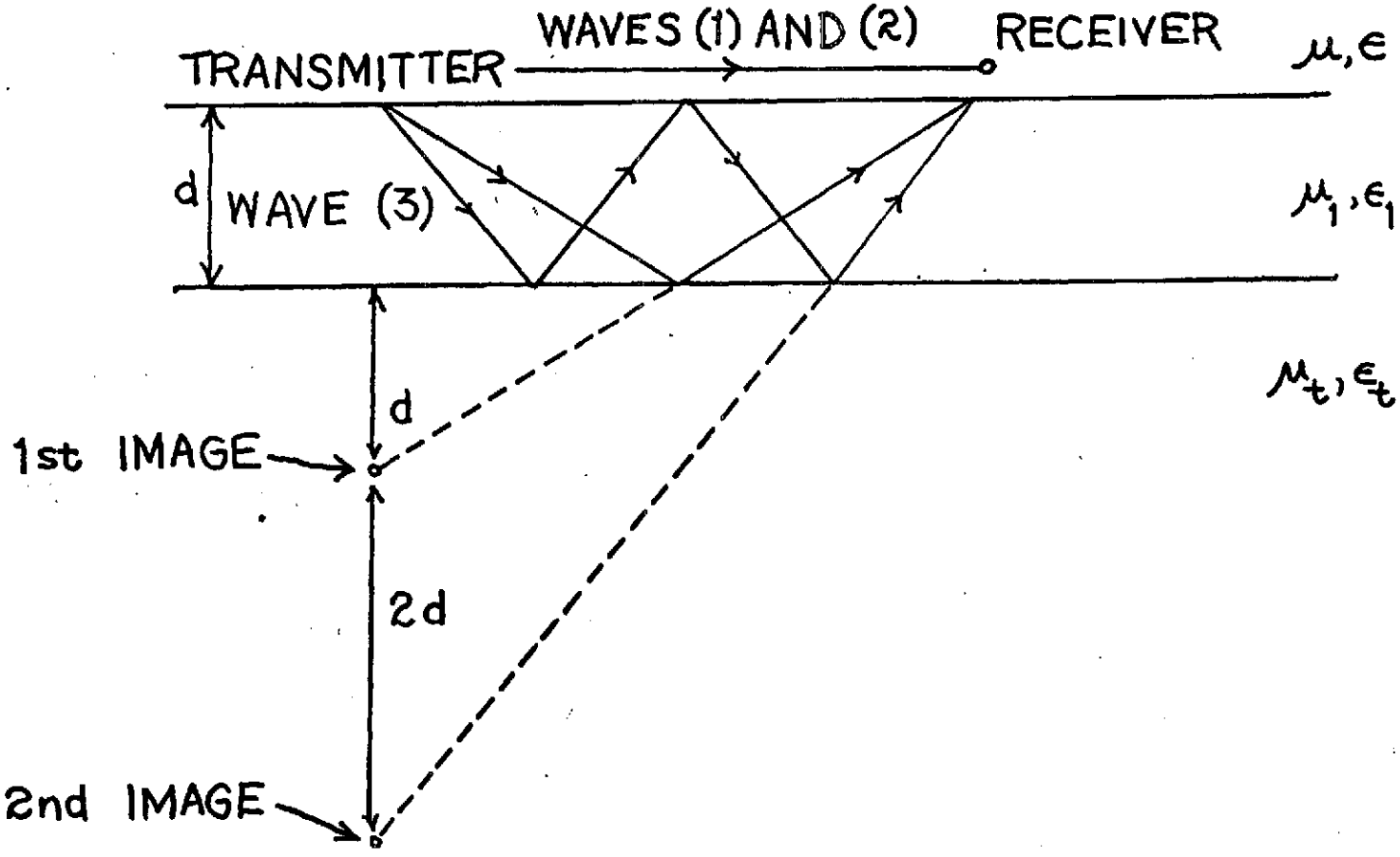
TRANSMITTER
WAVES (1) AND (2)
RECEIVER
μ, ε
d
WAVE (3)
μ1, ε1
μt, εt
d
1st IMAGE
2d
2nd IMAGE

Figure 4.1

Figure 4.2

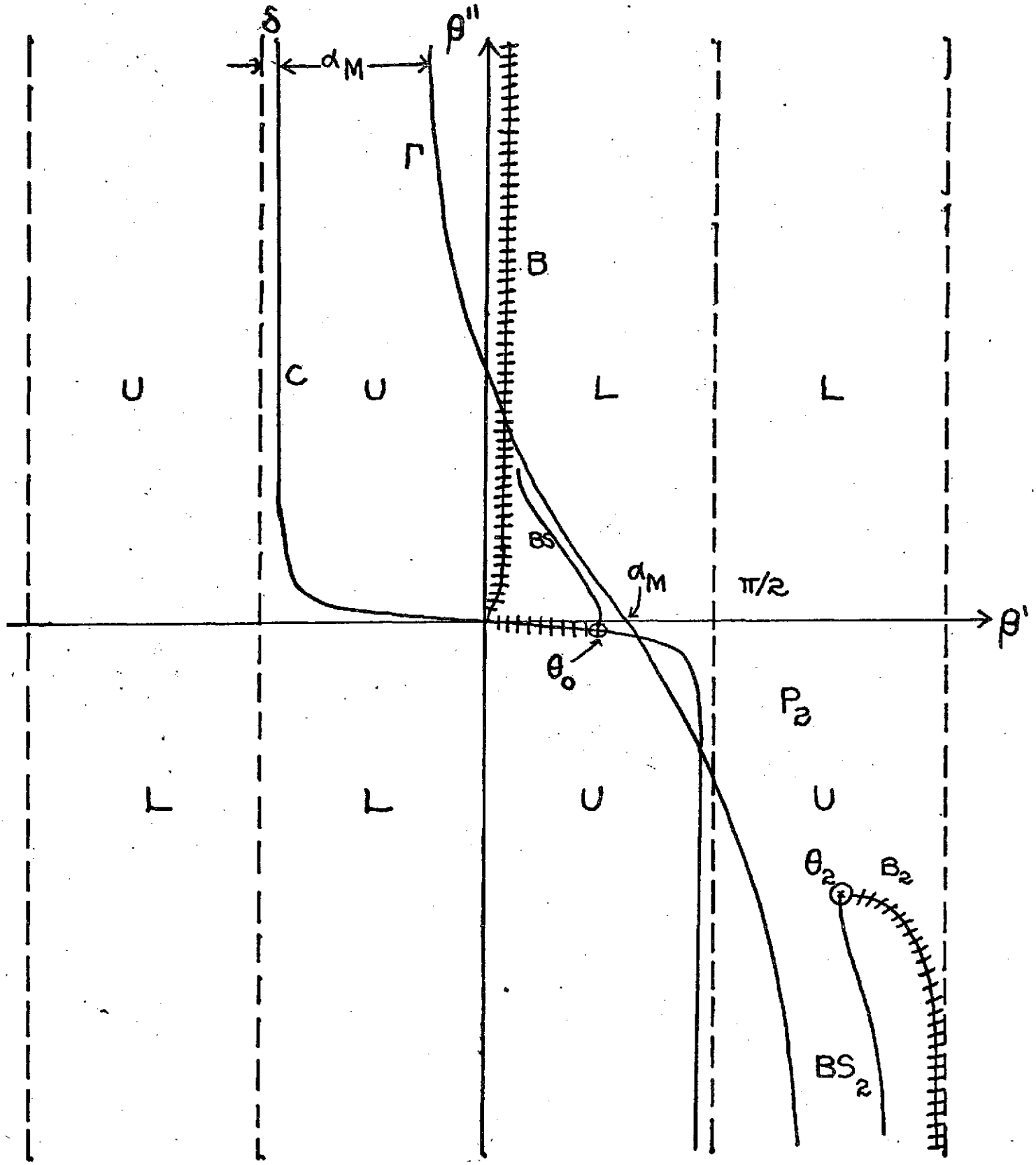

Figure 4.3

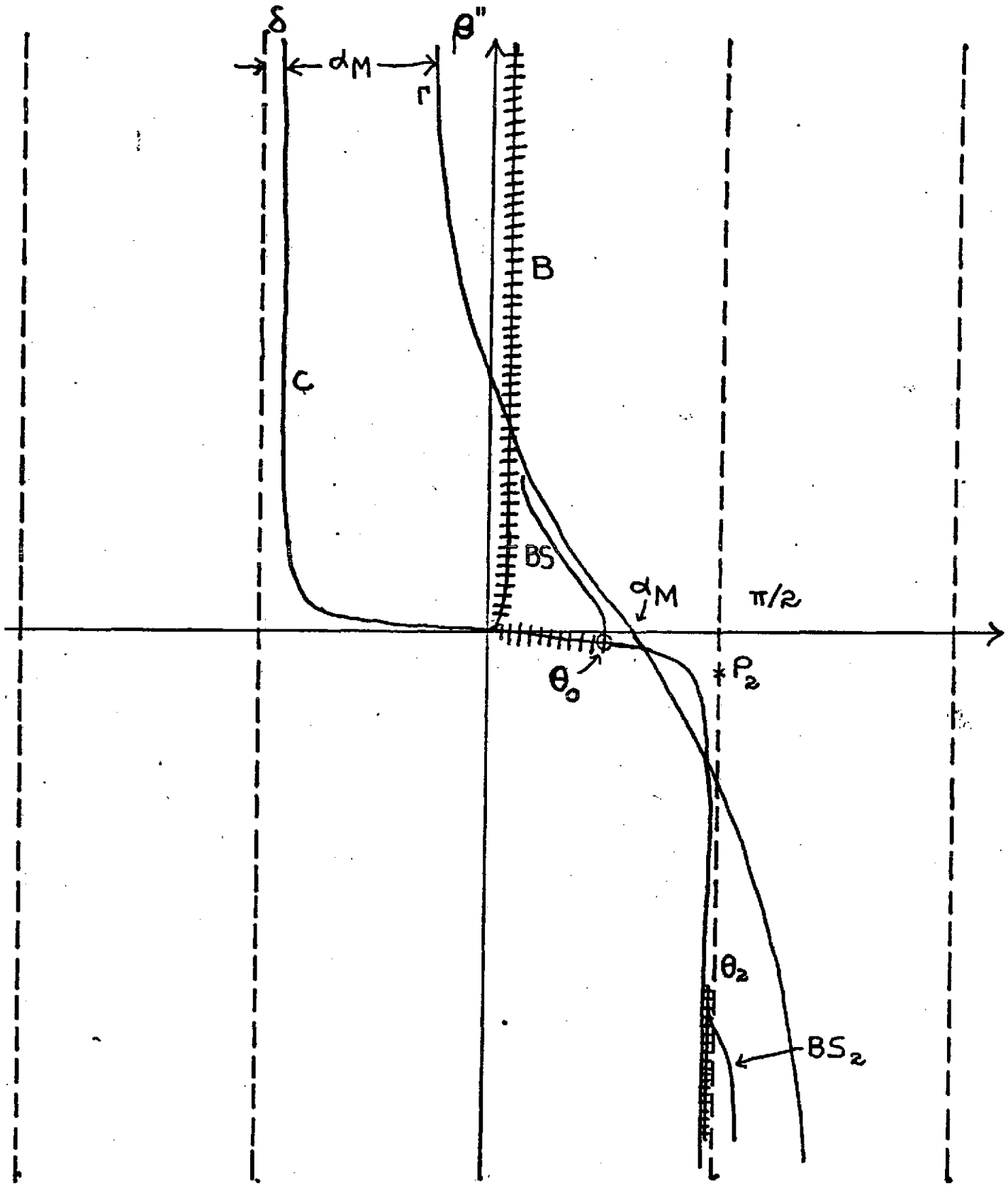

Figure 4.4

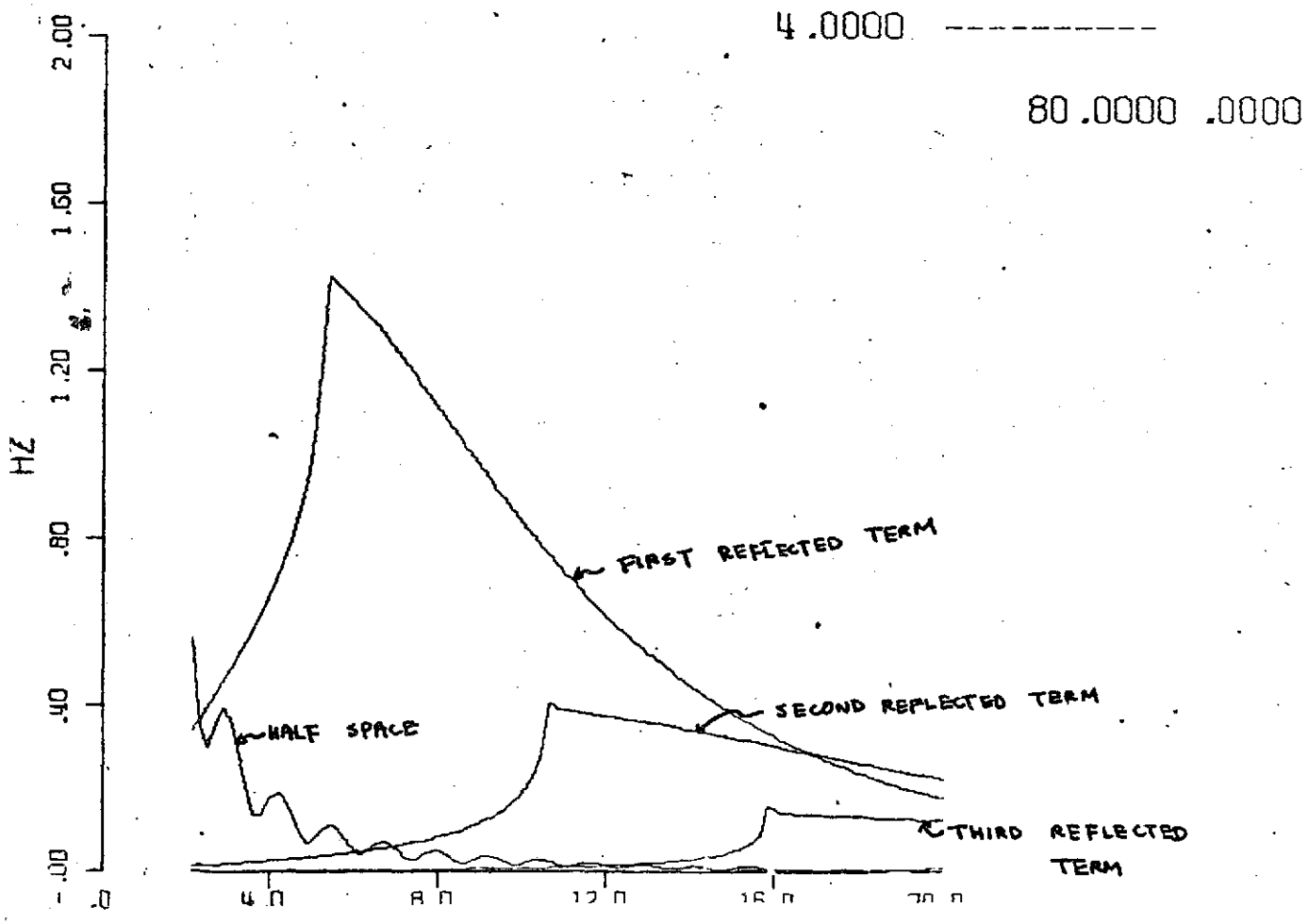
3.3000 .0050
4.0000
80.0000 .0000
HZ
2.00
1.60
1.20
.80
.40
.00
.0
4.0
8.0
FIRST REFLECTED TERM
SECOND REFLECTED TERM
HALF SPACE
THIRD REFLECTED TERM

Figure 4.5

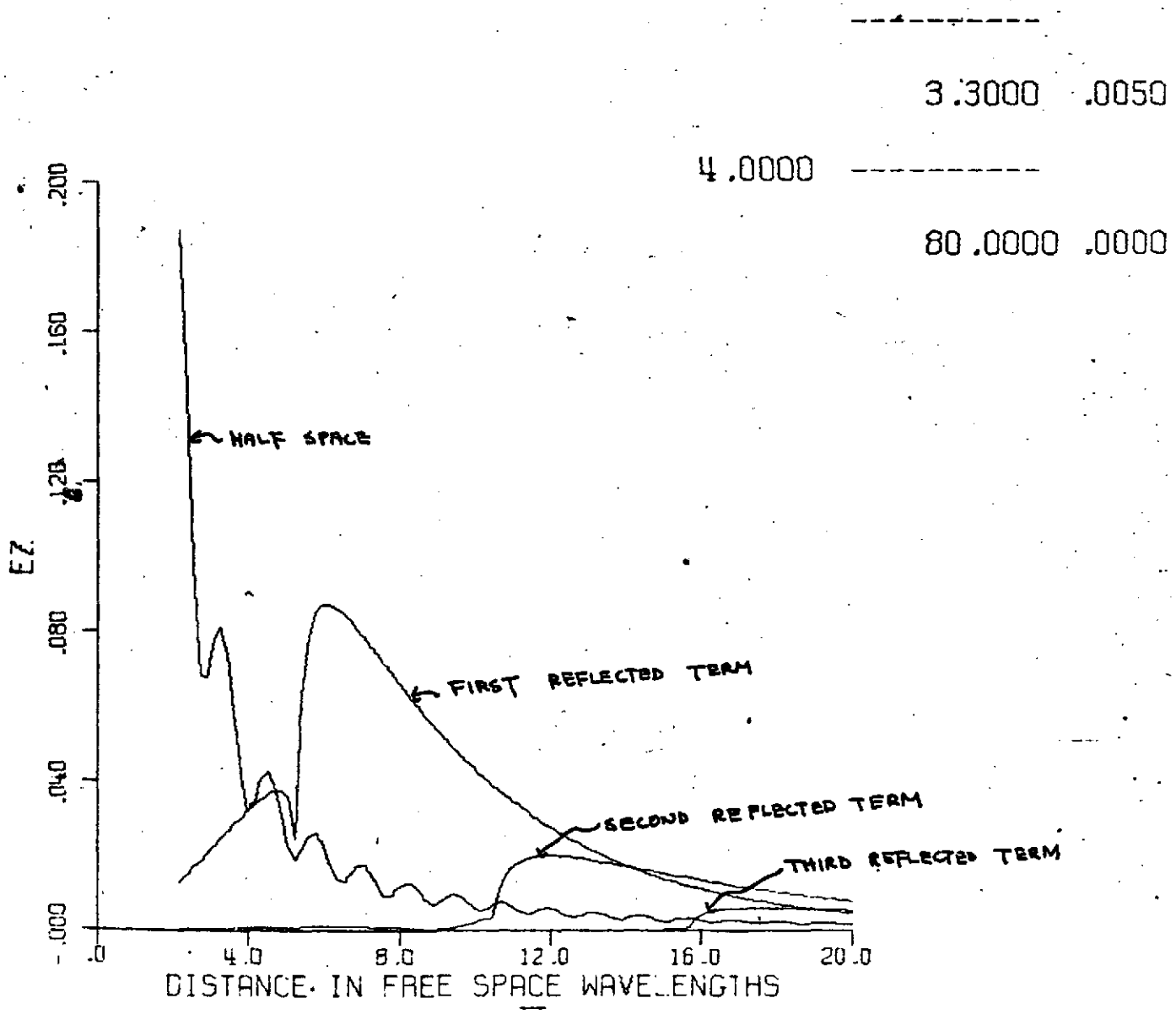
3.3000 .0050
4.0000
80.0000 .0000
.200
.160
.120
.080
.040
-.000
EZ
HALF SPACE
FIRST REFLECTED TERM
SECOND REFLECTED TERM
THIRD REFLECTED TERM
.0
4.0
8.0
12.0
16.0
20.0
DISTANCE IN FREE SPACE WAVELENGTHS

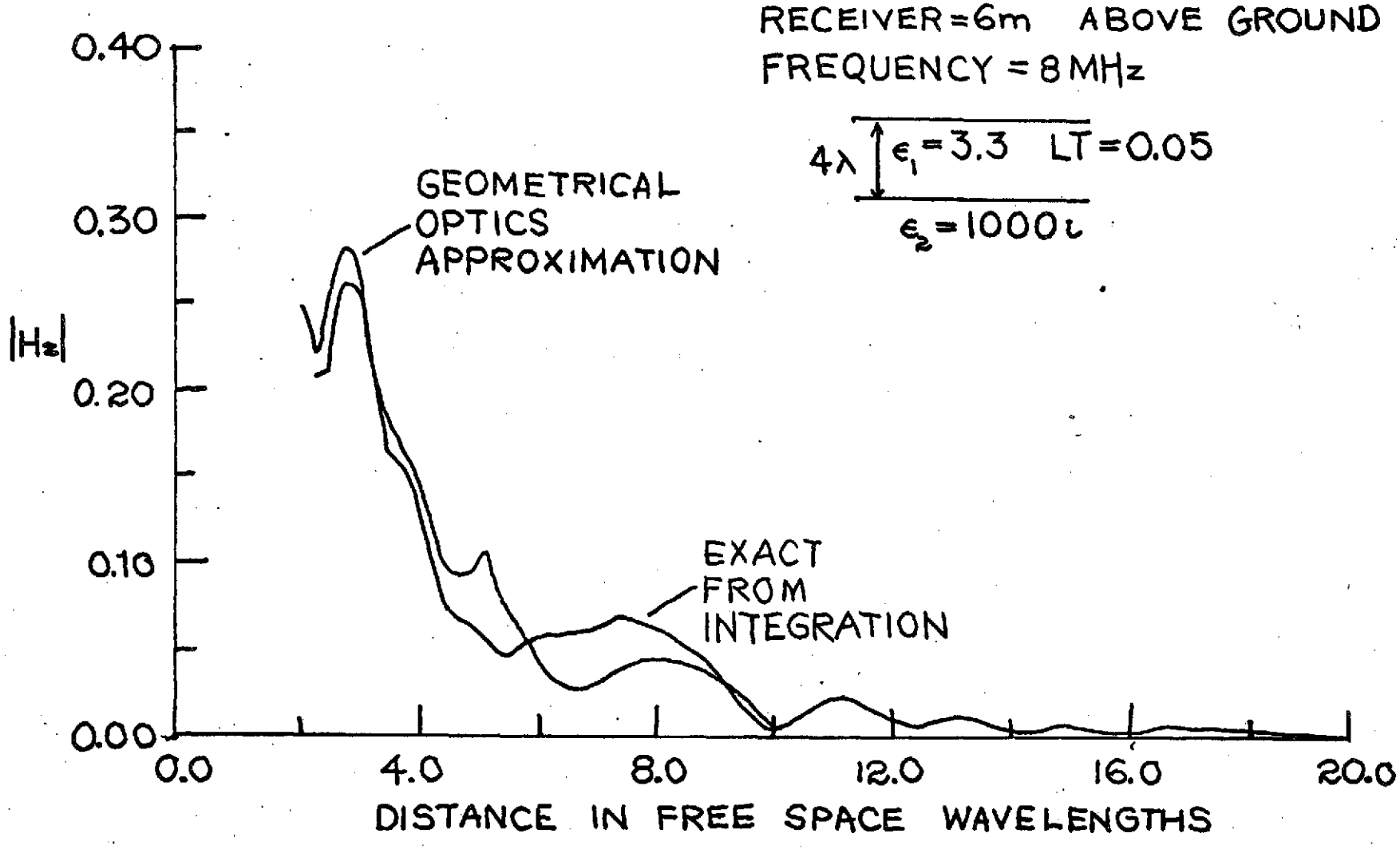
RECEIVER=6m ABOVE GROUND
FREQUENCY = 8 MHz
4λ
$\epsilon_1 = 3.3$ LT=0.05
$\epsilon_2 = 1000\iota$
GEOMETRICAL OPTICS APPROXIMATION
EXACT FROM INTEGRATION
$|H_z|$
0.40
0.30
0.20
0.10
0.00
0.0
4.0
8.0
12.0
16.0
20.0
DISTANCE IN FREE SPACE WAVELENGTHS

Figure 4.6

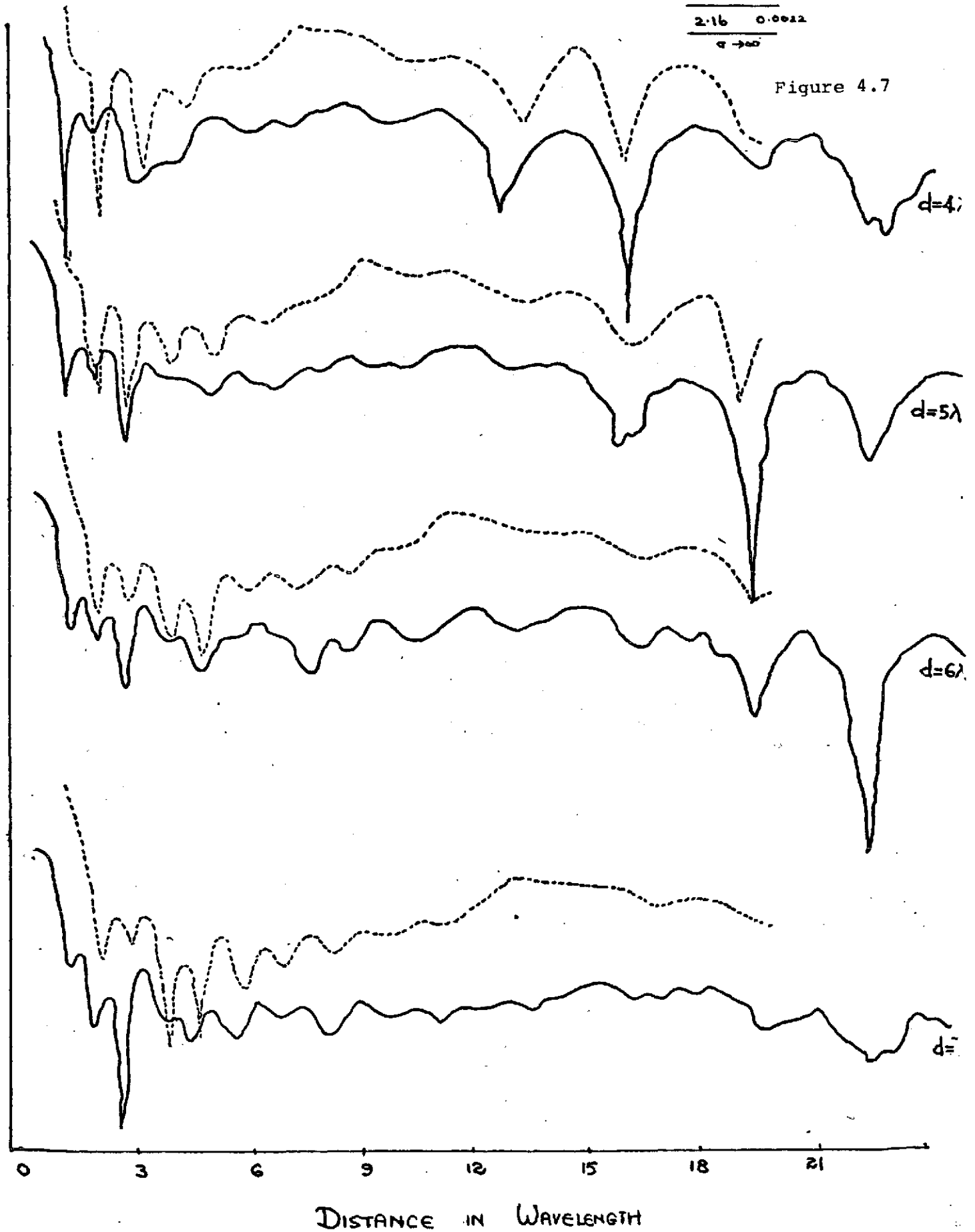
2·16 0·0022
a →∞
d=4λ
d=5λ
d=6λ
d=
0
3
6
9
12
15
18
21
DISTANCE IN WAVELENGTH

Figure 4.7

Figure 4.8

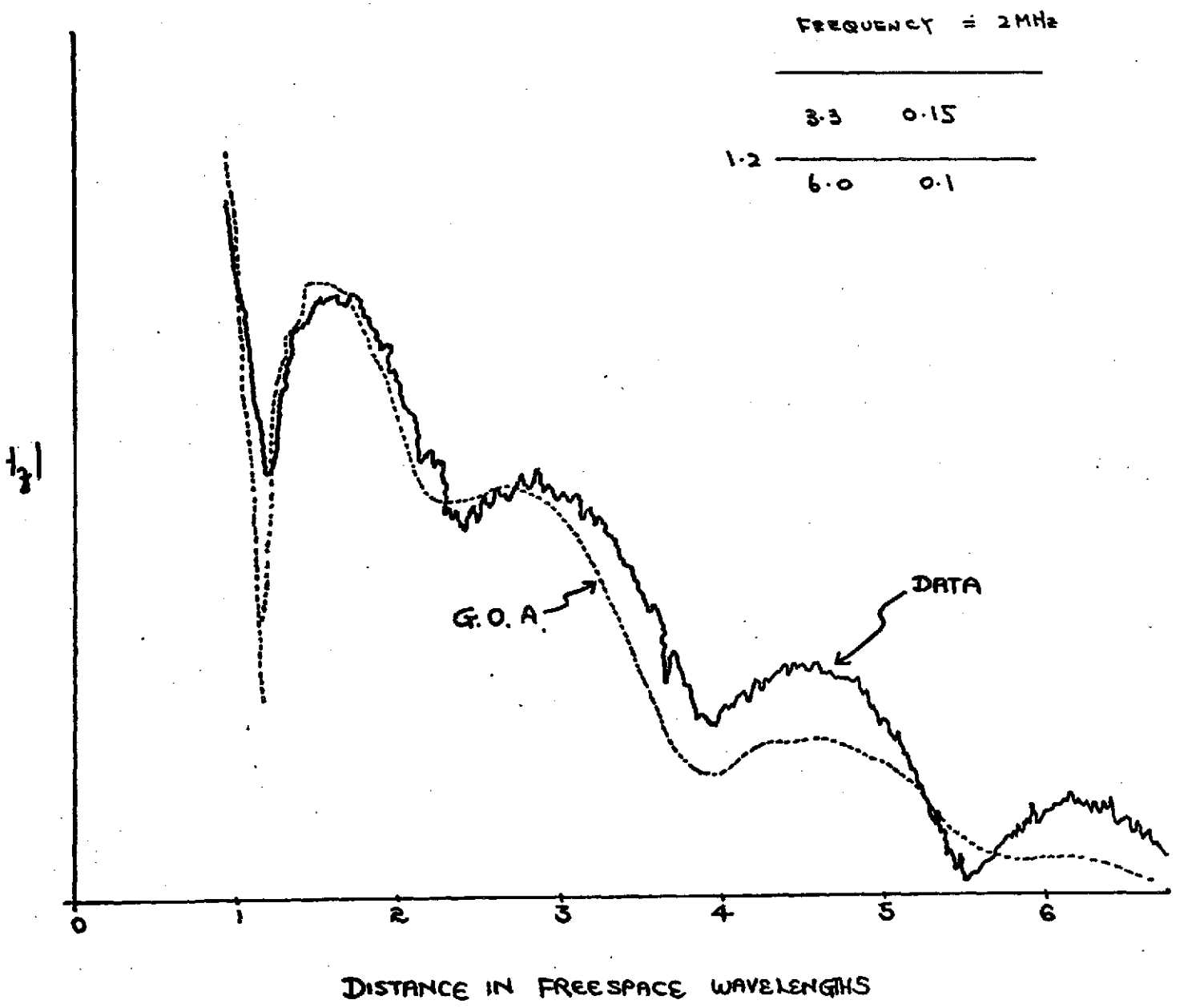
FREQUENCY = 2MHz
3·3
0·15
1·2
6·0
0·1
|t₂|
G.O.A
DATA
0
1
2
3
4
5
6
DISTANCE IN FREESPACE WAVELENGTHS

Chapter 5.

MODE APPROACH

In this chapter, we use the residue series method in combination with either the modified saddle point method or the numerical method to evaluate the integrals. Each term in the residue expansion can be attributed to a normal mode of the layered medium. The characteristics of mode solutions are then discussed. When the non-modal part is evaluated by the modified saddle point method, the results are applicable to the far field regions only. With a combination of the residue approach and the numerical method, the results can be extended to all regions of interest. The advantages and the disadvantages of the various limits are also discussed. Theoretical results are illustrated for the various field components plotted in the form of interference patterns.

5.1 METHODS OF APPROACH

Consider the integral

$$H_z = \int_{-\infty}^{\infty} dk_\rho \frac{iI\ell k_\rho^2}{8\pi k_z} (1+R^{TE}) e^{ik_z z} H_1^{(1)} (k_\rho \rho) \sin\phi \qquad (5.1)$$

where H_z denotes the z-component of the magnetic field vector. We use cylindrical coordinate system with z-axis perpendicular to the surface of the stratified medium and ρ denotes the

transverse distance with origin at the transmitting antenna, the azimuthal angle ϕ is measured with respect to the transmitting antenna axis. The propagation vector k in the free space region has components k_ρ and k_z. $I\ell$ denotes the antenna strength. $H_1^{(1)}(k_\rho\rho)$ is the first order Hankel function of first kind. R^{TE} represents the reflection coefficient for TE wave components due to the stratified medium.

For the two layer case, the reflection coefficient R^{TE} takes the following form

$$R^{TE} = \frac{1}{R_{01}^{TE}} \left[1 - \frac{1 - (R_{01}^{TE})^2}{1 + R_{01}^{TE} R_{12}^{TE} \exp(i2k_{1z}d)}\right] \tag{5.2}$$

where R_{01}^{TE} and R_{12}^{TE} are the usual Fresnel reflection coefficients for TE waves at interfaces between the first and the second boundaries.

In order to solve the integral in (5.1), we make the transformation

$$k_\rho = k\sin\theta \tag{5.3}$$

so that the two Riemann sheets due to the branch point k_z is unfolded. We then have four Riemann sheets due to Re k_{1z} and Re k_{2z}. In the integral (5.1), we can write $H_1(k_\rho\rho) = H_1(k_\rho\rho)e^{-ik_\rho\rho}$ and insert an exponential factor $\exp(ik_\rho\rho)$ which is in fact the factor for the Hankel function at its asymptotic limits when $k_\rho\rho$ tends to infinity. Correspond-

ing to this factor, there is a saddle point at $\theta = \pi/2$. We then detour, on the complex θ-plane, the original path of integration to the steepest decent path passing through the saddle point. The contribution to the integral is then composed of three parts

$H_z = I_p + I_s + I_b$. 1) I_p is $2\pi i$ times the residue series of the poles enclosed between the new and the old paths, 2) I_b is the branch cut contribution due to k_{1z} and k_{2z}, and 3) I_s is the saddle point contribution. Each pole on the θ-plane can be interpreted as a normal mode pertaining to the layer medium. We therefore discuss our solutions separately for the modal part corresponding to the residual series and the non-modal part corresponding to the branch cut and the saddle point contributions.

5.2 MODAL SOLUTIONS

In order to find the normal modes pertaining to the layered medium, we determine the poles of the integrand. Due to the two branch points at $k_\rho = k_1$ and $k_\rho = k_2$, there are four corresponding Riemann sheets. We are interested in the sheet where $\mathrm{Re}(k_{1z}) > 0$ and $\mathrm{Re}(k_{2z}) > 0$. The poles of the integrand are in turn determined by the zeros of the denominator of $1+R^{TE}$. Let

$$R_{12}R_{10} = e^{i\phi} \qquad 0 \leq \mathrm{Re}(\phi) \leq 2\pi \tag{5.4}$$

we can write, in view of the denominator of (2)

$$\phi + 2k_{1z}d = 2\pi\ell \qquad \ell = 1, 2, \ldots, \infty \tag{5.5}$$

For each ℓ, there are two roots corresponding to $Re(k_z) > 0$ and $Re(k_z) > 0$. A pole location plot on the complex θ-plane is illustrated in Fig. 5.1 for a layer of depth 4λ with permitivity $2.16(1+i0.0022)$ over a perfect conductor. The original path of integration and the new steepest descent path are also shown on the same figure.

The poles that lie between the new and the old paths of integration contribute to the integral in (5.1). The contribution is determined by $2\pi i$ times the residue series.

$$I_\rho = -\frac{I\ell}{4} \sum_{\text{poles}} \left\{ \frac{\frac{k_\rho^2}{k_z} X_{01}(1+R_{12}e^{i2k_{1z}d})}{\frac{d}{dk_\rho}[1+R_{12}R_{01}e^{i2k_{1z}d}]} H_1^{(1)}(k_\rho\rho)e^{ik_z z} \right\}_{k_\rho \text{ at the pole}} \tag{5.6}$$

Each term in the summation series corresponds to a normal mode. Note that each normal mode is a cylindrical wave. Note also that as $\rho \to \infty$, the Hankel function has the asymptotic limit $\sqrt{\frac{2}{\pi\rho}}e^{ik_\rho\rho - \frac{3i\pi}{4}}$.

With regard to the modes that are excited by the antenna, we have the following observations: 1) All excited modes have $Re(k_\rho) < k_1$. 2) For the class of modes having $Re(k_\rho) < k$, they all have $Re(k_z) > 0$ and $Im(k_z) < 0$. Physically these modes correspond to waves leaving the surface with increasing amplitude. We term these waves leakly modes, they can also be called radiation modes of the structure. 3) For the class of modes having $k < Re(k_\rho) < Re(k_1)$, all have

$\mathrm{Re}(k_z) < 0$ and $\mathrm{Im}(k_z) > 0$. Physically these modes correspond to waves coming toward the surface with increasing amplitudes away from the surface. We term these waves creeping modes. They are surface-like modes and are related to the waveguide modes. 4) For the leaky modes, the transverse wave number k_ρ has both positive real part and positive imaginary part. The magnitude of the imaginary part is large as compared with that of the creeping modes. The leaky modes decay very rapidly away from the transmitter and are important only in regions near the dipole. 5) The transverse components of the creeping modes have a positive real part and a positive imaginary part. The creeping waves decay relatively slower than the leaky waves with trasverse distance.
The creeping modes are the significant ones in regions far from the transmitting antenna. 6) The number of normal modes excited by the antenna depends on the thickness of the slab. If the slab is sufficiently thin no mode will be excited at all. We discuss the thin layer case in Section 5.4. The calculated results are presented in Appendix C for different layer thickness.

5.3 INTEGRATION AROUND THE SADDLE POINT

In the absence of any stratified medium, the saddle point contribution from the transmitter corresponds to the direct wave from the dipole. When there is stratified medium present, the evaluation of the saddle point contribution is complicated

by the poles in the neighborhood of the saddle point. Besides the pole effects, the saddle point contribution is also affected by the rapidly varying exponential $\exp(i2k_{1z}d)$ factor in the reflection coefficient. The oscillation of this factor is fast when d is large. We thus evaluate the saddle point contribution for the following three cases: 1) when $\rho >> d$, we use the ordinary saddle point method (OSP). 2) When $\rho > d$, we use the modified saddle point method (MSP). 3) When $\rho \sim d$, we resort to numerical evaluation by using the Gaussian Hermite Guadrature (GHQ) formula.

1) In applying the ordinary saddle point method, we transform the integral to the form

$$I_s = \int_{-\infty}^{\infty} \Phi(x) \exp(-x^2/2)\,dx; \quad \Phi(x) = \sum_{m=0}^{\infty} A_{2m} x^{2m} \tag{5.7}$$

The solution is then given by

$$I_s = OSP = \sqrt{2\pi}\{A_0 + A_2 + 3A_4 + \ldots\} \tag{5.8}$$

We include terms to ρ^{-3}.

The integral (1) can be transformed into the form (5.7) by setting

$$ik\rho(1 - \sin\theta) = x^2/2 \tag{5.9}$$

When $\rho >> d$, there are no poles near the saddle point and the integrand does not oscillate very fast. Thus the ordinary saddle point method is applicable.

2) Suppose there is a pole near the saddle point at $x = x_0$.

$$x_0 = [i2k\rho(1 - \sin\theta_p)]^{1/2} \tag{5.10}$$

where θ_p is the location of the pole. Let

$$M = \lim_{x \to x_0} \Phi(x)(x - x_0) \tag{5.11}$$

We can write

$$\Phi(x) = \psi(x) + \frac{M}{x - x_0} \tag{5.12}$$

and

$$I_s = W_s + W_p \tag{5.13}$$

where

$$W_\rho = \int_{-\infty}^{\infty} \frac{M}{x - x_0} dx = \begin{cases} +i\pi M e^{-x_0^2/2} \operatorname{erfc}(-iw_0) & \operatorname{Im} w_0 > 0 \quad (5.14) \\ -i\pi M e^{-x_0^2/2} \operatorname{erfc}(iw_0) & \operatorname{Im} w_0 < 0 \quad (5.15) \end{cases}$$

$$w_o = x_0/\sqrt{2}$$

With the effect of the poles being subtracted, W_s can be solved <u>asymptotically</u>

$$W_s = \int_{-\infty}^{\infty} \psi(x) e^{-x^2/2} dx = \mathrm{OSP} - [W_p] \tag{5.16}$$

where $[W_p]$ denotes W_p in inverse power series of w_0. We thus have the solution for the modified saddle point method.

$$I_s = \mathrm{MSP} = \mathrm{OSP} + \sum_{\text{poles}} \{W_p - [W_p]\} \tag{5.17}$$

Evidently, as $w_0 >> 1$, the modified saddle point result is identical to the ordinary saddle point result. The summation in (17) extends over all poles near the saddle point. Both OSP and $[W_p]$ are worked up to ρ^{-3} terms.

3) The Gaussian Hermite quadrature formula is particularly useful in evaluating the line integral along the steepest descent path. Let

$$ik\rho - ik_\rho \rho = x^2 \tag{5.18}$$

we have

$$k_z = - \frac{kx}{\sqrt{ik\rho}} \left[2 - \frac{x^2}{ik\rho}\right] \tag{5.19}$$

And the integral can be cast into the form

$$I_s = \int_{-\infty}^{\infty} f(x) \exp(-x^2)\, dx \tag{5.20}$$

where

$$f(x) = -\frac{I\ell}{4\pi} \frac{k_\rho^2}{k_z} \frac{x}{\rho} (1 + R^{TE}) H_1^{(1)}(k_\rho \rho) e^{ik_z z + x^2} \tag{5.21}$$

By the GHQ formula,

$$I_s = \sum_{j=1}^{n} w_i f(x_i) + R_n \tag{5.22}$$

where

x_i = ith zero of the Hermite polynominl $H_n(x)$

$$w_i = \sqrt{\pi}\, 2^{n-1}\, n!/n^2 [H_{n-1}(x_i)]^2 \tag{5.23}$$

is the weighting factor, and

$$R_n = \frac{\sqrt{\pi}\, n!}{2^n (2n)!} f^{(2n)}(\xi) \qquad -\infty < \xi < \infty \tag{5.24}$$

is the error term. For the case $\rho \lesssim d$, there are poles close to the contour of integration, and also the integrand oscillates rapidly due to the presence of the $\exp(i2k_{1z}d)$ factor in the reflection coefficient. With the knowledge of the locations of the poles, we can adjust n such that the error term R_n is vanishingly small.

Fig. 3 illustrates the case of a 4λ dielectric layer with permittivity $\varepsilon_1 = 2.16(1 + i0.002)$ over a perfect reflector. The saddle point contribution is calculated by using OSP, MSP and GHQ. It is seen that all three methods approach same values as $\rho > 100\lambda$. The MSP and GHQ coincides for $\rho > 10\lambda$. All three methods depart considerally for $\rho < 10\lambda$. Thus for $\rho < 10\lambda$, we recommand GHQ, for $10\lambda < \rho < 100\lambda$, one can use either MSP or GHQ. For $\rho > 100\lambda$, OSP is sufficiently accurate.

5.4 INTEGRATION ALONG THE BRANCHES CUTS

There are two branch points at $k_\rho = k_1$ and $k_\rho = k_2$. Correspondingly we choose two branch cuts $\mathrm{Re}(k_{1z}) = 0$ and $\mathrm{Re}(k_{2z}) = 0$. The integrand is an even function of k_{1z}. Thus the branch point at k_1 does not contribute to the integral. The contribution due to the branch point k_{2z} can be calculated by detouring the branch cut to a path parallel to the path of the steepest descent. The result is

$$I_b = \frac{I\ell}{2\pi}\left\{\frac{X_{01}X_{10}}{(1+e^{i2k_{1z}d}R_{01})^2}\ \frac{k_\rho^2 e^{-2\sqrt{k_2^2-k_1^2}\,d}}{k_{1z}k_z}\ \frac{e^{ik_2\rho}}{\rho^2}\right\}_{k_\rho = k_2} \tag{5.25}$$

Physically this corresponds to an inhomogeneous wave that decays away from the bottom surface with the exponential factor $\exp(-2\sqrt{k_2^2 - k_1^2}\,d)$.

Therefore, except in cases when the slab region is very thin, the effect due to the branch point k_2 is not observed on the surface of the layered medium.

In Figure 4, we show contributions due to the branch point for three cases. The permittivity of the first medium is $3.0(1 + i0.001)\varepsilon_0$ The permittivity of the second medium is $5.0(1 + i0.002)\varepsilon_0$ The depth varies from 0.05λ, 0.1λ, 0.2λ, 0.5λ, 1.0λ. Obviously, as the depth increases, the I_b effect diminishes.

5.5 RESULTS AND DISCUSSIONS

In the previous three sections, we have discussed the three separate contributions to the integral in (1). The total field at a receiving point due to a transmitting antenna is obtained by summing over all the three contributions. With applications to the radio frequency interferometry in mind, we illustrated the methods by calculating the interference patterns as a function of distance from the transmitter.

When the slab is sufficiently thin, no mode is excited and the integral is due to the saddle point and branch point k_2. Figure 5 shows interference patterns due to layers with $\varepsilon_1 = 3.0(1+i0.001)\varepsilon_0$ and depths 0.05λ and 0.1λ on top of a dielectric half-space with $\varepsilon_2 = 5.0(1+i0.002)\varepsilon_0$. The saddle point contribution is calculated by the ordinary saddle point method.

When the layer gets thicker, modes will be excited. We show in Figure 6 the interference patterns for the same media with depth .2, .5 and 1 wavelength. Only 1 to 3 creeping modes are excited. In Figure 7, we illustrated the case of a 4λ layer on top of a perfect conductor. The pole location plot has been shown in Figure 2. Because there are poles that are quite close to the saddle point, OSP and MSP are not applicable in near and intermediate ranges (Figure 3). The saddle point contribution in Figure 7 has been calculated with GHQ and MSP. GHQ result should be more accurate,especially in near field regions.

Thus the problem of electromagnetic fields due to a horizontal electric dipole antenna has been solved with the mode approach. We conclude that in calculating the saddle point contribution in the near field region, one should use the GHQ method. In intermediate regions, and in many cases far field zones, the MSP method whould be used when there are poles near the saddle point. When the layer is thick, all branch point contributions can be neglected. But when the layer is very thin, one must take into account the branch point contribution. Although the study is made for the two layer case, the approach can be readily extended to more than two layer cases.

FIGURE CAPTIONS

Figure 5.1 Pole plot on the complex θ-plane. The depth is $d = 4\lambda_0$, the permittivities are $\varepsilon_1 = 2.160 + i0.002$. The lower half-space is a perfect reflector.

Figure 5.2 Comparison of results by OSP, MSP and GHQ. The depth is $d = 4\lambda_0$, the permittivity is $\varepsilon_1 = 2.16(1+i0.002)$. The lower half-space is a perfect reflector.

Figure 5.3 Branch cut contribution compared for layer depths 0.05λ, 0.5λ and 1.0λ. The permittivities are $\varepsilon_1 = 3.0(1+i0.001)$ and $\varepsilon_2 = 5.0(1+i0.002)$. The vertical scale is 40db per division.

Figure 5.4 Interference patterns for thin layers. There is no pole contributions. The permitivitties are $\varepsilon_1 = 3.0(1+i0.001)$ and $\varepsilon_2 = 5.0(1+i0.002)$. The patterns are plotted for $d = 0.05\lambda$ and $d = 0.1\lambda$. Vertical scale is 20db/division.

Figure 5.5 Interference patterns for a layer with $\varepsilon_1 = 3.0(1+i0.001)$ on top of a half-space with $\varepsilon_2 = 5.0(1+i0.002)$. Calculations are done for three layer depths. When $d = 0.2\lambda$ and 0.5λ, there is only 1 creeping mode being excited. When $d = 1\lambda$, 3 creeping modes are excited. Vertical scale is 20db per division.

Figure 5.6 Interference patterns calculated with both MSP and GHQ. The depth is $d = 4\lambda$ and the permittivity is $\varepsilon_1 = 2.6(1+i0.0022)$. The subsurface is a perfect conductor.

Figure 5.1

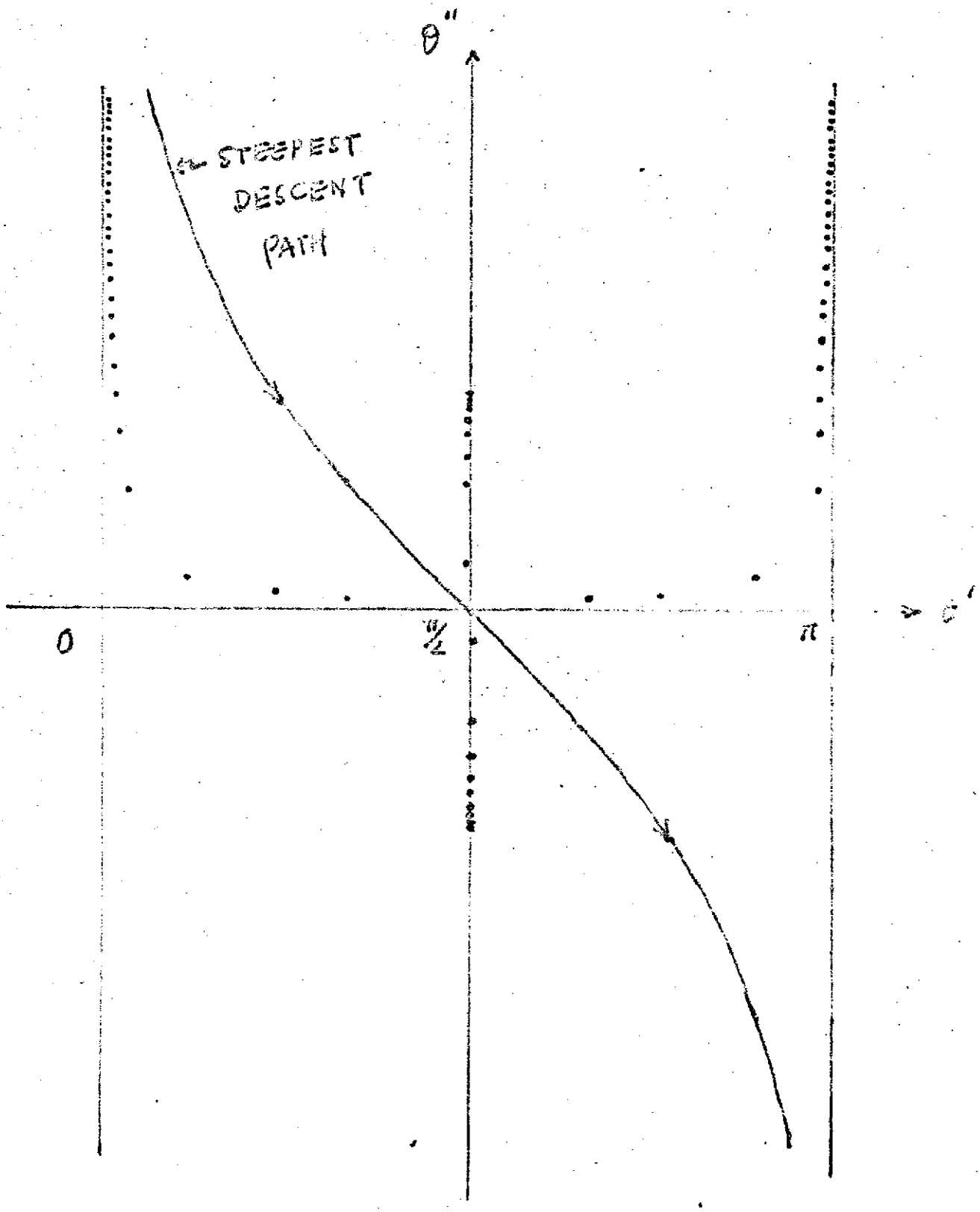

Figure 5.2

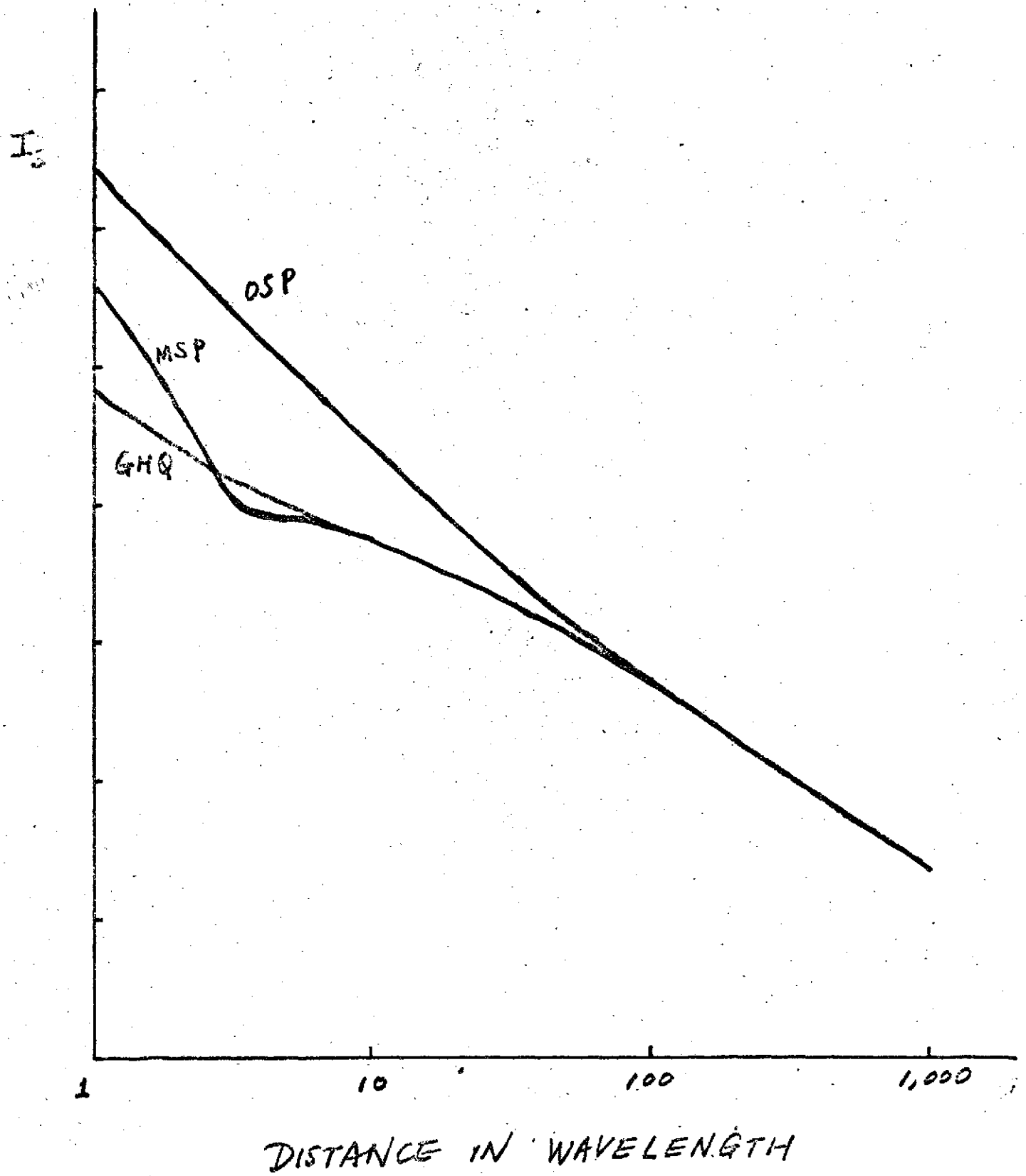

Figure 5.3

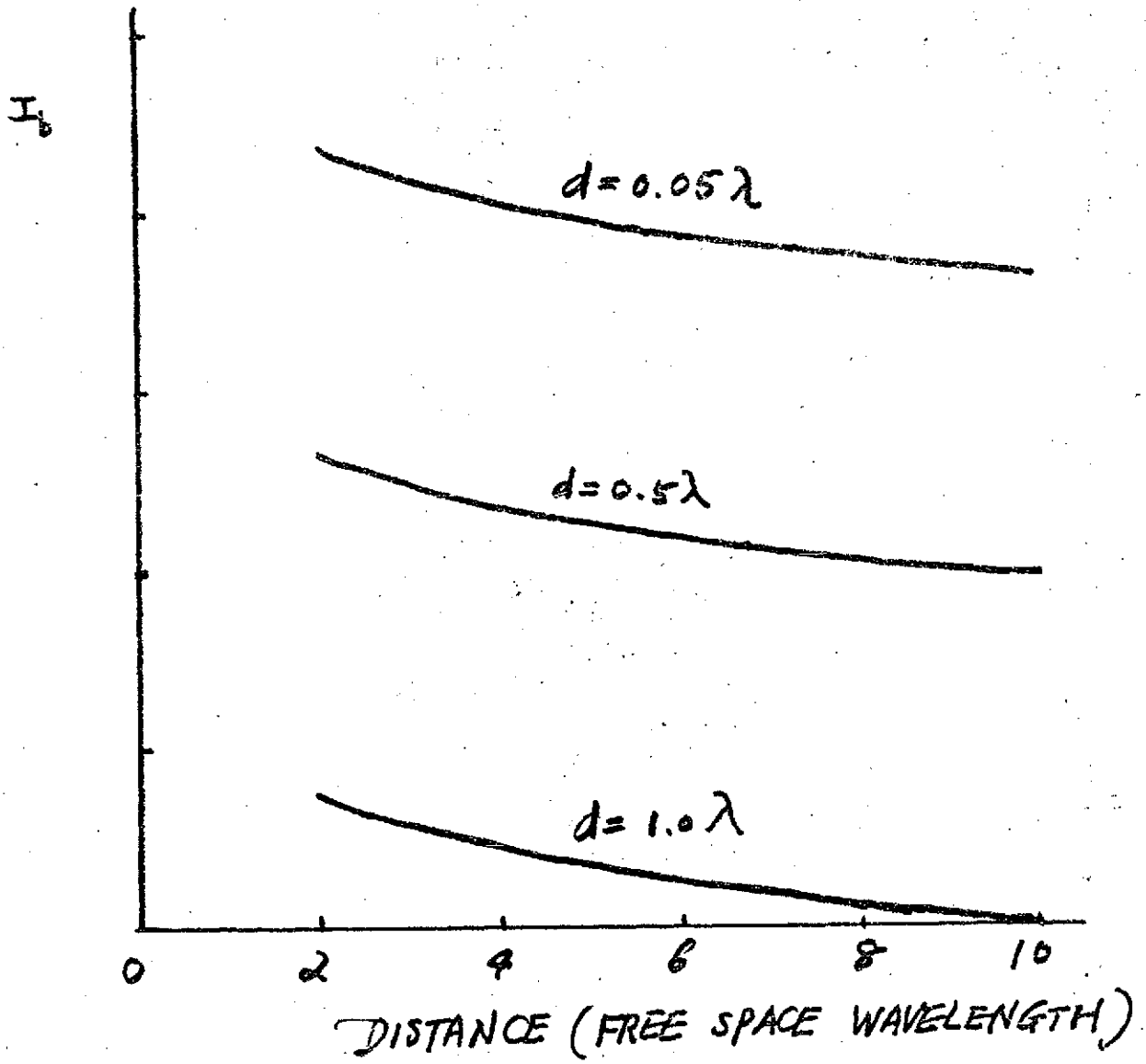
I_b
$d = 0.05\lambda$
$d = 0.5\lambda$
$d = 1.0\lambda$
0
2
4
6
8
10
DISTANCE (FREE SPACE WAVELENGTH)

Figure 5.4

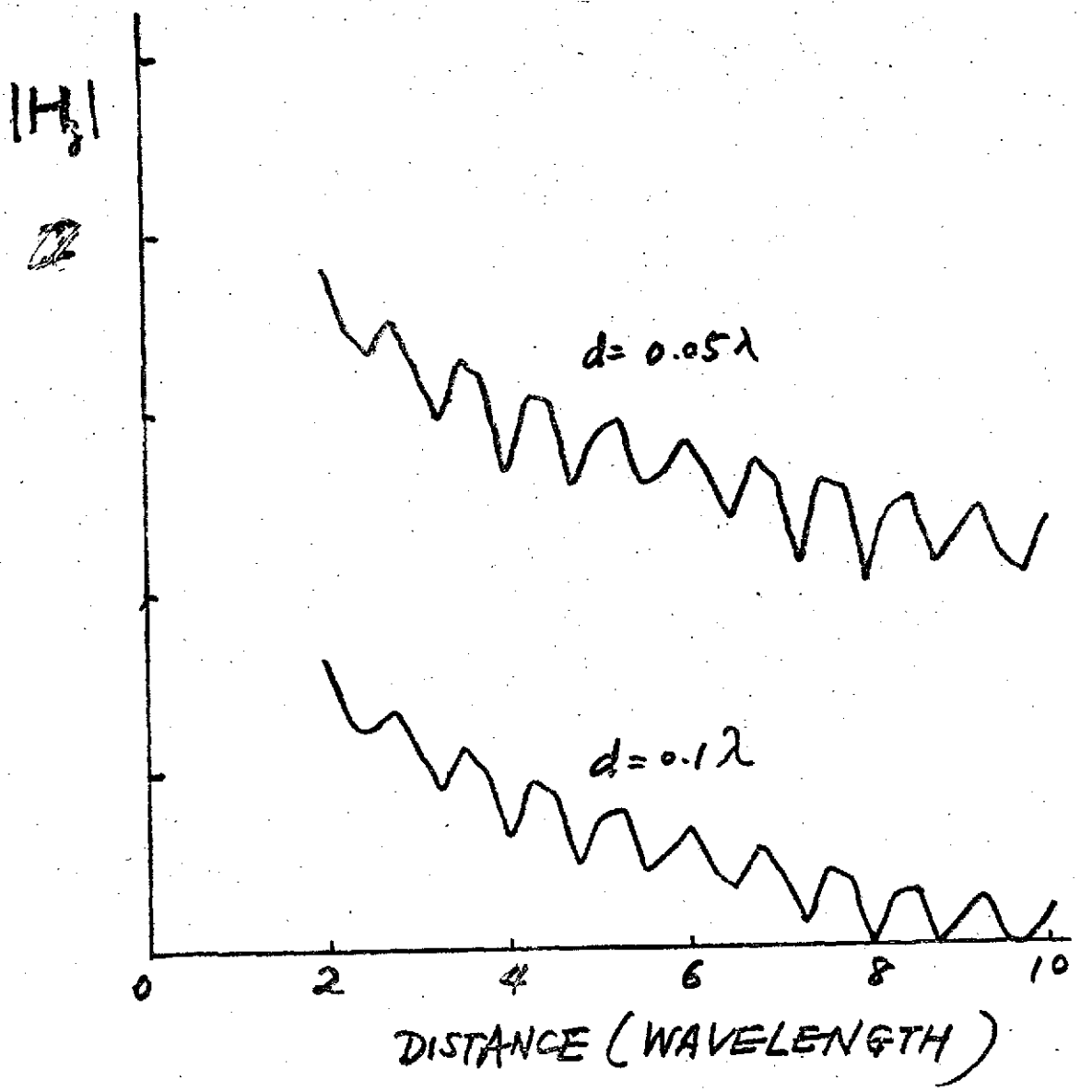

Figure 5.5

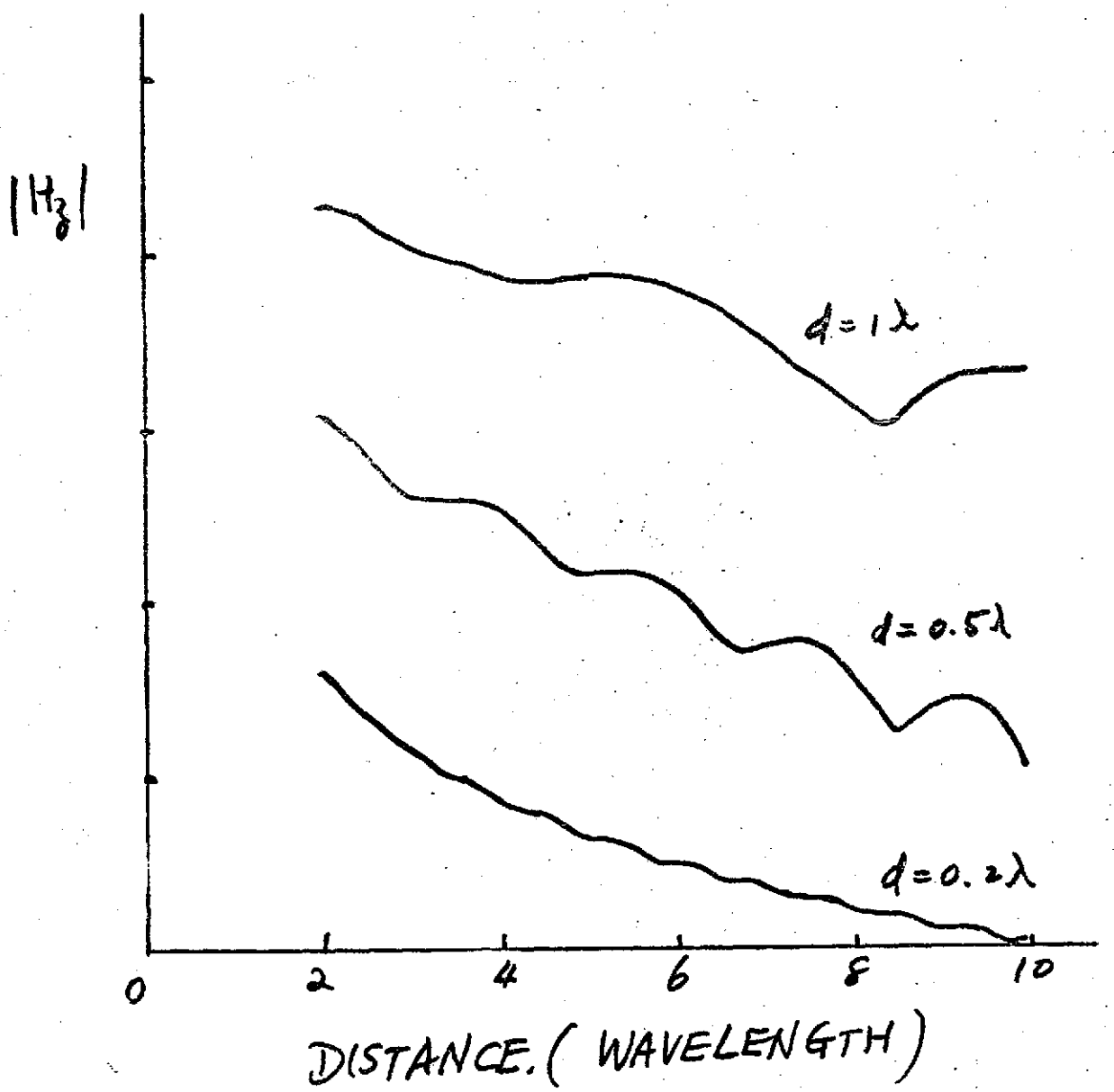
$|H_3|$
$d = 1\lambda$
$d = 0.5\lambda$
$d = 0.2\lambda$
0
2
4
6
8
10
DISTANCE. (WAVELENGTH)

Figure 5.6

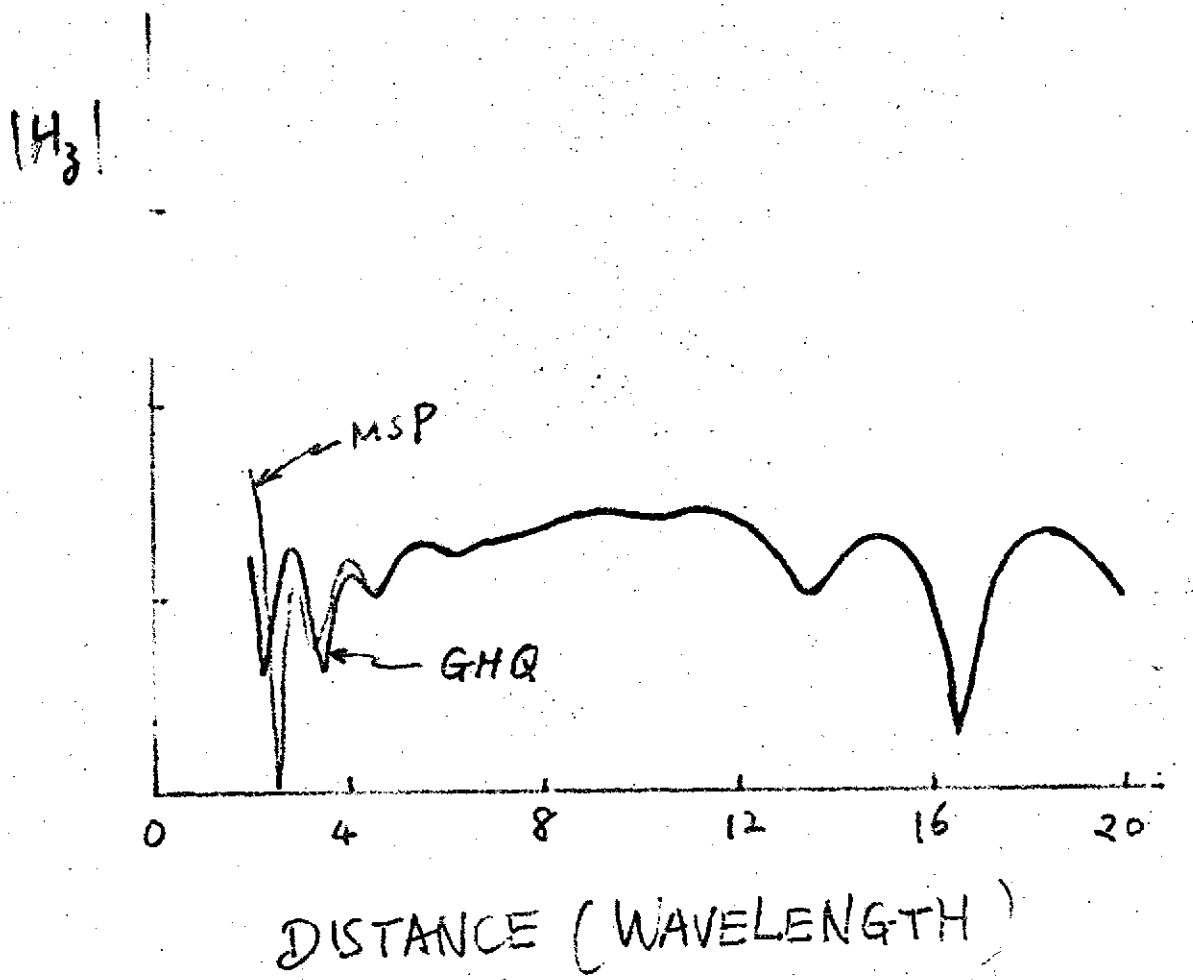

Chapter 6.

NUMERICAL APPROACH

6-1 SIMPSON'S RULE

The integrals in Eqs. (1) and (2) can be readily evaluated numerically provided they are well defined and properly convergent. In the actual computation procedures, we change the Hankel functions to Bessel functions and integrate from 0 to ∞ instead of from $-\infty$ to $+\infty$. Although the Hankel function has a singularity at $k_\rho = 0$, the integrand as a whole is regular at that point. For the integrands to be well defined, we must avoid the branch point $k_\rho = k$. When $\mathrm{Im}(k) \neq 0$, the branch point does not lie on the path of integration. If $\mathrm{Im}(k) = 0$, we choose the Sommerfeld path for the integration.

Simpson's rule is used in carrying out the numerical integration. The amount of computer time needed to obtain a given accuracy is reduced in two ways. First, because of the presence of the factor $\exp(ik_z z)$ in the integrand, we choose a non-zero z; the larger the z, the faster is the rate of convergence. Physically, this choice corresponds to having the receiving point above the surface. In the lunar experiment, the receiving antenna is about 2 to 3 meters above ground when mounted on the Lunar Roving Vehicle. Secondly, we vary the integration increments Δk_ρ as a function of distance from the transmitter. The magnitude of Δk_ρ depends mainly on the rate of oscillation of the

Bessel function which for large value of the argument $k_\rho\rho$ is proportional to $\cos k_\rho\rho$.

For comparison with other techniques, we have evaluated numerically the H_z-component of a two layer model with a perfect reflector. The frequency is 8MHz which corresponds to a free-space wavelength of $\lambda_0 = 37.5$ meters. The layer has dielectric constant $3.3\varepsilon_0$, loss tangent 0.01, and a layer thickness of $4\lambda_0$. The results are shown in Fig. 6. The receiving antenna has a height of 3 meters. We used $\Delta k_\rho\rho$ as small as 0.5 to determine the increment Δk_ρ. With a distance of $\rho \leq 14\lambda_0$, $\Delta k_\rho = 0.5/14\lambda_0 \simeq 0.004$. The computation is stopped when the absolute magnitude of the integrand becomes smaller than 0.002 of the accumulative area. A typical value of the number of increments used for computation is about 5,000. Computation time with the IBM 360-65 was about 2 minutes per point as shown in Figure .

6.2 FAST FOURIER TRANSFORM METHOD

Separate the integral (1) into two parts I_1 and I_2. The first part corresponds to solutions in the absence of any stratified medium, and the result is given by the identity

$$I_1 = \frac{\partial}{\partial \rho} \frac{e^{ikr}}{r} = \frac{-i}{2} \int_{-\infty}^{\infty} \frac{k_\rho^2}{k_z} e^{ik_z z} H_1^{(1)} (k_\rho \rho) \, dk_\rho \tag{6.1}$$

The second part includes all effects due to the reflection coefficient R^{TE} and after changing to Bessel functions,

$$I_2 = \int_0^{\infty} dk_\rho \frac{iI\ell k_\rho^2}{4\pi k_z} R^{TE} e^{ik_z z} J_1(k_\rho \rho) \sin\phi \tag{6.2}$$

which is the integral that we want to solve with the FFT.

In applying the FFT, we use the formula (Gradshteyn and Ryzhik, 1965)

$$\int_0^{\infty} e^{-\nu k\rho} J_1(k_\rho \rho) dk_\rho = \frac{1}{\rho} \left(1 - \frac{\nu}{\sqrt{\nu^2 + \rho^2}}\right) \tag{6.3}$$

$$\nu = \nu_R + i\nu_I, \quad \mathrm{Re}\{\nu + i\rho\} > 0$$

The integral is written in the following form

$$I_2 = \int_0^{\infty} dk_\rho \, g(k_\rho) e^{-\nu_R k\rho} J_1(k_\rho \rho) dk_\rho \tag{6.4}$$

where

$$g(k_\rho) = i \frac{I\ell}{4\pi} \frac{k_\rho^2}{k_z} R^{TE} e^{ik_z z + \nu_R k_\rho} \tag{6.5}$$

We can write (Cooley, 1967) for $\Delta k_\rho \simeq 1/2F$ where F is the Nyquist frequency

$$g(k_\rho) = \frac{1}{N\Delta k_\rho} \sum_{n=-\frac{N}{2}}^{\frac{N}{2}-1} a(f) \; e^{i2\pi f k_\rho} \text{for } 0 < k_\rho < (\tfrac{N}{2} - 1)\Delta k_\rho \tag{6.6}$$

where

$$a(f) = \int_{-\infty}^{\infty} g(k_\rho) e^{-2\pi i f k_\rho} \, dk_\rho$$

$$f = n/N\Delta k_\rho$$

The factor $-2\pi f$ corresponds to ν_I in Equation (6). The right hand side of (9) is periodic and does not tend to zero at ∞. We can multiply (9) by $\exp(-\nu_R k_\rho)$ so that the right hand side of (9) is sufficiently small for the range of k_ρ between $(\frac{N}{2} - 1)\Delta k_\rho$ and ∞. Then the final solution becomes, in view of the identity (6)

$$I_2 = \frac{1}{N\Delta k_\rho} \sum_{n=-N/2}^{\frac{N}{2}-1} a(\frac{n}{N\Delta k_\rho}) \frac{1}{\rho} \left[1 - (\nu_R - \frac{i2\pi n}{N\Delta k_\rho}) / \sqrt{(\nu_R - i2\pi n/N\Delta k_\rho)^2 + \rho^2}\right] \tag{6.7}$$

In choosing the increment Δk_ρ, we recall the two alternatives suggested in Section II. If we make the upper half space slightly conductive, which corresponds to Im k $\neq$ 0, then we choose Δk_ρ to be smaller than the distance of the branch point from the real axis on the complex k_ρ-plane. If we insist on a real k, then we choose Δk_ρ such that one of the data points coincides with the branch point and such that Δk_ρ is smaller than the distance of the pole or branch point closest to the real axis on the complex k_ρ-plane.

To calculate the expansion coefficient a in Equation (9) we use the FFT algorithm in a subroutine which, for a given set of data d_k, returns the result

$$T_j = \sum_{n=0}^{N-1} d_k e^{-i\frac{2\pi jn}{N}} \qquad j = 0, 1, \ldots N-1 \qquad (6.8)$$

We first alias the function $g(k_\rho)$ with period $N\Delta k_\rho$ and denote the aliased version by $g_p(k_\rho)$. The subroutine requires data points of $g_p(k_\rho\rho)$ between 0 and $(N-1)\Delta k_\rho$. Note that the function $g_p(k_\rho\rho)$ is equal to $g(k_\rho)$ between 0 and $(N/2-1)\Delta k_\rho$ but $g_p(k_\rho)$ between $(\frac{N}{2}-1)\Delta k_\rho$ and $(N-1)\Delta k_\rho$ is equal to $g(k_\rho)$ between $-(N/2)\Delta k_\rho$ and $-\Delta k_\rho$. In the subroutine we calculate

$$a_p\left(\frac{n}{N\Delta k_\rho}\right) = \Delta k_\rho \sum_{\ell=0}^{N-1} g_p(\ell\Delta k_\rho)\, e^{-i2\pi\ell n/N} \qquad n = 0, 1, \ldots N-1 \tag{6.9}$$

and returns the aliased version of $a(n/N\Delta k_\rho)$, $a_p(n/N\Delta k_\rho)$. We must be careful in translating from $a_p(n/N\Delta k_\rho)$ to $a(n/N\Delta k_\rho)$ within the limits $-\frac{1}{2\Delta k_\rho}$ to $\frac{1}{2\Delta k_\rho}$ in order to use the result (10).

We must choose $N\Delta k_\rho$ such that the function $g(k_\rho)$ is sufficiently near zero outside the limits $-N\Delta k_\rho/2$ to $N\Delta k_\rho/2$. Although mathematically, we could choose z to be large, its value is predetermined by the experimental arrangement. ν_R must not be too small. Note that ν_R must be greater than zero but cannot be larger than z or the exponent in (8) will cause $g(k_\rho)$ to diverge. We choose $\nu_R = z/2$.

In Figure 1 and Figure 2, we show the interference patterns for H_z calculated with FFT on the IBM 360/65 computer for a three layer and a six layer case, respectively. The height of the observation point, $z = 0.213\lambda_0$ which corresponds to 2 meters for a frequency of 32 MHz (values that were used in the lunar experiment). The computation time was about 2.5 minutes for both cases. These results are to be compared with the results obtained with Simpson's rule and shown also in Figures 1 and 2.

6.3 DISCUSSION

We have shown that with the reflection coefficient formulation, the problem of calculating the electromagnetic field components due to a dipole transmitting antenna on a stratified medium can be solved readily with the FFT algorithm and the Simpson's rule and illustrated for H_z for a three layer and a six layer case. See Figures 1 and 2.

In Figure 3, we compare the FFT method with results from the geometrical optics approximation and the mode analysis. The analytical methods consume very little time, but they are applicable only in certain regions according to the nature of the approximations involved. The geometrical optics result applies when the distance is far from the transmitting antenna and when the layer is thick and lossy. The mode method can be applied to general cases, and is extremely useful for thin layers. The FFT results for some general stratified media are also presented in Figures 4 - 9.

FIGURE CAPTIONS

Figure 1. Comparison of the direct and FFT methods for a three layer model in which

$\varepsilon_1 = (3.3)(1 + i0.01)\varepsilon_0$ $\quad d_1 = 1\lambda$

$\varepsilon_2 = (5.0)(1 + i0.02)\varepsilon_0$ $\quad d_2 = 2\lambda$

$\varepsilon_3 = (8.0)(1 + i0.04)\varepsilon_0$

Vertical scale is 10 db per division.

Figure 2. Comparison of the direct and FFT methods for a six layer model in which

$\varepsilon_1 = (2.0)(1 + i0.01)\varepsilon_0$ $\quad d_1 = 0.5\lambda$

$\varepsilon_2 = (3.0)(1 + i0.02)\varepsilon_0$ $\quad d_2 = 1\lambda$

$\varepsilon_3 = (4.0)(1 + i0.03)\varepsilon_0$ $\quad d_3 = 2\lambda$

$\varepsilon_4 = (5.0)(1 + i0.04)\varepsilon_0$ $\quad d_4 = 3\lambda$

$\varepsilon_5 = (6.0)(1 + i0.05)\varepsilon_0$ $\quad d_5 = 4\lambda$

$\varepsilon_t = (8.0)(1 + i0.06)\varepsilon_0$

Vertical scale is 10 db per division.

Figure 3. Comparison of the FFT, Geometrical Optics (GOA), and Mode Theory (MODE) for a two layer model in which

$\varepsilon_1 = 3.3(1 + i0.02)\varepsilon_0$ $\quad d_1 = 4\lambda$

$\varepsilon_t = 6.0(1 + i0.04)\varepsilon_0$

Vertical scale is 10 db per division.

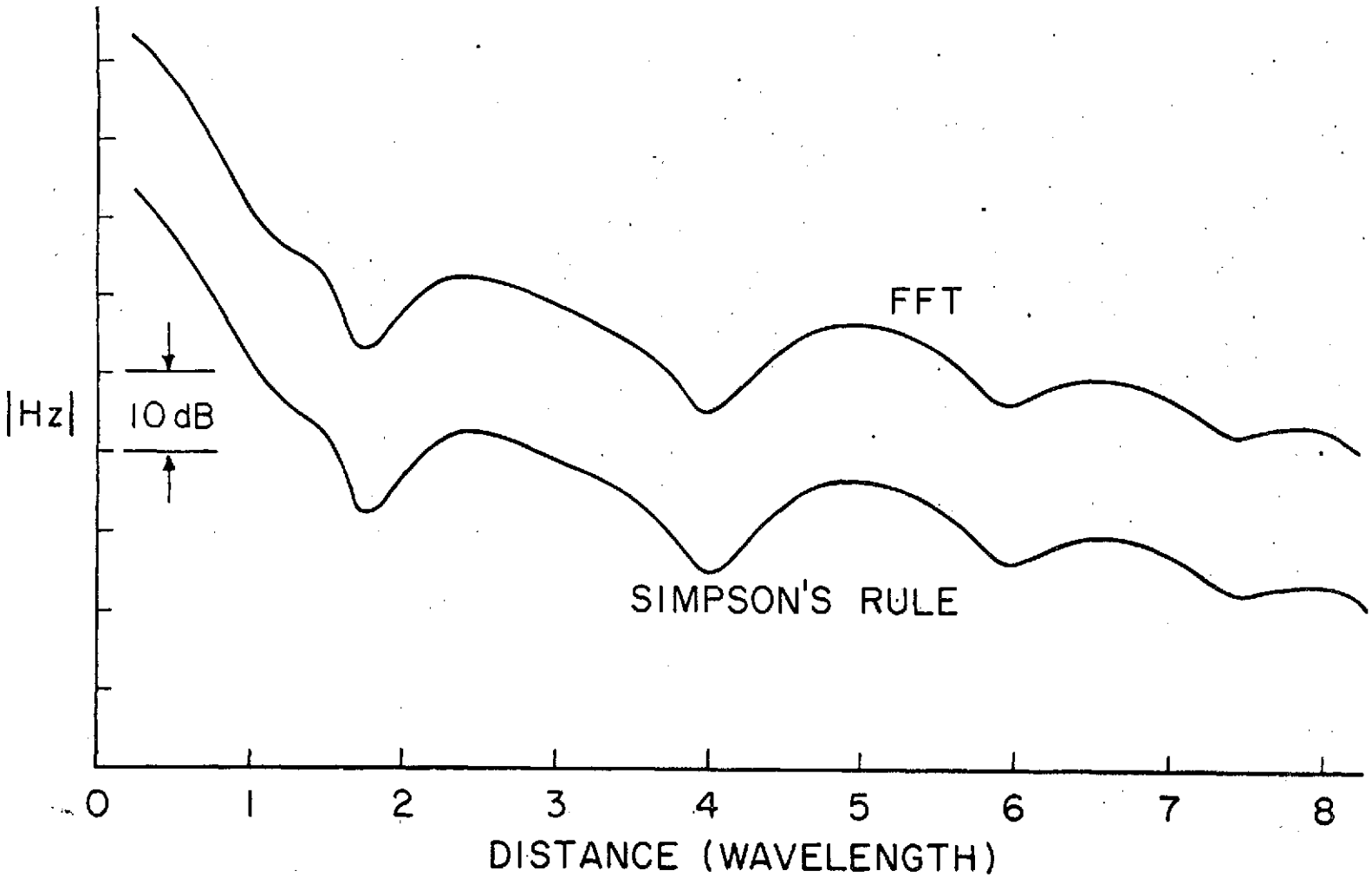

Figure 6.1

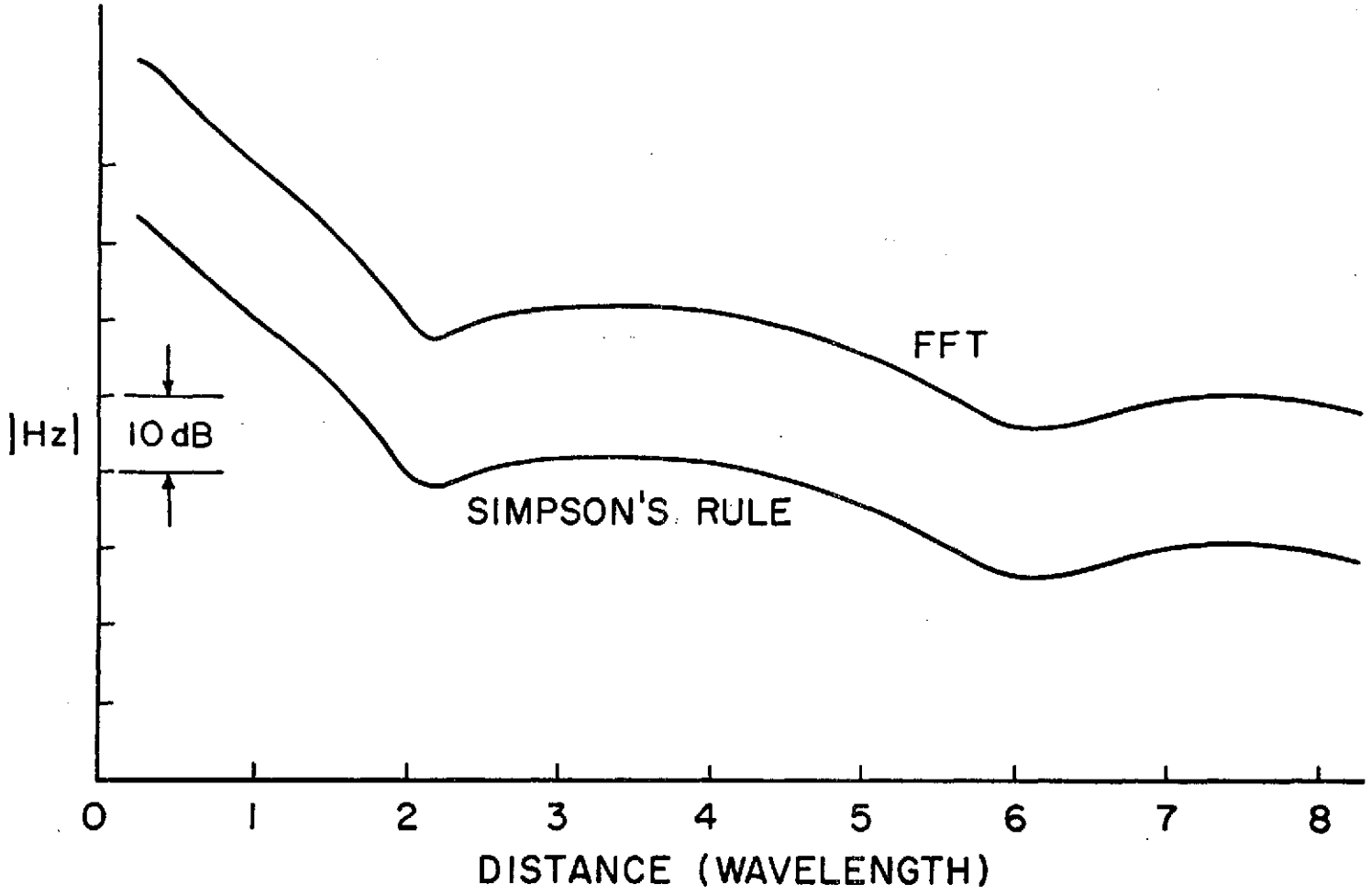

Figure 6.2

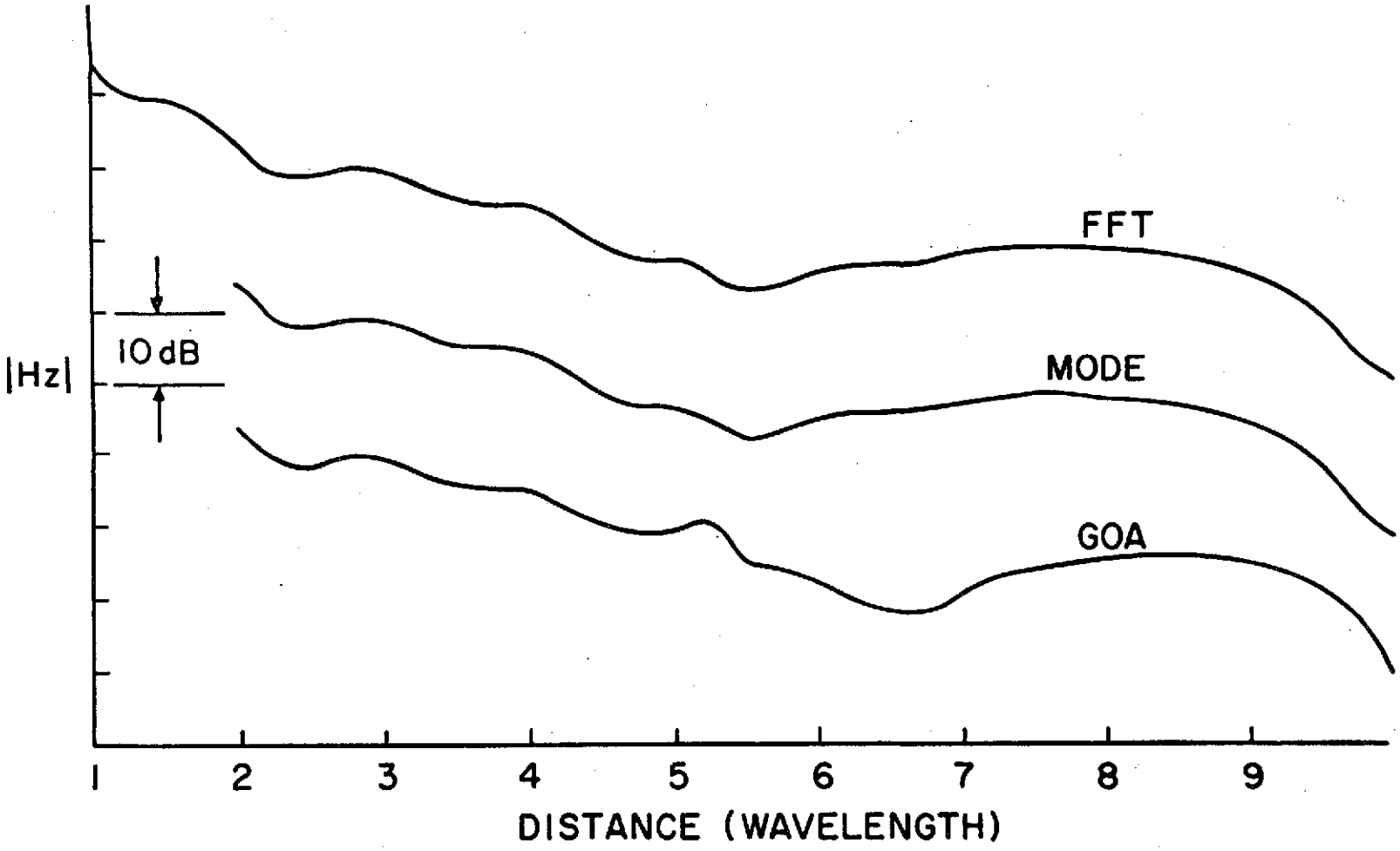

Figure 6.3

Figure 6.4

NLAYS= 4 FREQ= 32.000000

DL, LT, PERM, ANIS				DEPTH in meters
1.000	0.0	1.000	1.000	
				0.0
3.200	0.003125	1.000	1.000	
				15.0
4.200	0.003125	1.000	1.000	
				45.0
5.400	0.003125	1.000	1.000	
				******

Z= 0.213333 λ_0

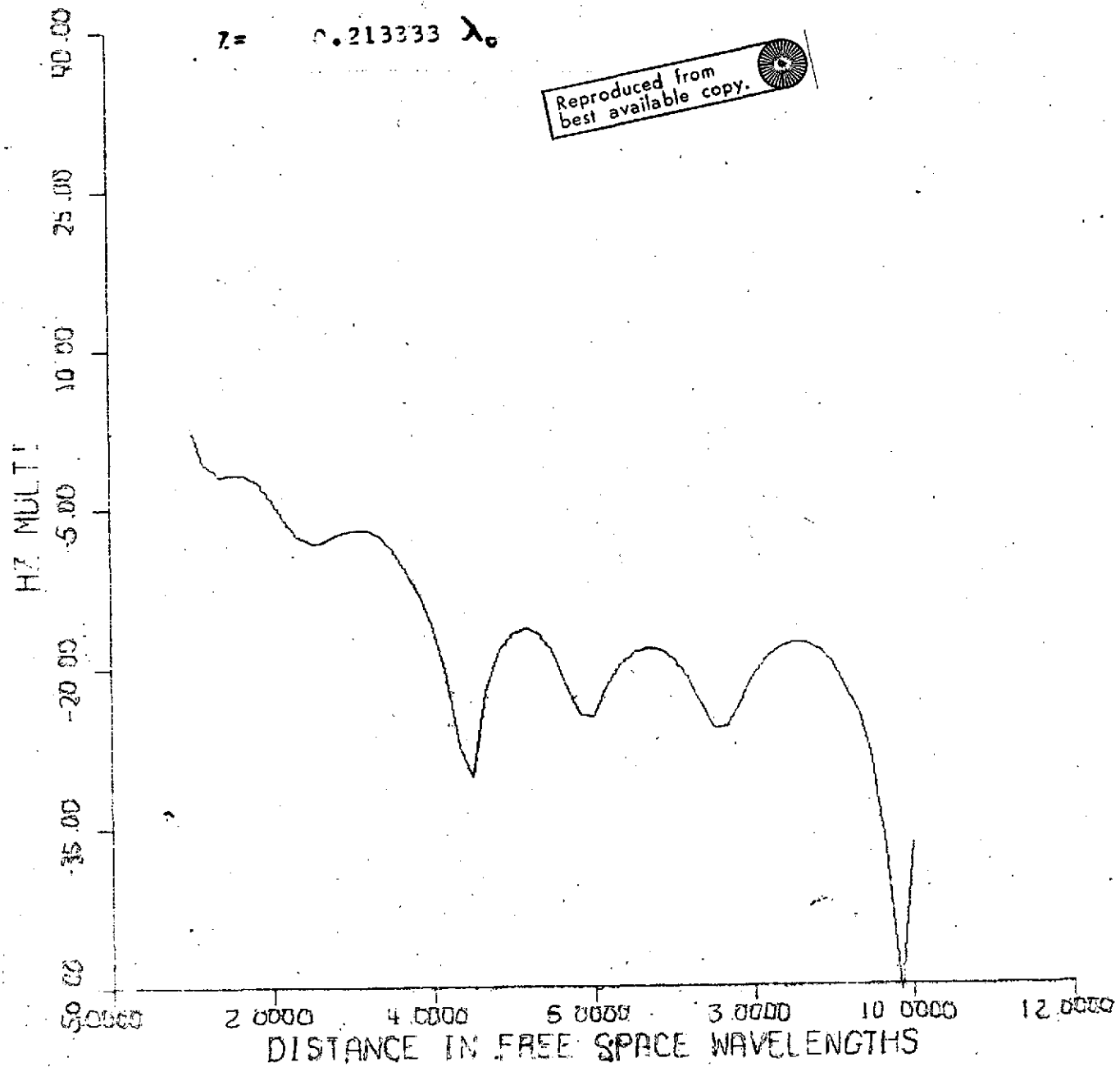

Figure 6.6

NLAYS= 4 FREQ= 8.000000

DEPTH in meters	DELT, PERM, ANIS			
	1.000	0.0	1.000	1.000
0.0	3.200	0.012500	1.000	1.000
15.0	4.200	0.012500	1.000	1.000
45.0	5.400	0.012500	1.000	1.000
******				

Z= 0.053333 λ_0

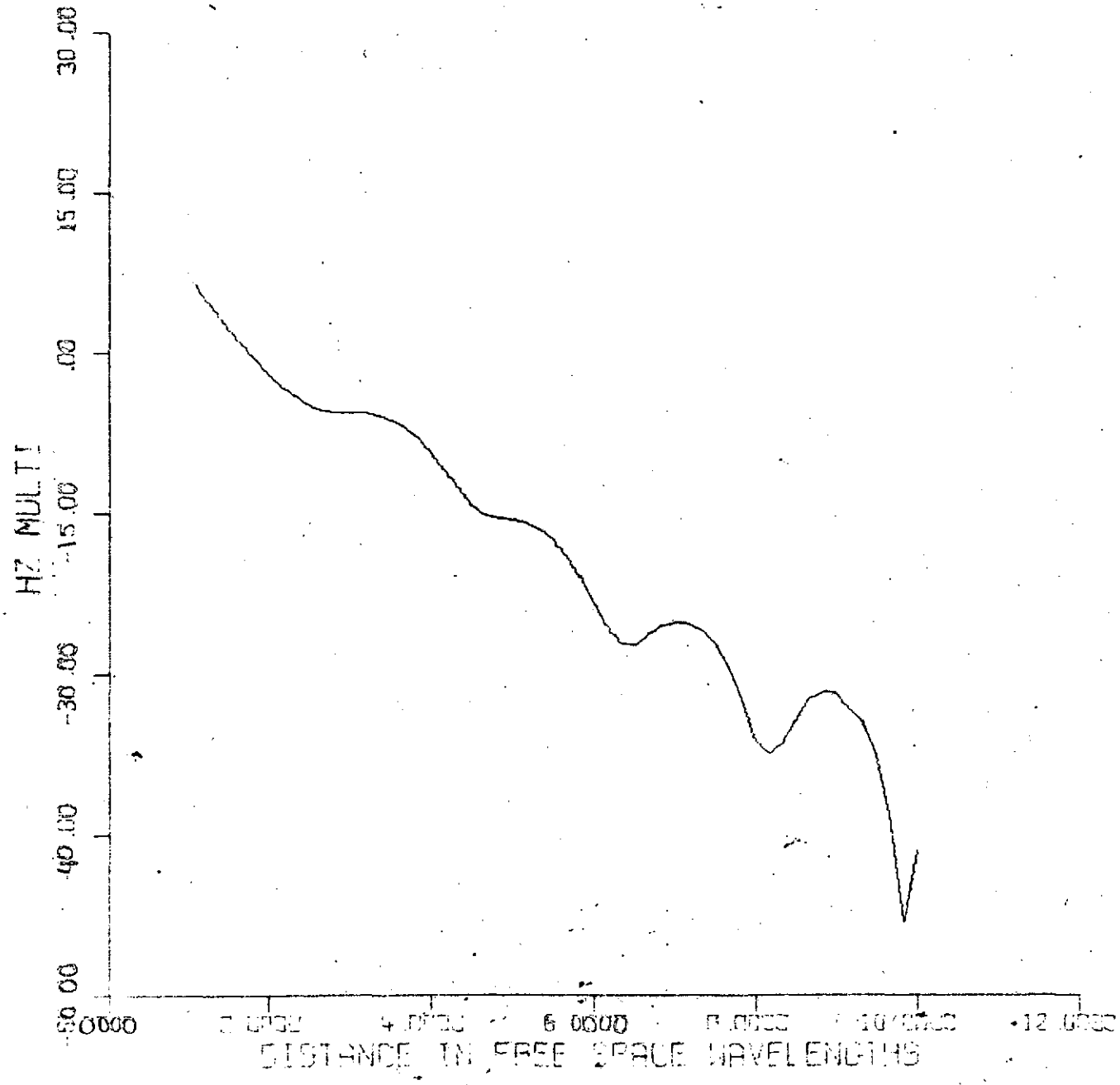

Figure 6.5

NLAYS= 4 FREQ= 16.000000

DL,LT,PERM,ANIS				DEPTH in metres
1.000	0.0	1.000	1.000	
				0.0
3.200	0.006250	1.000	1.000	
				15.0
4.200	0.006250	1.000	1.000	
				45.0
5.400	0.006250	1.000	1.000	
				******

$\dot{Z}$= 0.106667 λ_0

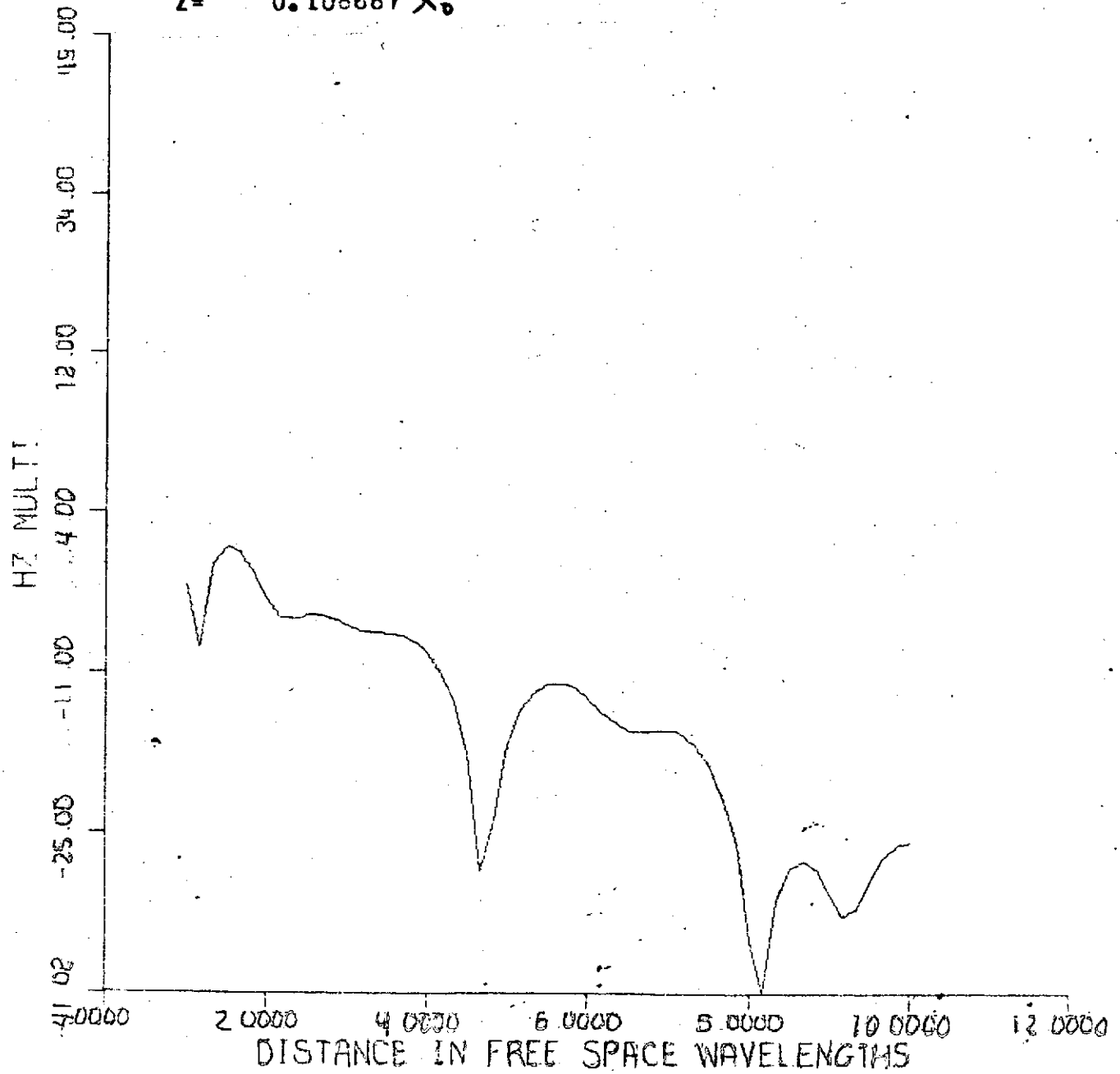

Figure 6.7

NLAYS= 4 FREQ= 32.000000

CL,LT,PERM,ANIS				DEPTH in meters
1.200	0.0	1.000	1.000	
3.200	0.003125	1.000	1.200	0.0
4.200	0.003125	1.000	1.200	15.0
5.400	0.003125	1.000	1.200	45.0
				******

Z= 0.213333 λ_0

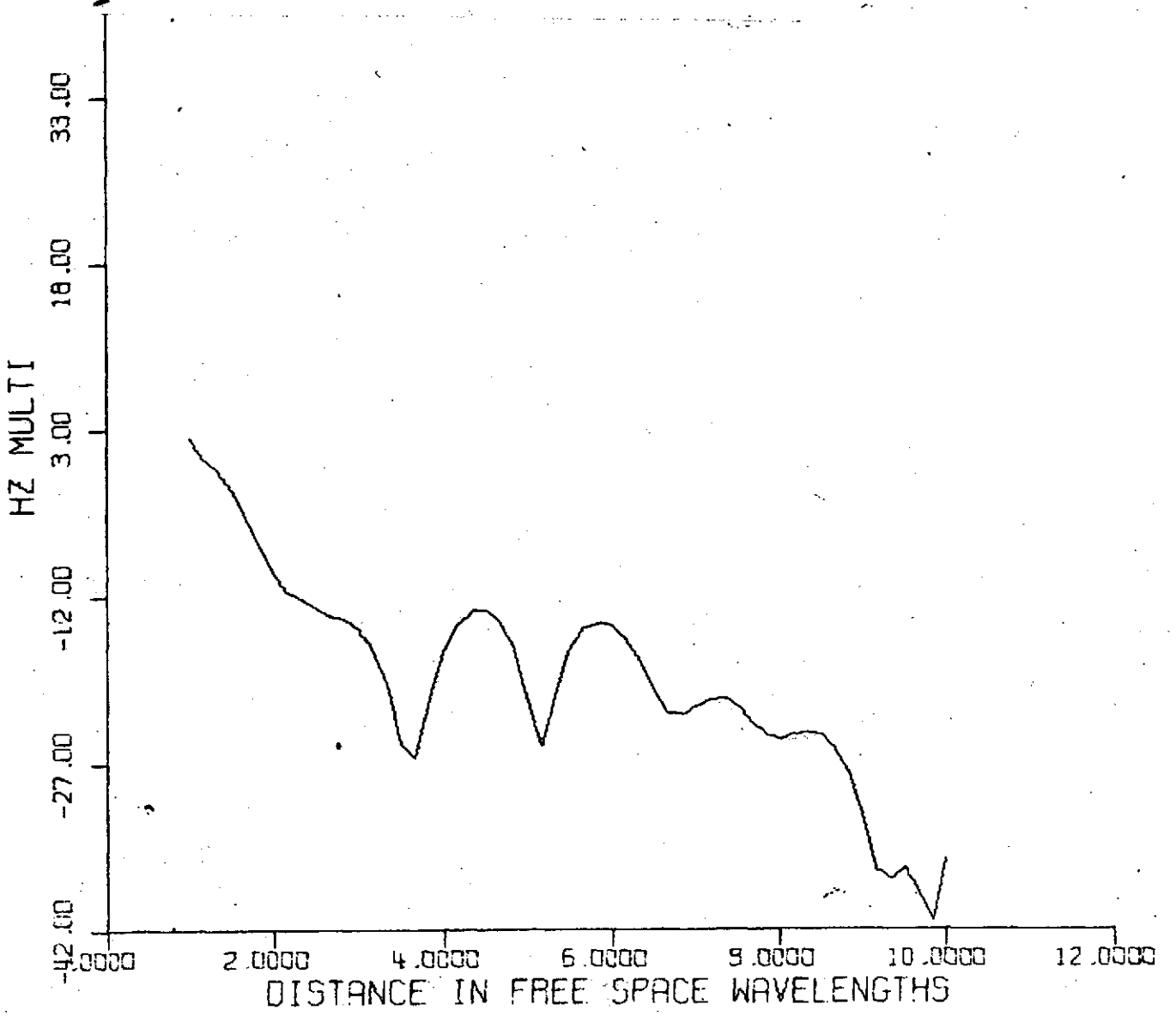

Figure 6.8

NLAYS= 4 FREQ= 16.000000

DL,LT,PERM,ANIS				DEPTH in water
-1.000	0.0	1.000	1.000	
				0.0
3.200	0.000250	1.000	1.200	
				15.0
4.200	0.000250	1.000	1.200	
				45.0
5.400	0.000250	1.000	1.200	
				******

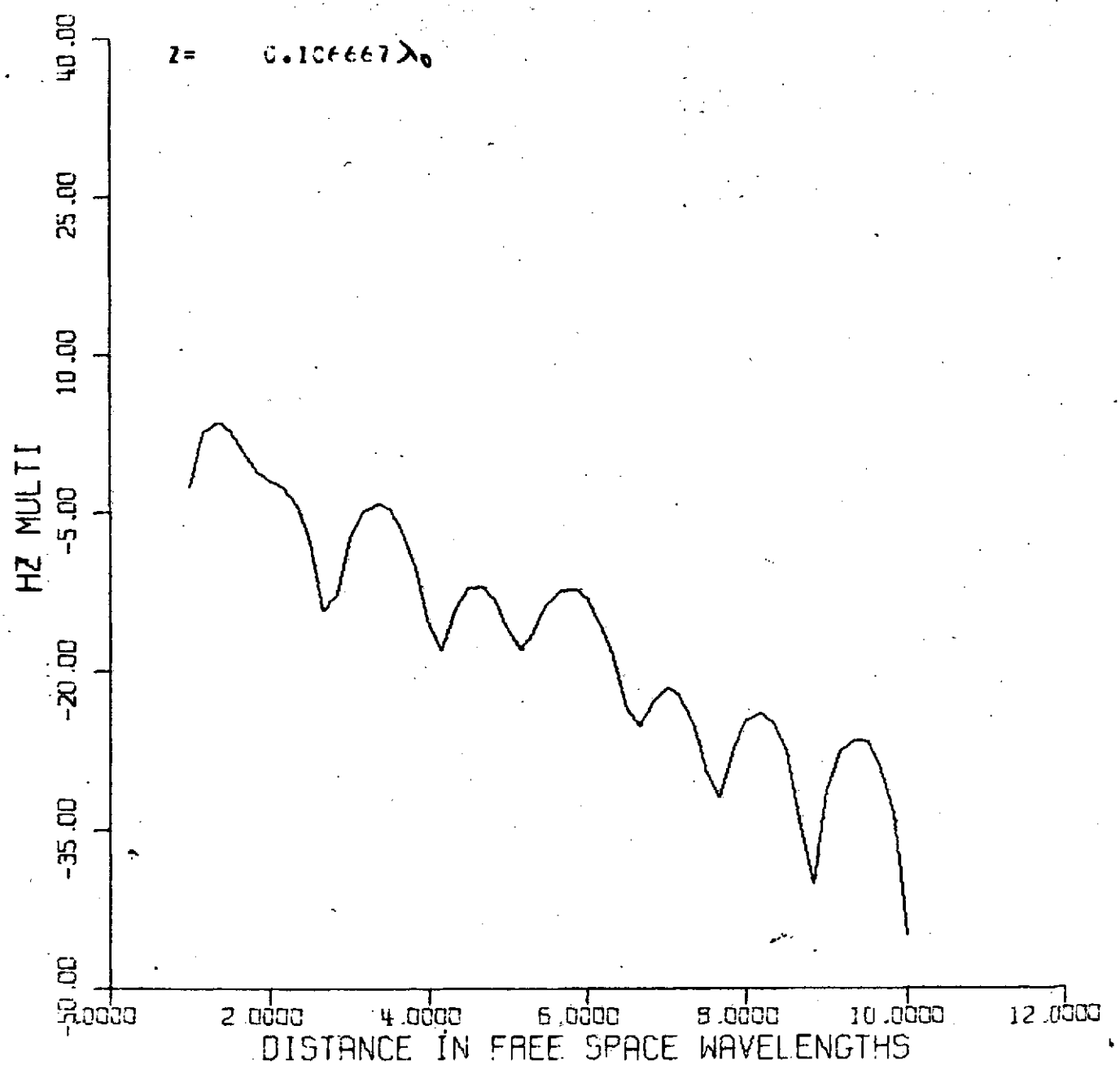

Figure 6.9

NLAYS= 4 FREQ= 8.000000

DL,LT,PERM,ANIS				DEPTH in meters
1.000	0.0	1.000	1.000	0.0
3.200	0.012500	1.000	1.200	15.0
4.200	0.012500	1.000	1.200	45.0
5.400	0.012500	1.000	1.200	******

z= 0.053333 λ_0

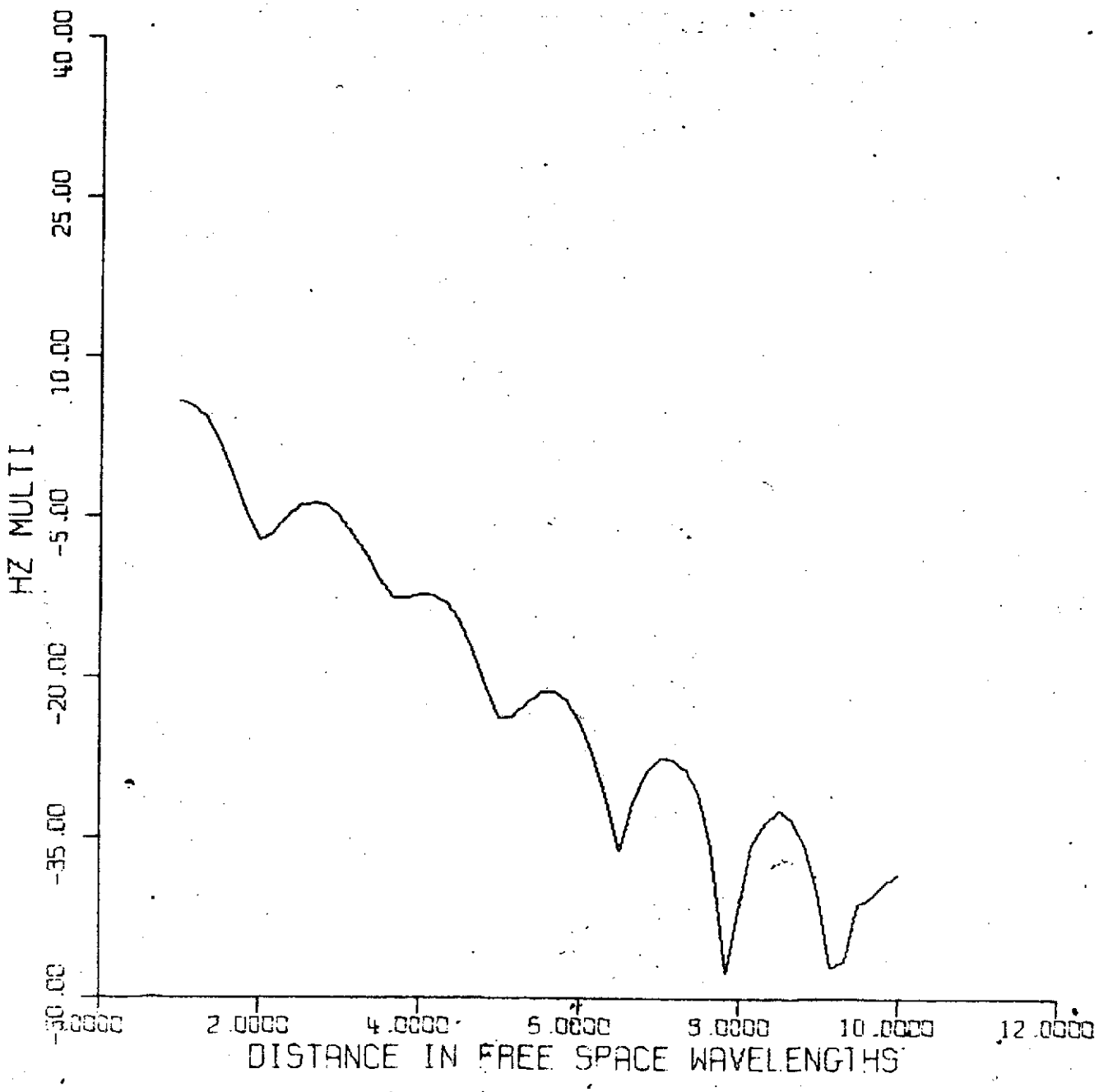

Chapter 7.

DISCUSSIONS

7.1 COMPARISON OF THEORETICAL SOLUTIONS

In Figure 7.1, we show H_z as a function of distance calculated on the basis of the tree different approaches for a single model. The model consists of a single layer, 4λ in thickness, with $\varepsilon = 33\varepsilon_0$ and $\tan\delta = 0.01$, between free space above and a perfect conductor below. The fields are calculated for a receiver at a height of 3 meters above surface at 8 MH_z. Inspection of the figure shows that the results from the mode analysis agree well with those obtained from numerical integration. Note in particular that the positions of the first peaks in the geometrical optics approximation and in the mode analysis occur at different locations. In the geometrical optics approach, if this peak is used to predict the depth of the subsurface reflector, we see that the mode analysis will predict a smaller depth. In the following sections, the theoretical calculations are compared with the various experimental results.

7.2 EXPERIMENTAL CONFIRMATION

Both the concept of this experiment and the equipment have been tested extensively on glaciers and with laboratory-sized scale models. Because of the variability of natural materials, we used three different glaciers— the Goner Glacier in Switzer-

land, the Athabasca Glacier in Alberta, and several glaciers that drain the Juneau, Alaska icefields. Each of these glaciers had been studied previously. Because the shape, depth, and physical properties of each glacier were known already, the data obtained on the glaciers can be used to check our theoretical expressions. Although we have collected data on several profiles on the Gorner, about 50 profiles on the Athabasca and about 120 profiles on the Juneau glacidrs, with lengths of 1 to $1\frac{1}{2}$ km, we shall cite results for only two profiles. These results are typical of the other profiles.

The Gorner glacier, located in southern Switzerland, has been studied for more than a century. The rather extensive set of data includes the results of gravity, seismic, and (D.C.) electrical resistivity surveys. The thickness and shape of the glacier were well-determined. Our field gear was quite simple and included a General Radio 1330A bridge oscillator for the transmitter, a Galaxy R530 communications receiver, and homemade antennas. The glacier was quite thick in our test area. In Fig. 7.2 we show the interference pattern of the vertical magnetic component for the broadside transmitting antenna at 10 MHz. The observed peaks and troughs match very well the corresponding features in the theoretical curve calculated for a one layer medium with dielectric constant $3.2\varepsilon_0(1 + i0.03)$.

The Athabasca glacier, located about 75 miles south of Jasper, Alberta, Canada, has been thoroughly studied[9-10] also by such other methods as seismology, gravity, electrical resistivity measure-

ments, and drill holes. The ice thicknesses measured by seismic reflections and by direct measurement in boreholes agree quite well and we use the profiles reported by Paterson and Savage as standards with which to compare the thicknesses determined from our electrical sounding technique. In figure 7.3, we show typical results, the interference pattern of the vertical magnetic component at 2 MHz. Note the excellent match between the experiment curve and the theortical curves obtained with both the geometrical optics approximation and the mode analysis. Our interferometry data indicate a depth of 180 meters which is in good agreement with the results of drilling, seismic and gravity surveys.

A scaled model tank, operating at 6 GHz, was used to obtain interference patterns for a dielectric layer with dielectric constant $2.16\varepsilon_o(1 + i0.0022)$ over an aluminum reflector. The general features of the model tank were described by Rossiter et al.[8], and some results from the study of this particular case for depths greater than 2λ were reported there, with our mode analysis, we are now able to match the experimental curves for shallower depths. In fig. 7.4, we show results for layer thicknesses of 1λ and 2λ. The curves are comapred with theoretical calculations from both the geometrical optics and the mode approaches. Note specifically that for these shallow depths the geometrical optics approximation fails to account for even the fross features whereas the mode approach fits the experimental data excellently.

CONCLUSIONS

The radiation fields due to a horizontal electric dipole laid on the surface of a stratified medium have been calculated with three different approaches and compared with the various experimental results. The solutions are obtained from the refflection coefficient formulation and written in integral forms. In the near field of the transmitting antenna, analytical methods involving asymptotic expansion are not applicable. Direct numerical integration of the integrals by a computer is the simplest and the most useful. The numerical method for near field calculations also yields accurate results and uses less computer time than far field calculations. When the receiver is far away from the transmitting antenna, the integrals can be evaluated asymptotically by the method of steepest decents. For high lossy media and large layer thickness, the geometical optics approach gives rather accurate results. The interference patterns calculated from this approach can be easily interpreted in terms of ray optics. When losses are small and layers are thin, the mode approach is most attractive. The results can be interpreted in terms of normal modes of the layered medium. Although the calculations and illustrations presented in this paper were done for the one layer and the two layer cases, the calculations can be readily generalized to handle more layers.

FIGURE CAPTIONS

Fig. 7.1 Comparison of theoretical results. These interference patterns are calculated for a dielectric layer with dielectric constant $3.3\varepsilon_o(1 + i0.01)$ overlying a perfect conductor. The receiver has a height of 0.08 wavelength.

Fig. 7.2 Comparison of Gorner glacier data with theoretical results for the vertical magnetic field component H_z at 10 MHz. The theoretical curve is calculated for a one-layer medium with dielectirc constant $3.2\varepsilon_o(1 + i0.03)$

Fig. 7.3 A set of Athabasca data taken at 2 MHz, site 3 compared with the theoretical results obtained with mode approach and geometircal optics approach. The theoretical results are calculated for a layer of ice with dielectric constant $3.3\varepsilon_o(1 + i0.15)$ and depth 1.2λ = 180meters.

Fig. 7.4 Scaled Model Tank experimental data compared with theoretical results obtained with the mode approach and the geometrical optics approximation. The model consists of a layer of oil with dielectric constant $\varepsilon = 2.16\varepsilon_o$ $(1 + i0.0022)$. The subsurface reflector is an aluminum plate. The upper set of curves is for a layer thickness of 1λ, the lower set for 2λ, λ being the free space wavelength.

Figure 7.1

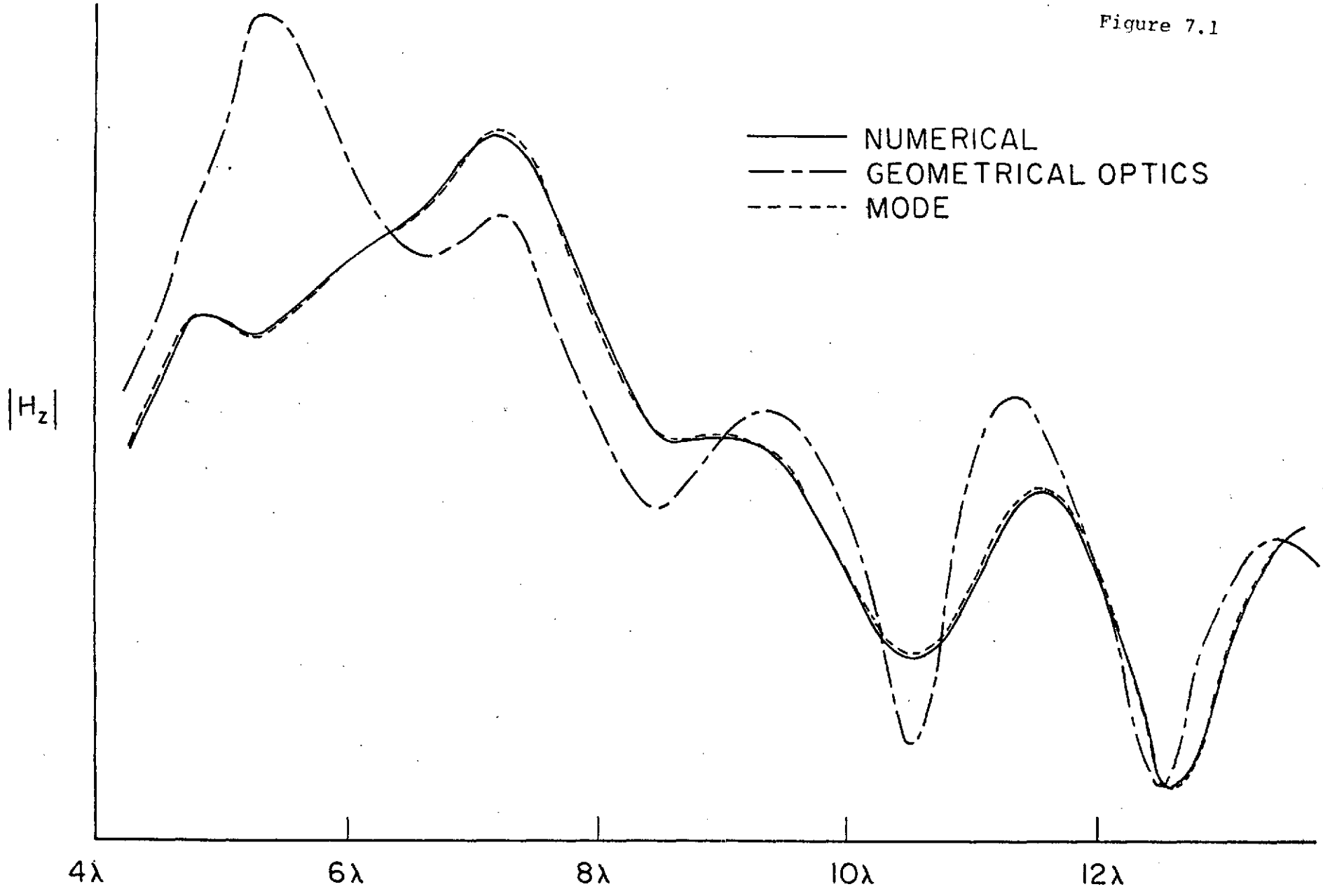

Figure 7.2

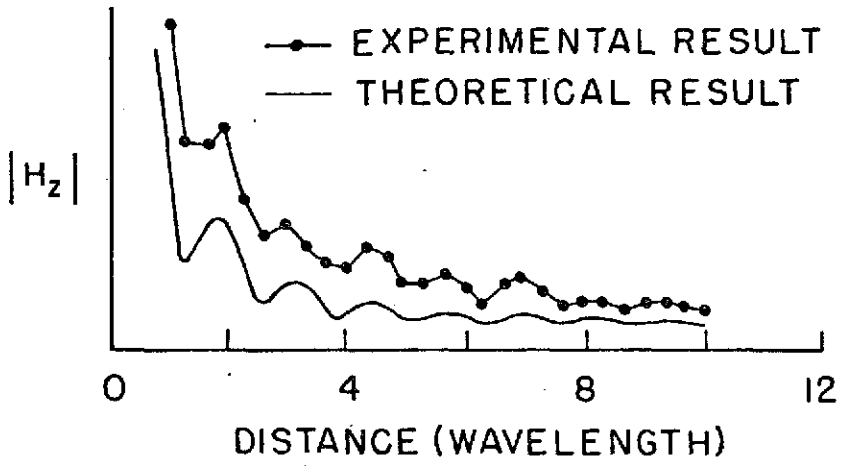
EXPERIMENTAL RESULT
THEORETICAL RESULT
|Hz|
0
4
8
12
DISTANCE (WAVELENGTH)

Figure 7.3

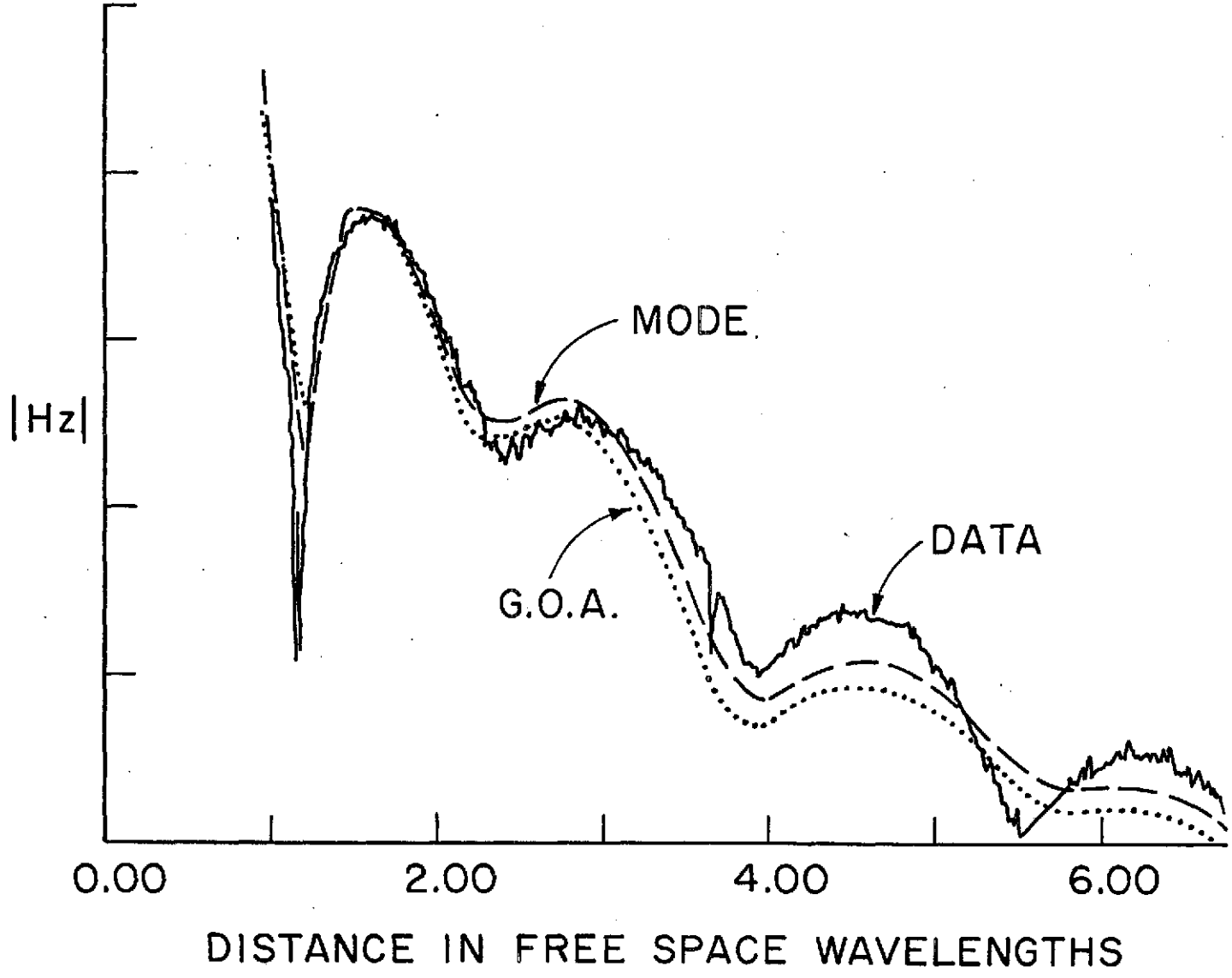
|Hz|
MODE
G.O.A.
DATA
0.00
2.00
4.00
6.00
DISTANCE IN FREE SPACE WAVELENGTHS

Figure 7.4

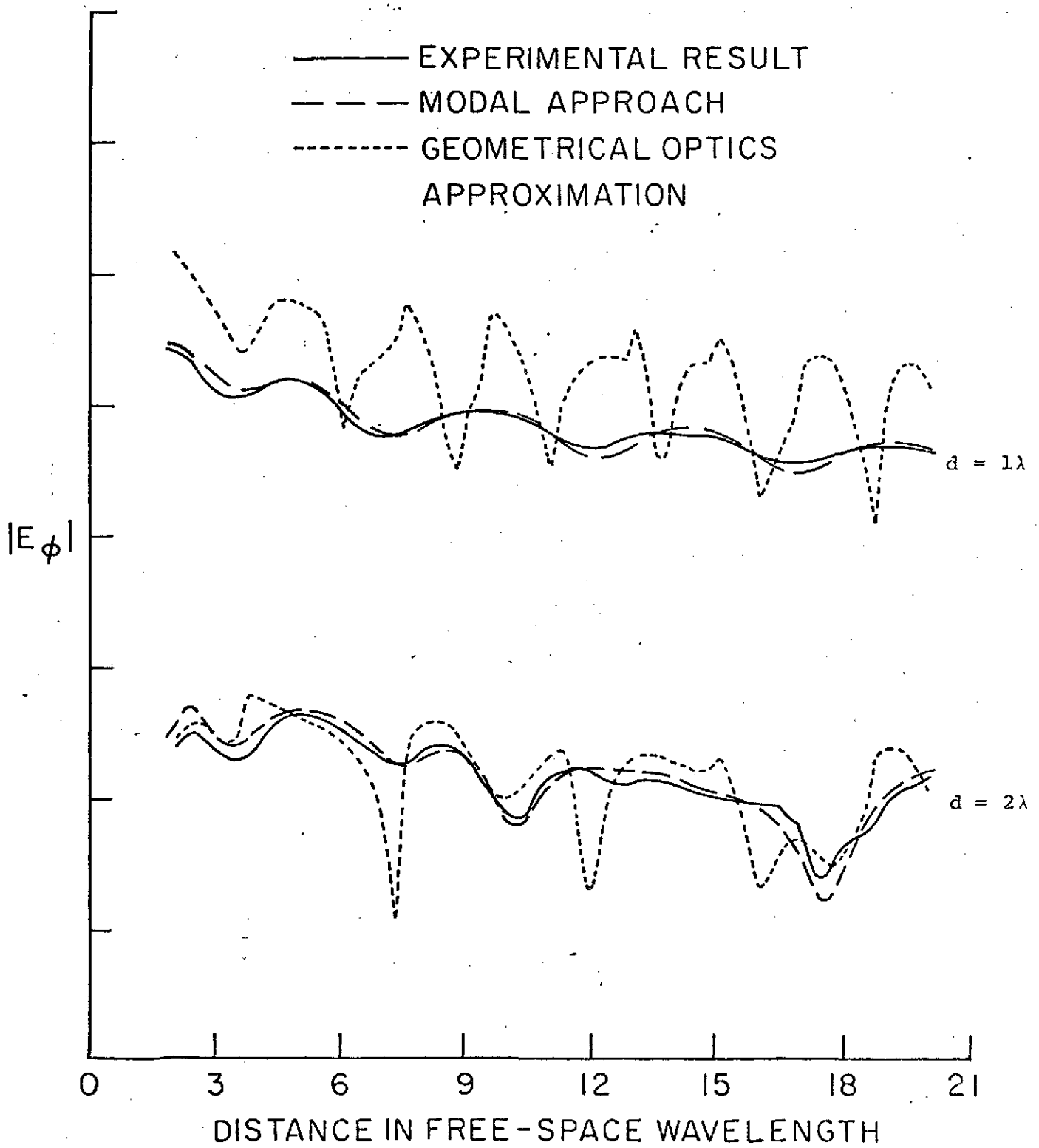
EXPERIMENTAL RESULT
MODAL APPROACH
GEOMETRICAL OPTICS APPROXIMATION
$|E_\phi|$
d = 1λ
d = 2λ
0
3
6
9
12
15
18
21
DISTANCE IN FREE-SPACE WAVELENGTH

REFERENCES

1. R. B. Adler, L. J. Chu, and R. M. Fano, Electromagnetic Energy Transmission and Radiation, John Wiley and Sons, Inc., NY, Chapter 10, 1960.

2. A. P. Annan, "Radio Interferometry Depth Sounding, Part I- Theoretical Discussion," Geophysics, 1973.

3. A. Banos, Jr., Dipole Radiation in the Presence of a Conducting Half Space, Pergammon, NY, 1966.

4. B. K. Bhattacharya, Electromagnetic Fields of a Vertical Magnetic Dipole Placed Above the Earth's Surface, Geophysics, Vol. 28, No. 3, pp. 408-425, 1963.

5. L. M. Brekhovski, Waves in Layered Media, Academic Press, NY, 1960.

6. D. N. Chetaev, "On the field of a Low-frequency Electric Dipole Situated on the Surface of a Uniform Anisotropic Conducting Half-space," Soviet Phys.- Tech. Phys., Vol. 7, No. 11, pp. 991-995, 1963.

7. J. W. Cooley, P. A. W. Lewis, and P. D. Welch, "Application of the Fast Fourier Transform to Computation of Fourier Integrals, Fourier Series, and Convolution Integrals, IEEE Trans. on Audio and Electroacoustics, AU-15, 79, 1967.

8. W. W. Cooper, TE/TM Patterns of Herzian Dipole in Two of Three Layered Medium, to be published, 1971.

9. M. A. H. El-Said, "Geophysical Prospection of Underground Water in the Desert by Means of Electromagnetic Interference Fringes," Proc. IRE, Vol. 44, pp. 24-30, Jan 1956, and p. 940, July 1956.

10. M. A. H. El-Said, "A New Method for the Measurement of the Average Dielectric Constant of the Underground Medium on Site," IEEE PGAP, Vol. AP-4, pp. 601-604, Oct. 1956.

11. S. Evans, "Dielectric Properties of Ice and Snow - a Review," J. Glaciology, Vol. 5, pp. 773-792, 1965.

12. L. B. Felsen and N. Marcuvitz, Radiation and Scattering of Waves, Prentice Hall, 1973.

13. I. S. Gradsheteyn, and I. W. Ryshik, "Tables of Integrals Series and Products, P. 707, Academic Press, NY, 1965.

14. P. Gudmandsen, "Electromagnetic Probing of Ice: in Electromagnetic Probing in Geophysics (J. R. Wait, Ed.), The Golem Press, 1972.

15. E. T. Kanasewich, "Gravity Measurements of the Athabasca Glacier, Alberta, Canada," J. Glaciology, Vol. 4, pp. 617-631, 1963.

16. J. A. Kong, "Quantization of Electromagnetic Waves in Moving Uniaxial Media", J. Appl. Phys., Vol. 41, No. 2, pp.554-559, 1970.

17. J. A. Kong, "Reflection and Transmission of Electromagnetic Waves by Stratified Moving Media", Can. J. Phys., Vol. 49, No. 22, pp. 2785-2792, 1971.

18. J. A. Kong and L. Tsang, Comparison of Results from Geometrical Optics Approach, Memorandum to Professor Gene Simmons, Oct. 1972.

19. J. A. Kong, "Electromagnetic Fields due to Dipole Antennas over Stratified Anisotropic Media," Geophysics, Vol. 37, No. 6, pp. 985-996, Dec. 1972.

20. J. A. Kong, L. Tsang, and G. Simmons, "Lunar Subsurface Probing with Radio Frequency Interferometry," to be published 1973.

21. G. LaTorraca, "Half Wavelength Dipole Antennas over Stratified Media," Master's Degree Thesis, Massachusetts Institute of Technology, MA, 1972.

22. V. P. Nanda and E. J. Groener, "A Study of Theoretical Interference Plots for Horizontal Electric Dipole in Three Layer Geometry and Estimation of Medium Parameters," Center for Space Research Memorandum, Massachusetts Institute of Technology, MA, Sept. 1971.

23. D. C. Pearce and J. W. Walker, "An Empirical Determination of the Relative Dielectric Constant of the Greenland Ice Cap," J. Geophsical Research, Vol. 72, No. 22, pp. 5743-5747, 1967.

24. O. Praus, "Field of Electric Dipole above Two-later Anisotropic Medium," Stud. Geoph. et Geodaet., Vol. 9, pp. 359-380, 1965.

25. J. R. Rossiter, G. A. LaTorraca, A. P. Annan, D. W. Strangway, and Gene Simmons, "Radio Interferometry Depth Sounding, Part 11 - Experimental Results," Geophysics, 1973.

26. J. C. Savage and W. S. B. Paterson, "Borehole Measurements in the Athabasca Glacier," J. Geophysical Research, Vol. 68, No. 15, pp. 4521-4536, 1963.

27. G. Simmons, D. W. Strangway, L. Bannister, D. Cubley and G. LaTorraca, "The Surface Electric Properties Experiment," Proc. Conf. Lunar Geophys., Houston, 1972.

28. G. Simmons, D. W. Strangway, L. Bannister, D. Cubley, and G. LaTorraca, "The Surface Electric Properties", The Moon, 6, 258, 1973.

29. G. Simmons, D. W. Strangway, A. England P. Annan, R. Baker, L. Bannister, R. Brown, D. Cubley, J. Groener, J. Kong, G. LaTorraca, P. Mason, J. Meyer, V. Nanda, D. Redman, J. Rossiter, L. Tsang, W. Waller, and R. Watts, "Radio Frequency Interferometry: Electrical Structure at the Apollo 17 Site (Abstract), Trans. Am. Geophys. Union, in press, 1973.

30. A. K. Sinha and P. K. Bhattacharya, "Electric Dipole over an Anisotropic and Inhomogeneous Earth," Geophysics, Vol. 32, No. 4, pp. 652-667, 1967.

31. A. K. Sinha, "Electromagnetic Fields of an Oscillazing Magnetic Dipole over an Anisotropic Earth," Geophysics, Vol. 33, No. 2, pp. 346-353, 1968.

32. A. K. Sinha, "Vertical Electric Dipole over an Inhomogeneous and Anisotropic Earth," Pure and Applied Geophysics, Vol. 72, No. 1, pp. 123-147, 1969.

33. A. K. Sinha, "Radio Frequency Interometry Depth Sounding Part I - Fields from a Horizontal Electric Dipole over a lossy Dielectric Media," submitted to Radio Science, 1972a.

34. A. K. Sinha, "Radio Frequency Interometry Depth Sounding Part II - Fields from a Horizontal Electric Dipole on a Dielectric Layer over a Perfect Reflector," submitted to Radio Science, 1972b.

35. A. K. Sinha, "Radio Frequency Interometry Depth Sounding Part III- Horizontal Electric Dipole on a Dielectric Layer over an Arbitrary Reflector," submitted to Radio Science, 1972c.

36. A. Sommerfeld, Partial Differential Equations, Academic Press, NY, 1949.

37. D. W. Strangway, G. Simmons, R. Watts, G. LaTorraca, L. Bannister, R. Baker, J. E. Redman and J. R. Rossiter, "Radio Frequency Interferometry--A New Technique for Study Glaciers," J. Glaciology, 1972.

38. D. W. Strangway, A. P. Annan, and R. Watts, "Model and Theoretical Solutions," Memorandum to Dr. Gene Simmons, Oct. 1972.

39. L. Tsang, "Electromagnetic Near Dields of Horizontal Dipole on Stratified Lunar Surface," Bachelor's Degree Thesis, Massachusetts Institute of Technology, MA, 1971.

40. L. Tsang, "Comments on Cooper's Mathematical Approaches," Memorandum to Professor Gene Simmons, Oct. 1972.

41. L. Tsang, J. A. Kong, and Gene Simmons, "Interference Patterns of a Horizontal Electric Dipole over Layered Dielectric Media," J. Geophysical Rearch, June 1973.

42. J. R. Wait, "The Magnetic Dipole over the Horizontally Stratified Earth," Can. J. Phys., Vol. 29, pp. 577-592.

43. J. R. Wait, "Radiation from a Vertical Electric Dipole over a Stratified Ground", IRE Trans. on Ant. and Prop., Vol. AP-1, pp. 9-11, 1953.

44. J. R. Wait, "Fields of a Horizontal Dipole over a Stratified Anisotropic Half-space," IEEE Trans. Ant. Prop., AP-14, pp. 790-792, 1966a.

45. J. R. Wait, "Fields of a Horizontal Dipole over an Anisotropic Half-space," Can. J. Phys., Vol. 44, pp. 2387-2401, 1966b.

46. J. R. Wait, Electromagnetic Waves in Stratified Media, Pergamon Press, 1970.

47. S. H. Ward, "Electromagnetic Theory for Geophysical Applications," Mining Geophysics, Vol. 2, Part A, pp. 10-196, Tulsa, Society of Exploration Geophysicists, 1967.

48. A. Wolf, "Electric Field of an Oscillating Dipole on the Surface of a Two Later Earth," Geophysics, Vol. 11, pp. 518-534, 1946.